View metadata, citation and similar papers at core.ac.uk
brought to you by CORE
provided by King Fahd University of Petroleum and Minerals

# PERFORMANCE OF PUNCTURED SPACE-TIME CODES OVER WIRELESS CHANNELS AND THEIR APPLICATIONS

by

**SAMI ABDUL-HADI FARAJ AL-ANAZI**

A Thesis Presented to the
DEANSHIP OF GRADUATE STUDIES

In Partial Fulfillment of the Requirements
for the Degree

**MASTER OF SCIENCE**

in

**ELECTRICAL ENGINEERING**

**KING FAHD UNIVERSITY OF PETROLEUM & MINERALS**

**DHAHRAN, SAUDI ARABIA**

**DECEMBER 2004**

**KING FAHD UNIVERSITY OF PETROLEUM & MINERALS**
**DHAHRAN 31261, SAUDI ARABIA**

**DEANSHIP OF GRADUATE STUDIES**

This thesis, written by SAMI ABDUL-HADI FARAJ AL-ANAZI under the direction of his thesis advisor and approved by this thesis committee, has been presented to and accepted by the Dean of Graduate Studies, in partial fulfillment of the requirements for the degree of MASTER OF SCIENCE IN ELECTRICAL ENGINEERING.

Thesis Committee

Dr. Saud Al-Semari
Thesis Advisor

Dr. Mahmoud Dawoud
Member

Dr. Maan Kousa
Member

Dr. Jamil M. Bakhashwain
Department Chairman

Dr. Mohammad A. AL-Ohali
Dean of Graduate Studies

15 December 2004
Date

***Dedicated to***

**My Parents**

**and**

**My Family**

# ACKNOWLEDGMENT

*In the name of Allah, the Most Gracious and the Most Merciful*

All praise and glory goes to Almighty Allah. Peace and blessings of Allah be upon His last Prophet Muhammad and all his Sahaba.

Acknowledgment is due to King Fahd University of Petroleum and Minerals for providing support for this work.

Deepest gratitude goes to Dr. Saud Al-Semari my thesis advisor for his strong and continuous support, and the numerous moments of attention he devoted throughout this research work.

Gratitude also due to my thesis committee members Dr. Mahmoud Dawoud and Dr. Maan Kousa for their encouragement, cooperation and for their valuable time that spent reviewing and correcting this work.

Acknowledgment is due to my fellow and friend Hesham Al-Salman, who provided me with many important resources and was very helpful and cooperative

at all times. I also thank my friends Dr. Salam Zummo and Badr Al-Dohan for their support in various stages during this research. Special thanks are due to other colleagues and my friends for their encouragement, motivation and pivotal support.

I would like to thank my parents. Their prayers and encouragement have always helped me take the right steps in life. May Allah reward them with the highest degrees in Jannah. Thanks are also due to my relatives and to all whom support me even without I know them.

# TABLE OF CONTENTS

# List of Tables

# List of Figures

# THESIS ABSTRACT


**NAME:** SAMI ABDUL-HADI FARAJ AL-ANAZI


**TITLE:** PERFORMANCE OF PUNCTURED SPACE-TIME CODES OVER WIRELESS CHANNELS AND THEIR APPLICATIONS

**MAJOR:** ELECTRICAL ENGINEERING

**DATE OF DEGREE:** DECEMBER, 2004


In recent years, demand of high data rates wireless communication systems is exponentially increases where space-time (ST) codes have been introduced as one of the efficient solutions for this problem. In this thesis ST coding system throughput and reliability have been improved. There are two methods to improve throughput; the first one is by using high-rate ST codes and the second method is based on symbol puncturing, which is the main idea of this thesis. Design criteria of PST codes over quasi-static and rapid fading channels are derived and five ST codes are found. Simulation shows that the new codes have comparable performance with out puncturing and superior performance under puncturing compared to some existing codes. ST coding system reliability is improved by using hybrid forward error correction and automatic repeat request (HARQ) schemes. There are six type-I and type-II HARQ protocols that employ either ST, high-rate ST or PST codes. Simulation shows that type-II protocols have better performance and throughput efficiencies than type-I protocols employing the same coding scheme.

خلاصة الرسالة

**الاسم :** **سامي بن عبدالهادي بن فرج العنزي**

**العنوان :** **اداء الترميزات الفراغية الوقتية المعطوبة عبر القنوات اللاسلكية وتطبيقاتها**

**التخصص :** **هندسة كهربائية**

**التاريخ :** **ذو القعدة 1425 هـ ، ديسمبر 2004**

في السنوات الاخيرة ، ازداد الطلب على نظم الاتصالات اللاسلكية ذات معدلات البيانات العالية بشكل مطرد ، حيث طرحت الترميزات الفراغية الوقتية كاحد الحلول الفعالة لهذه المشكلة . في هذه الرسالة ، تم تحسين سعة واعتمادية نضم الترميز الفراغي الوقتي . هنالك طريقتان لتحسين السعة : الطريقة الاولى باستخدام الترميزات الفراغية الوقتية ذات المعدلات العالية والطريقة الثانية تعتمد على تعطيب الرمز وهي الفكرة الرئيسية لهذه الرسالة . تم اشتقاق قوانين تصميم الترميزات الفراغية الوقتية عبر القنوات شبة الثابتة وسريعة التغير ، كم تم ايجاد خمس ترميزات فراغية وقتية . اظهرت المحاكاة ان اداء الترميزات الجديدة مقارن بدون تعطيب وفائق مع التعطيب مقارنة مع بعض الترميزات الفراغية الوقتية الاخرى . تم تحسين اعتمادية نظم الترميز الفراغي الوقتي باستخدام مركب طرق تحسين الخطأ الامامي واعادة الطلب التلقائي . هنالك ستة اتفاقية مركبة من النوع الاول والنوع الثاني والتي تستخدم اما الترميزات الفراغية الوقتية او الترميزات الفراغية الوقتية ذات المعدلات العالية او الترميزات الفراغية الوقتية المعطوبة . اظهرت المحاكاة ان المركبات من النوع الثاني لها اداء افضل وسعة اكفئ من المركبات من النوع الاول والتي تستخدم نفس نوع الترميز .

# CHAPTER 1

# INTRODUCTION

## 1.1 GENERAL OVERVIEW

In the last few years, there has been a strong demand to achieve higher data rates over wireless channels, in order to support high-speed data services. Such applications and services include high audio quality, fast data transfer and video applications such as online video conferencing. However, wireless communication systems suffer from time varying characteristics of the communication channel and fading phenomena. These cause in some cases substantial attenuations in the received signal, which results in a dramatic degradation in the overall communication system performance.

In 1998, *space-time* (ST) codes [1] were proposed for high data rate wireless

communication systems. Space-time codes implement the idea of combining multi-transmit antennas with trellis-coded modulation. This coding technique results in a significant improvement on wireless communication systems performance. Moreover, it results in a very good tradeoff between data rate, diversity advantage and trellis complexity.

A fundamental method of increasing the throughput of a wireless communication system is to use a higher signal constellation size. However, increasing the constellation size reduces the Euclidean distance between the constellation symbols, which increases the probability of error. Another way of increasing the throughput especially for space-time codes is by increasing the rate of the channel encoder and using the same signal constellation size. This would also increase the probability of error but if a proper high-rate channel encoder is used the probability of error due to increasing the code rate can be made small. Instead, puncturing techniques could be used to increase the throughput of the communication system. These techniques could also be used to produce variable rate codes [2]. Puncturing methods could be combined with space-time codes to generate a new class of codes.

In this Chapter, the wireless communication channel models used are given with a brief description of diversity. Then, a space-time coding system is studied with detailed statement of performance criteria over quasi-static and rapid fading channels. Simulation results for some of the existing QPSK ST codes are reproduced in the same section. Next, an up to date literature survey is given.

Finally, thesis contributions are stated.

## 1.2 Channel Model

Wireless fading channels are classified (depending on the rate of change of the channel gains) into fast fading (FF) and slow fading (SF) channels. In the fast fading environments, channel gains change in a rate higher than the symbol rate. While in the slow fading environments, channel gains change in a rate further slower than the symbol rate. The *additive white Gaussian noise* (AWGN) exists in both fading channels.

Slow fading channels could farther be classified into quasi-static and rapid fading channels. In the quasi-static channels, channel gains are assumed to remain constants during frame transmission and change independently from one frame to another. Whereas, rapid fading channel gains vary independently from one symbol to another.

Channel models used throughout the thesis work are the quasi-static fading channel and the rapid fading channel models. Both channels are statistically modeled by a Rayleigh distribution. Therefore, the envelope of the channel samples ($|a|$) has a probability density function (pdf) that is given by:

$$p_a(|a|) = \frac{|a|}{\sigma^2} \exp\left(\frac{-|a|^2}{2\sigma^2}\right) \qquad a > 0 \tag{1.1}$$

where $2\sigma^2$ is the mean square average power of the fading samples and the phase is uniformly distributed in $[0, 2\pi]$. If a direct path between the mobile and the base station exists, the fade samples are modeled by Rician distribution.

The single most important way to reduce error probability and achieve reliable communication with a Rayleigh fading channel is diversity [1]. Severe attenuation of the transmitted signal due to deep-fade makes it impossible for the receiver to determine the transmitted signal unless a less-attenuated replica is available.

Consequently, the idea of diversity is to supply the receiver with replicas of the transmitted signal through different paths (links) using space, time and/or frequency. These paths could be independently affected by multipath fade, which increases the probability of receiving a less-attenuated replica of the transmitted signal. The following are examples of diversity techniques:

- *Time Diversity*: Channel coding in conjunction with time interleaving is used. Replicas of the transmitted signal are provided to the receiver in the form of redundancy in the temporal domain.

- *Frequency Diversity*: The fact that waves transmitted on different frequencies induce different multi-path structure in the propagation media is exploited. Replicas of the transmitted signal are provided to the receiver in the form of redundancy in the frequency domain.

- *Space Diversity*: Spatially separated antennas are used. The replicas of the transmitted signal are provided to the receiver in the form of redundancy

in spatial domain. This can be provided with no penalty in bandwidth efficiency.

The mobile communication system should implement all possible diversity techniques available. In space diversity, there is a variety of ways to combine diversity information from the various antennas, but the most efficient one is called *maximal ratio combining* (MRC) which gives the highest weight to the strongest signal.

## 1.3 Space-Time Codes

It has long been known that antenna diversity is an effective technique to improve the performance of wireless systems in fading channels. The greater the number of diversity antennas, the better the chances that at least one of the antennas receives a strong signal.

Recently, it has been shown that the use of space diversity (at the transmitter side) combined with error-correction coding allows dramatic increase in data rates achievable over wireless channels [1]. This combination of transmit diversity with error-correction coding is called *Space-Time Coding*, and the system with multiple transmit and receive antennas is called a *Multiple-Input Multiple-Output* (MIMO) system. Space-time codes could be viewed as a *multiple trellis coded modulation* (MTCM) but the branch transition symbols are transmitted in parallel.

### 1.3.1 ENCODER/DECODER OF ST CODING SYSTEMS

A general block diagram of a space-time coding system is shown in Figure 1.1. The $k$ source bits are encoded using error-correction codes, and then the encoder output bits are divided into $N$ groups each with $m$ bits. The $m$ bits of each group are mapped to a constellation point with $2^m$-constellation size. The generated $N$ symbols $(c_t^i, i = 1, 2, \cdots, N)$ are modulated and transmitted each via one of the $N$ transmit antennas simultaneously with the same transmission period. It is assumed that the points of the signal constellation are multiplied by a factor of $\sqrt{E_s}$ so that the average energy of the constellation is one.

As an example of space-time trellis code, the QPSK 4-state trellis code designed in [1] is studied. The code trellis diagram is shown in Figure 1.2(b). This code is designed for two transmit antennas. The encoder takes two input bits each time, therefore, there are four branches diverging form each trellis state. The trellis transition branch labels indicate the symbols to be transmitted, the first symbol via the first transmit antenna and the second symbol via the second transmit antenna. Depending on current trellis state and input bits, two QPSK symbols are generated and transmitted simultaneously. For example, if the input bits are (01) (11) (10) (00) (01), and the encoder is at initial state (00), the output symbols are $(3, 1)$ $(2, 3)$ $(0, 2)$ $(1, 0)$ $(0, 1)$. This code can also be viewed as delay diversity where symbols transmitted over the second antenna at a given time slot will be transmitted over the first antenna at the next time slot.

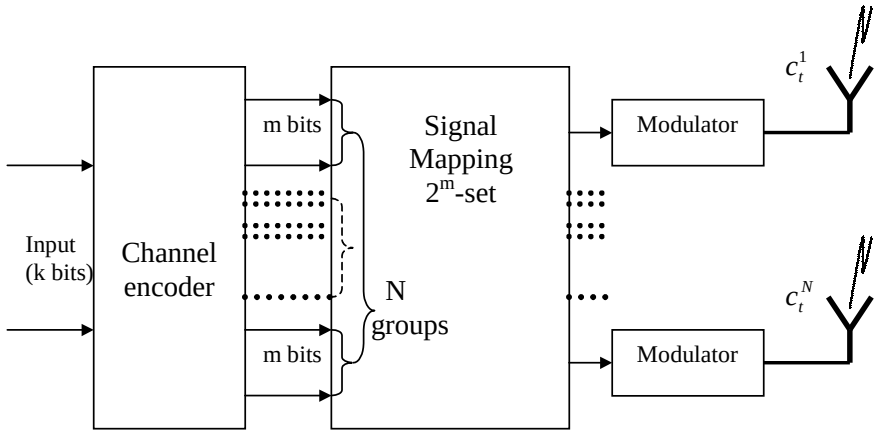


(a)

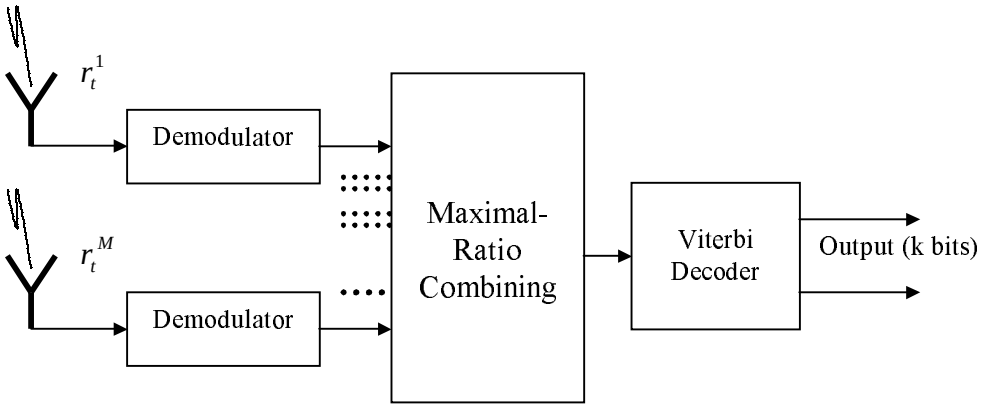


(b)

Figure 1.1: General block diagram of ST coding system (a) Encoder (b) Decoder

At the receiver, the received signal at each of the $M$ receive antennas is a noisy superposition of all transmitted signals from the $N$ transmit antennas corrupted by Rayleigh fading. The received signal at the $j^{th}$ receive antenna ($Rx$ antenna) is:

$$\mathbf{r}_t^j = \sum_{i=1}^{N} \alpha_{i,j}(t) c_t^i \sqrt{E_s} + n_t^j \tag{1.2}$$

where $n_t^j$ are samples of independent zero-mean complex Gaussian random variables with variance $N_0/2$ per dimension, and $c_t^i$ is the transmitted symbol from transmit antenna ($Tx$ antenna) $i$ at time $t$. The coefficient $\alpha_{i,j}(t)$ is the path gain from transmit antenna $i$ to receive antenna $j$ at time $t$ and it is modeled as independent samples of Gaussian random variable with zero mean and variance 0.5 per dimension.

The Viterbi decoder selects a cumulative branch metric, which is given for a single branch by:

$$\sum_{j=1}^{M} \left| r_t^j - \sum_{i=1}^{N} \alpha_{i,j}\left(t\right) c_t^i \right|^2 \tag{1.3}$$

### 1.3.2 Performance Analysis and Design Criteria

Performance analysis of ST codes is mainly carried in the mean of the pairwise error probability (PEP) expression approximations. The design criteria then are derived from these approximations. In the design of ST trellis codes for fading channels, parallel transitions must be avoided, because the parallel transitions limit the minimum time diversity to one. So if a spectral efficiency of $k$ b/s/Hz

is targeted, there will be $2^k$ branches diverging from and merging into each trellis state. Thus, the encoder should have at least $v = k$ memory elements (at least $2^k$ trellis states) such that parallel transitions are avoided since there is only one branch connecting each two trellis states.

Performance of ST trellis codes has been derived and studied by many researchers for different wireless communication channel models. These studies lead to the design of many ST codes. Following [1] and [3], performance analysis started by stating the notations used. Considering a transmitted codeword denoted by $\mathbf{c}$, which is given by the codeword matrix:

$$\mathbf{c} = \begin{bmatrix} c_1^1 & c_2^1 & \cdots & c_l^1 \\ c_1^2 & c_2^2 & \cdots & c_l^2 \\ \vdots & \vdots & \ddots & \vdots \\ c_1^N & c_2^N & \cdots & c_l^N \end{bmatrix} \tag{1.4}$$

where the $i^{th}$ row $\mathbf{c}^i = [c_1^i, c_2^i, \cdots, c_l^i]$ is the encoder-mapper output sequence transmitted via the $i^{th}$ transmit antenna ($i = 1, 2, \cdots, N$), and the $t^{th}$ column $\mathbf{c}_t = \left[c_t^1, c_t^2, \cdots, c_t^N\right]^T$ is the transmitted space-time symbol at the $t^{th}$ transmission time ($t = 1, 2, \cdots, l$).

At the receiver, the received signal at the $j^{th}$ receive antenna ($j = 1, 2, \cdots, M$) is a noisy superposition of the $N$ transmitted symbols corrupted by channel fading.

If $\mathbf{r}$ denotes the received signal sequence, where:

$$\mathbf{r} = \begin{bmatrix} r_1^1 & r_2^1 & \cdots & r_l^1 \\ r_1^2 & r_2^2 & \cdots & r_l^2 \\ \vdots & \vdots & \ddots & \vdots \\ r_1^M & r_2^M & \cdots & r_l^M \end{bmatrix} \tag{1.5}$$

and $\mathbf{r}_t = \left[r_t^1, r_t^2, \cdots, r_t^M\right]^T$ is the received sequence at the $M$ receive antennas at the $t^{th}$ reception time ($t = 1, 2, \cdots, l$), then the signal at the $j^{th}$ receive antenna after the match filter is given by:

$$r_t^j = \sum_{i=1}^{N} \alpha_{i,j}(t)\, c_t^i + n_t^j \tag{1.6}$$

where $n_t^j$ is the noise component of the $j^{th}$ receive antenna at time $t$, and it is modeled as independent complex Gaussian random variable with zero mean and variance $N_0/2$ per dimension. The fade coefficients $\alpha_{i,j}(t)$, $t = 1, 2, \cdots, l$ $i = 1, 2, \cdots, N$ $j = 1, 2, \cdots, M$, are modeled as complex Gaussian random variables with zero mean and variance $1/2$ per dimension. The fade coefficients vary independently from one symbol interval to other in rapid fading channels and from one frame interval to other in quasi-static fading channels. Moreover, the fade coefficients for paths from the $N$ transmit antennas to the $M$ receive antennas at time $t$ are uncorrelated. Hence, the received signals at time $t$ can be written in

terms of the transmitted ST symbol as:

$$\mathbf{r}_t = \mathbf{a}(t)\,\mathbf{c}_t + \mathbf{n}_t \tag{1.7}$$

where $\mathbf{a}(t)$ is the fading coefficients matrix at time $t$, which equals:

$$\mathbf{a}(t) = \begin{bmatrix} \alpha_{1,1}(t) & \alpha_{2,1}(t) & \cdots & \alpha_{N,1}(t) \\ \alpha_{1,2}(t) & \alpha_{2,2}(t) & \cdots & \alpha_{N,2}(t) \\ \vdots & \vdots & \ddots & \vdots \\ \alpha_{1,M}(t) & \alpha_{2,M}(t) & \cdots & \alpha_{N,M}(t) \end{bmatrix} \tag{1.8}$$

and $\mathbf{n}_t = \left[n_t^1, n_t^2, \cdots, n_t^M\right]^T$ is the noise vector at time $t$. The rows $\mathbf{a}_j(t)$ of the fade matrix are the channel path gains from the $N$ transmit antennas to the $j^{th}$ receive antenna at time $t$.

$$\mathbf{a}_j(t) = \left[\alpha_{1,j}(t), \alpha_{2,j}(t), \cdots, \alpha_{N,j}(t)\right] \tag{1.9}$$

The pairwise error probability $P(\mathbf{c} \to \mathbf{e})$ is defined as the probability that a maximum-likelihood decoder decides on the sequence $\mathbf{e}$ while the transmitted sequence was in fact $\mathbf{c}$. This event happens when:

$$\sum_{t=1}^{l}\sum_{j=1}^{M}\left|r_t^j - \sum_{i=1}^{N}\alpha_{i,j}(t)\,c_t^i\right|^2 \geq \sum_{t=1}^{l}\sum_{j=1}^{M}\left|r_t^j - \sum_{i=1}^{N}\alpha_{i,j}(t)\,e_t^i\right|^2 \tag{1.10}$$

Substituting (1.6) in (1.10) and simplifying the result leads to [3]:

$$\sum_{t=1}^{l}\sum_{j=1}^{M} 2Re\left(n_t^{j*}\sum_{i=1}^{N}\alpha_{i,j}\left(t\right)\left(e_t^i-c_t^i\right)\right) \geq \sum_{t=1}^{l}\sum_{j=1}^{M}\left|\sum_{i=1}^{N}\alpha_{i,j}\left(t\right)\left(e_t^i-c_t^i\right)\right|^2 = |e-c| \tag{1.11}$$

where $Re\left(\cdot\right)$ denotes the real part of a complex variable and $\left(\cdot\right)^*$ denotes the complex conjugate. The term on the right hand side of inequality (1.11) is a constant, called square Euclidean distance (in [3] it is called modified Euclidean distance) and it is denoted by $d^2\left(\mathbf{c},\mathbf{e}\right)$. This constant is a measure of how far the two ST codewords $\mathbf{c}$ and $\mathbf{e}$ are from each other.

$$d^2\left(\mathbf{c},\mathbf{e}\right) = \sum_{t=1}^{l}\sum_{j=1}^{M}\left|\sum_{i=1}^{N}\alpha_{i,j}\left(t\right)\left(c_t^i-e_t^i\right)\right|^2 \tag{1.12}$$

The term on the left hand side of inequality (1.11) is a Gaussian random variable with zero mean and variance $4\sigma^2 d^2\left(\mathbf{c},\mathbf{e}\right)$. Thus, the conditioned pairwise error probability is given by:

$$P\left(\mathbf{c}\rightarrow\mathbf{e}|\alpha_{i,j}\left(t\right),i,j,t\right) = Q\left(\sqrt{\frac{d^2\left(\mathbf{c},\mathbf{e}\right)E_s}{2N_0}}\right) \leq \frac{1}{2}\exp\left(-d^2\left(\mathbf{c},\mathbf{e}\right)\frac{E_s}{4N_0}\right) \tag{1.13}$$

where $Q\left(x\right)$ is the complementary error function defined as:

$$Q\left(x\right) = \frac{1}{\sqrt{2\pi}}\int_x^{\infty} e^{\frac{-t^2}{2}}dt \tag{1.14}$$

The $Q(x)$ is approximated by the following inequality:

$$Q(x) \leq \frac{1}{2} e^{\frac{-x^2}{2}} \qquad x \geq 0 \tag{1.15}$$

**Quasi-Static Rayleigh Fading Channels**

As mentioned earlier, in quasi-static fading channels, the fade coefficients remain constant during frame transmission time $l$ and vary independently from one frame to another. Therefore

$$\alpha_{i,j}(1) = \alpha_{i,j}(2) = \cdots = \alpha_{i,j}(l) = \alpha_{i,j}$$

and the $j^{th}$ row of the coefficients matrix will be:

$$\mathbf{a}_j = [\alpha_{1,j} \quad \alpha_{2,j} \quad \cdots \quad \alpha_{N,j}] \tag{1.16}$$

Let a codeword difference matrix $\mathbf{B}(\mathbf{c}, \mathbf{e})$ be defined by [1]:

$$\mathbf{B}(\mathbf{c}, \mathbf{e}) = \begin{bmatrix} c_1^1 - e_1^1 & c_2^1 - e_2^1 & \cdots & c_l^1 - e_l^1 \\ c_1^2 - e_1^2 & c_2^2 - e_2^2 & \cdots & c_l^2 - e_l^2 \\ \vdots & \vdots & \ddots & \vdots \\ c_1^N - e_1^N & c_2^N - e_2^N & \cdots & c_l^N - e_l^N \end{bmatrix} \tag{1.17}$$

which is a square root of a distance matrix $\mathbf{A}(\mathbf{c},\mathbf{e})$ given by:

$$\mathbf{A}(\mathbf{c},\mathbf{e}) = \mathbf{B}(\mathbf{c},\mathbf{e}) \cdot \mathbf{B}^H(\mathbf{c},\mathbf{e}) \tag{1.18}$$

where the superscript $H$ denotes the Hermitian (transpose conjugate) of a matrix. $\mathbf{A}(\mathbf{c},\mathbf{e})$ is a nonnegative definite Hermitian [1]. So, there is a unitary matrix $\mathbf{V}$ such that:

$$\mathbf{V}\mathbf{A}(\mathbf{c},\mathbf{e})\mathbf{V}^H = \mathbf{D} \tag{1.19}$$

where $\mathbf{D}$ is a real diagonal matrix of the eigenvalues of $\mathbf{A}(\mathbf{c},\mathbf{e})$, with diagonal elements $\lambda_i$, $i = 1, 2, \cdots, N$ counting multiplicity and $\lambda_1 \geq \lambda_2 \geq \cdots \geq \lambda_n \geq 0$. The rows $[\mathbf{v}_1, \mathbf{v}_2, \cdots, \mathbf{v}_N]^T$, (eigenvectors of $\mathbf{A}(\mathbf{c},\mathbf{e})$) of $\mathbf{V}$ form a complete orthonormal basis of the $N$-dimensional vector space.

Using the above results, and substituting (1.16) in the expression of $d^2(\mathbf{c},\mathbf{e})$, (1.12) will result in:

$$d^2(\mathbf{c},\mathbf{e}) = \sum_{j=1}^{M} \mathbf{a}_j \mathbf{A}(\mathbf{c},\mathbf{e})\mathbf{a}_j^H = \sum_{j=1}^{M}\sum_{i=1}^{N} \lambda_i |\beta_{i,j}|^2 \tag{1.20}$$

where $\beta_{i,j} = \mathbf{a}_j \cdot \mathbf{v}_i$, and the $\cdot$ is the inner complex vectors product. Substituting (1.20) in (1.13) leads to:

$$P(\mathbf{c} \to \mathbf{e}|\alpha_{i,j}, i, j) \leq \frac{1}{2}\exp\left(-\sum_{j=1}^{M}\sum_{i=1}^{N} \lambda_i |\beta_{i,j}|^2 \frac{E_s}{4N_0}\right) \tag{1.21}$$

$\beta_{i,j}$ is independent complex Gaussian random variables with variance 1/2 per dimension and mean $E[\mathbf{a}_j \cdot \mathbf{v}_i]$, where $E[\cdot]$ denotes the expectation. Letting

$$K_{i,j} = |E[\beta_{i,j}]|^2 = |E[\mathbf{a}_j] \cdot E[\mathbf{v}_i]|^2 = |[E[a_{1,j}], E[a_{2,j}], \cdots, E[a_{N,j}]] \cdot v_i|^2 \quad (1.22)$$

thus $|\beta_{i,j}|$ are independent Rician distributions [1] with probability density function (pdf):

$$p(|\beta_{i,j}|) = 2|\beta_{i,j}| \exp\left(-|\beta_{i,j}|^2 - K_{i,j}\right) I_0\left(2|\beta_{i,j}|\sqrt{K_{i,j}}\right) \qquad |\beta_{i,j}| \geq 0 \quad (1.23)$$

where $I_0(\cdot)$ is the zero-order modified Bessel function of the first kind. Therefore the unconditioned upper bound on the pairwise error probability is simply computed by averaging the right hand side of inequality (1.21) with respect to independent Rician distribution of $|\beta_{i,j}|$ to arrive at [1]:

$$P(\mathbf{c} \to \mathbf{e}) \leq \prod_{j=1}^{M} \left( \prod_{i=1}^{N} \frac{1}{1 + \frac{E_s}{4N_0}\lambda_i} \exp\left( -\frac{K_{i,j}\frac{E_S}{4N_0}\lambda_i}{1 + \frac{E_S}{4N_0}\lambda_i} \right) \right) \quad (1.24)$$

A special case of Rayleigh fading where $E[\alpha_{i,j}] = 0$ and thus $K_{i,j} = 0$ results in an upper bound on PEP given by:

$$P(\mathbf{c} \to \mathbf{e}) \leq \left( \prod_{i=1}^{N} \left( 1 + \lambda_i \frac{E_s}{4N_0} \right) \right)^{-M} \quad (1.25)$$

Let $r$ denote the rank of $\mathbf{A}(\mathbf{c}, \mathbf{e})$, then there are exactly $r$ nonzero eigenvalues of

$\mathbf{A}(\mathbf{c}, \mathbf{e})$. Therefore, inequality (1.25) can be written as:

$$P(\mathbf{c} \to \mathbf{e}) \leq \left(\prod_{i=1}^{r} \lambda_i\right)^{-M} \left(\frac{E_s}{4N_0}\right)^{-rM} \tag{1.26}$$

From (1.26), a diversity advantage of $rM$ and a coding advantage of $(\lambda_1 \lambda_1 \cdot \lambda_r)^{1/r}$ are achieved.

Inequality (1.26) is valid for small values of $rM$ [3]. For large values of $rM$, since the $|\beta_{i,j}|$ in (1.21) follows a Rician distribution, there are $rM$ noncentral Chi-Square-distributed random variables $|\beta_{i,j}|^2$ with 2 degrees of freedom, noncentrality parameter $S = |E[\beta_{i,j}]|^2 = K_{i,j}$, variance $1 + 2K_{i,j}$, and mean value $1 + K_{i,j}$. Since for a large values of $rM$, there are a large number of independent sub-channels and according to the central limit theorem, the expression $\sum_{j=1}^{M} \sum_{i=1}^{N} \lambda_i |\beta_{i,j}|^2$ approaches a Gaussian random variable with variance $\sum_{j=1}^{M} \sum_{i=1}^{N} \lambda_i (1 + 2K_{i,j})$, and mean value $\sum_{j=1}^{M} \sum_{i=1}^{N} \lambda_i (1 + K_{i,j})$. For Rayleigh fading channels where $E[\mathbf{a}_j] = 0$ and thus $K_{i,j} = 0$, and following [3], the upper bound on the unconditional PEP can be obtained by averaging (1.21) with respect to those random variables, to get:

$$\begin{aligned} P(\mathbf{c} \to \mathbf{e}) \quad \leq \quad & \frac{1}{2} \exp\left(\frac{ME_s}{4N_0}\left(\frac{E_s \sum_{i=1}^{r} \lambda_i^2}{8N_0} - \sum_{i=1}^{r} \lambda_i\right)\right) \cdot \\ & Q\left(\frac{\sqrt{M}\left(\sum_{i=1}^{r} \lambda_i^2 - \frac{E_s}{4N_0} \sum_{i=1}^{r} \lambda_i\right)}{\frac{E_s}{4N_0}\sqrt{\sum_{i=1}^{r} \lambda_i^2}}\right) \end{aligned} \tag{1.27}$$

Using inequality (1.15), the expression (1.27) can be approximated by [3]:

$$P\left(\mathbf{c} \rightarrow \mathbf{e}\right) \leq \exp\left(-\frac{ME_s}{4N_0}\sum_{i=1}^{r}\lambda_i\right) \tag{1.28}$$

The above performance analysis of ST codes in quasi-static fading channels was divided into two parts depending on the value of $rM$. The maximum value of $rM$ is $NM$. For small values of $NM$, where there is a small number of independent sub-channels, the PEP is dominated by the rank and the product of nonzero eigenvalues (determinant) of $\mathbf{A}\left(\mathbf{c}, \mathbf{e}\right)$, Inspection of inequality (1.26), leads to the following design criteria for small values of $NM$.

**Design Criteria Set I [1]**

- *The Rank Criterion:* Maximize the minimum rank of the matrix $\mathbf{A}\left(\mathbf{c}, \mathbf{e}\right)$ for all distinct codeword pairs.

- *The Determinant Criterion:* Maximize the minimum determinant of $\mathbf{A}\left(\mathbf{c}, \mathbf{e}\right)$ corresponding to distinct codeword pairs with the minimum rank.

From the rank criterion, it is clearly seen that to achieve a full diversity advantage of $NM$, the rank of $\mathbf{A}\left(\mathbf{c}, \mathbf{e}\right)$ must equal to N for all distinct codeword pairs $\mathbf{c}$ and $\mathbf{e}$. If the minimum rank of $\mathbf{A}\left(\mathbf{c}, \mathbf{e}\right)$ is $r$, then the achievable diversity advantage equals $rM$. Since minimum determinant of $\mathbf{A}\left(\mathbf{c}, \mathbf{e}\right)$ is a measure of the coding advantage [1], maximizing the minimum determinant maximize the coding advan-

tage. The minimum determinant can be used to choose between codes with the same minimum rank.

For large values of $NM$, which corresponds to a large number of independent sub-channels, it is seen from (1.28) that PEP is determined by the minimum rank and the summation of the nonzero eigenvalues of $\mathbf{A}(\mathbf{c}, \mathbf{e})$. For square matrix, the summation of the eigenvalues equals the summation of the main diagonal elements and it is called the trace. For practical systems, which operate at high SNR such that:

$$\frac{E_S}{4N_0} \geq \frac{\sum_{i=1}^{r} \lambda_i}{\sum_{i=1}^{r} \lambda_i^2} \tag{1.29}$$

the design criteria mainly depends on the maximization of the minimum trace.

**Design Criteria Set II [3]**

- Maximize the minimum rank of the matrix $\mathbf{A}(\mathbf{c}, \mathbf{e})$ for all distinct codeword pairs such that $rM \geq 4$.
- Maximize the minimum trace of $\mathbf{A}(\mathbf{c}, \mathbf{e})$ for all distinct codeword pairs.

The first criterion indicates that a diversity advantage of four is enough and the system performance is determined by the minimum trace. The trace of $\mathbf{A}(\mathbf{c}, \mathbf{e})$ is related to the squared Euclidean distance by:

$$tr\left(\mathbf{A}(\mathbf{c}, \mathbf{e})\right) = \sum_{t=1}^{l} \sum_{i=1}^{N} \left| c_t^i - e_t^i \right|^2 \tag{1.30}$$

Maximizing the minimum trace is equivalent to maximizing the minimum Euclidean distance. Since for large $NM$ the channel converges to Gaussian channel and the main design criterion is maximization of the minimum Euclidean distance.

**Rapid Rayleigh Fading Channels**

In rapid fading channels, channel gains ($\alpha_{i,j}(t)$) vary independently form one symbol interval to another. As in quasi-static fading channels, let $\mathbf{F}(\mathbf{c}_t, \mathbf{e}_t)$ denotes a ST symbols difference vector that is given by:

$$\mathbf{F}(\mathbf{c}_t, \mathbf{e}_t) = \left[c_t^1 - e_t^1, c_t^2 - e_t^2, \cdots, c_t^N - e_t^N\right]^T \tag{1.31}$$

Then, an $N \cdot N$ matrix $\mathbf{C}(\mathbf{c}_t, \mathbf{e}_t)$ defined by [1]:

$$\mathbf{C}(\mathbf{c}_t, \mathbf{e}_t) = \mathbf{F}(\mathbf{c}_t, \mathbf{e}_t) \cdot \mathbf{F}^H(\mathbf{c}_t, \mathbf{e}_t) \tag{1.32}$$

is a Hermitian matrix. So there exist a unitary matrix $\mathbf{V}(t)$ such that:

$$\mathbf{V}(t)\,\mathbf{C}(\mathbf{c}_t, \mathbf{e}_t)\,\mathbf{V}^H(t) = \mathbf{D}(t) \tag{1.33}$$

where $\mathbf{D}(t)$ is a real diagonal matrix with diagonal elements $D_{i,i}(t)$, $i = 1, 2, \cdot, N$ are the eigenvalues of $\mathbf{C}(\mathbf{c}_t, \mathbf{e}_t)$. The rows of $\mathbf{V}(t)$, $[\mathbf{v}_1(t), \mathbf{v}_2(t), \cdots, \mathbf{v}_N(t)]^T$ eigenvectors of $\mathbf{C}(\mathbf{c}_t, \mathbf{e}_t)$ form a complete orthonormal basis of the $N$-dimensional

vector space.

If $\mathbf{c}_t = \mathbf{e}_t$, then $\mathbf{C}(\mathbf{c}_t, \mathbf{e}_t)$ has all its eigenvalues equal zero. Otherwise, when $\mathbf{c}_t \neq \mathbf{e}_t$, then there is only one nonzero eigenvalue of $\mathbf{C}(\mathbf{c}_t, \mathbf{e}_t)$. Let this eigenvalue be denoted by $D_{1,1}(t)$ and let the eigenvector corresponding to $D_{1,1}(t)$ be denoted by $\mathbf{v}_1(t)$. The value of this nonzero element $D_{1,1}(t)$ is the squared Euclidean distance between $\mathbf{c}_t$ and $\mathbf{e}_t$.

$$D_{1,1}(t) = |\mathbf{c}_t - \mathbf{e}_t|^2 = \sum_{i=1}^{N} \left| c_t^i - e_t^i \right|^2 \tag{1.34}$$

The square Euclidean distance $d^2(\mathbf{c}, \mathbf{e})$ (1.12) could be expressed as:

$$d^2(\mathbf{c}, \mathbf{e}) = \sum_{t=1}^{l} \sum_{j=1}^{M} \sum_{i=1}^{N} |\beta_{i,j}(t)|^2 \cdot D_{i,i}(t) \tag{1.35}$$

where $\beta_{i,j}(t) = \mathbf{a}_j(t) \cdot \mathbf{v}_i(t)$ are independent complex Gaussian variables with zero mean and variance $1/2$ per dimension, and $\mathbf{a}_j(t)$ is given by (1.9). While there is at most one nonzero eigenvalue $D_{1,1}(t)$ at each time $t$, equation (1.35) will be:

$$d^2(\mathbf{c}, \mathbf{e}) = \sum_{t \in \gamma(\mathbf{c},\mathbf{e})} \sum_{j=1}^{M} |\beta_{1,j}(t)|^2 D_{1,1}(t) = \sum_{t \in \gamma(\mathbf{c},\mathbf{e})} \sum_{j=1}^{M} |\beta_{1,j}(t)|^2 |\mathbf{c}_t - \mathbf{e}_t|^2 \tag{1.36}$$

where $\gamma(\mathbf{c}, \mathbf{e})$ represents the set of time instances where $|\mathbf{c}_t - \mathbf{e}_t| \neq 0$ and $\delta_H$ (called the ST symbol-wise Hamming distance) equals the number of elements on $\gamma(\mathbf{c}, \mathbf{e})$. Substituting the value of $d^2(\mathbf{c}, \mathbf{e})$ from equation (1.36) into inequality (1.21), the

conditional PEP upper bound will be:

$$P\left(\mathbf{c}\rightarrow\mathbf{e}|\alpha_{i,j}\left(t\right),i,j,t\right)\leq\frac{1}{2}\exp\left(-\sum_{t\in\gamma(\mathbf{c},\mathbf{e})}\sum_{j=1}^{M}\left|\beta_{1,j}\left(t\right)\right|^{2}\left|\mathbf{c}_{t}-\mathbf{e}_{t}\right|^{2}\frac{E_{s}}{4N_{0}}\right) \quad (1.37)$$

By noting that $D_{1,1}\left(t\right)$ given by (1.34) is the only nonzero eigenvalue, and averaging (1.37) with respect to the Rayleigh distribution of $\left|\beta_{1,j}\left(t\right)\right|$, the unconditional PEP upper bound will be [1]:

$$P\left(\mathbf{c}\rightarrow\mathbf{e}\right)\leq\prod_{t\in\gamma(\mathbf{c},\mathbf{e})}\left(\left|\mathbf{c}_{t}-\mathbf{e}_{t}\right|^{2}\frac{E_{S}}{4N_{0}}\right)^{-M}=\prod_{t\in\gamma(\mathbf{c},\mathbf{e})}\left|\mathbf{c}_{t}-\mathbf{e}_{t}\right|^{-2M}\left(\frac{E_{S}}{4N_{0}}\right)^{-\delta_{H}M} \quad (1.38)$$

From this inequality, a diversity of $\delta_H M$ is achieved.

As in quasi-static fading channels, inequality (1.38) is valid for small values of $\delta_H M$ [3]. For large values of $\delta_H M$, and Rayleigh fading channels, inequality (1.13) will be [3]:

$$\begin{aligned}P\left(\mathbf{c}\rightarrow\mathbf{e}\right) \quad\leq\quad & \frac{1}{2}\exp\left(\frac{ME_{s}}{4N_{0}}\left(\frac{E_{s}\sum_{t\in\gamma(\mathbf{c},\mathbf{e})}\left|\mathbf{c}_{t}-\mathbf{e}_{t}\right|^{4}}{8N_{0}}-\sum_{t\in\gamma(\mathbf{c},\mathbf{e})}\left|\mathbf{c}_{t}-\mathbf{e}_{t}\right|^{2}\right)\right)\cdot\\ & Q\left(\frac{\sqrt{M}\left(\sum_{t\in\gamma(\mathbf{c},\mathbf{e})}\left|\mathbf{c}_{t}-\mathbf{e}_{t}\right|^{4}-\frac{E_{S}}{4N_{0}}\sum_{t\in\gamma(\mathbf{c},\mathbf{e})}\left|\mathbf{c}_{t}-\mathbf{e}_{t}\right|^{2}\right)}{\frac{E_{S}}{4N_{0}}\sqrt{\sum_{t\in\gamma(\mathbf{c},\mathbf{e})}\left|\mathbf{c}_{t}-\mathbf{e}_{t}\right|^{4}}}\right)\end{aligned} \quad (1.39)$$

Using inequality (1.15), the PEP upper bound in (1.39) can be approximated by [3]:

$$P\left(\mathbf{c}\rightarrow\mathbf{e}\right)\leq\exp\left(-\frac{ME_{s}}{4N_{0}}\sum_{t\in\gamma(\mathbf{c},\mathbf{e})}\left|\mathbf{c}_{t}-\mathbf{e}_{t}\right|^{2}\right) \quad (1.40)$$

The design criteria of space-time code in rapid Rayleigh fading channels are also divided into two parts. For small values of $\delta_H M$, the error performance is upper bounded by (1.38). In this case the error probability is dominated by the minimum ST symbol-wise Hamming distance and the product distance $d_p^2$ defined as:

$$d_p^2 = \sum_{t \in \gamma(\mathbf{c},\mathbf{e})} |\mathbf{c}_t - \mathbf{e}_t|^2 \tag{1.41}$$

The design criteria for small values of $\delta_H M$ were derived in [1].

**Design Criteria Set III [1]**

- *The Distance Criterion*: Maximize the minimum ST symbol-wise Hamming distance between all distinct codeword pairs.
- *The Product Criterion*: Maximize the product distance $d_p^2$ corresponding to the path with minimum $\delta_H$.

From the distance criterion, to achieve the most diversity advantage in a rapid fading environment, the ST symbol-wise Hamming distance $\delta_H$ between any codeword pair $\mathbf{c}$ and $\mathbf{e}$ must be maximized. Since the product distance is a measure of coding advantage [1], the minimum product distance must be maximized between all codeword pairs so that the coding advantage is maximized.

For large value of $\delta_H M$, the PEP is upper bounded by (1.40). For practical

systems, which operate at high SNR such that:

$$\frac{E_S}{4N_0} \geq \frac{\sum_{t\in\gamma(\mathbf{c},\mathbf{e})} |\mathbf{c}_t - \mathbf{e}_t|^2}{\sum_{t\in\gamma(\mathbf{c},\mathbf{e})} |\mathbf{c}_t - \mathbf{e}_t|^4} \tag{1.42}$$

the design criteria were derived in [3].

**Design Criteria Set IV [3]**

- Maximize the minimum ST symbol-wise Hamming distance between all distinct codeword pairs such that $\delta_H M \geq 4$.
- Maximize the minimum Euclidean distance between all distinct codeword pairs.

It is interesting to notice that design criteria set IV is similar to design criteria set II. This indicates that for large number of independent sub-channels, the channel model achieves the AWGN channel. Thus the design criterion used for AWGN channels (maximization of Euclidean distance) is valid here.

The design criteria for other wireless channels are also derived in [1] (such as correlated quasi-static flat Rayleigh fading channel, and Rican channels).

**Some QPSK ST Codes**

The derived design criteria were used to design ST trellis codes for transmission of 2 b/s/Hz and 3 b/s/Hz over quasi-static fading channels using two transmit antennas with 4-PSK and 8-PSK constellations respectively. Figure 1.2(a) shows the QPSK

signal constellation, and Figure 1.2(b), (e), and (h) show the trellis diagram of the 4-, 8-, and 16-state QPSK ST trellis codes designed in [1] respectively. These codes are used as a reference codes since they are the first proposed ones. Three more QPSK 4-, 8-, and 16-state ST codes design in [4] are shown in Figure 1.2(c), (f), and (i) respectively, where these codes are claimed to be optimum (having optimum coding gain) in quasi-static fading channels. The QPSK 4-, 8-, and 16-state ST codes designed in [5] are also shown in Figure 1.2(d), (g), and (j) respectively, where these codes are considered to be from the best codes found in the literature for rapid fading channels, Performance of the 4-, 8-, and 16-state codes from [1] are shown in Figure 1.3 in quasi-static fading channel and in Figure 1.7 in rapid fading channel. From both figures, the 16-state code outperform the 4- and 8-state codes. The QPSK 4-, 8-, and 16-state ST codes from Figure 1.2 are simulated using a computer program in quasi-static and rapid fading channel models for one and two receive antennas where the simulation results are given in Figure 1.4 to Figure 1.10.

## 1.4 Literature Survey

The design criteria in [1] were set to design ST trellis codes with two transmit antennas to achieve maximum diversity advantage. These design criteria were derived from matrices of codeword pairs. In [6], binary design rules of ST codes were found for any number of transmit antennas, any number of states, but only for BPSK and QPSK signal constellations. These rules uniquely define the ST

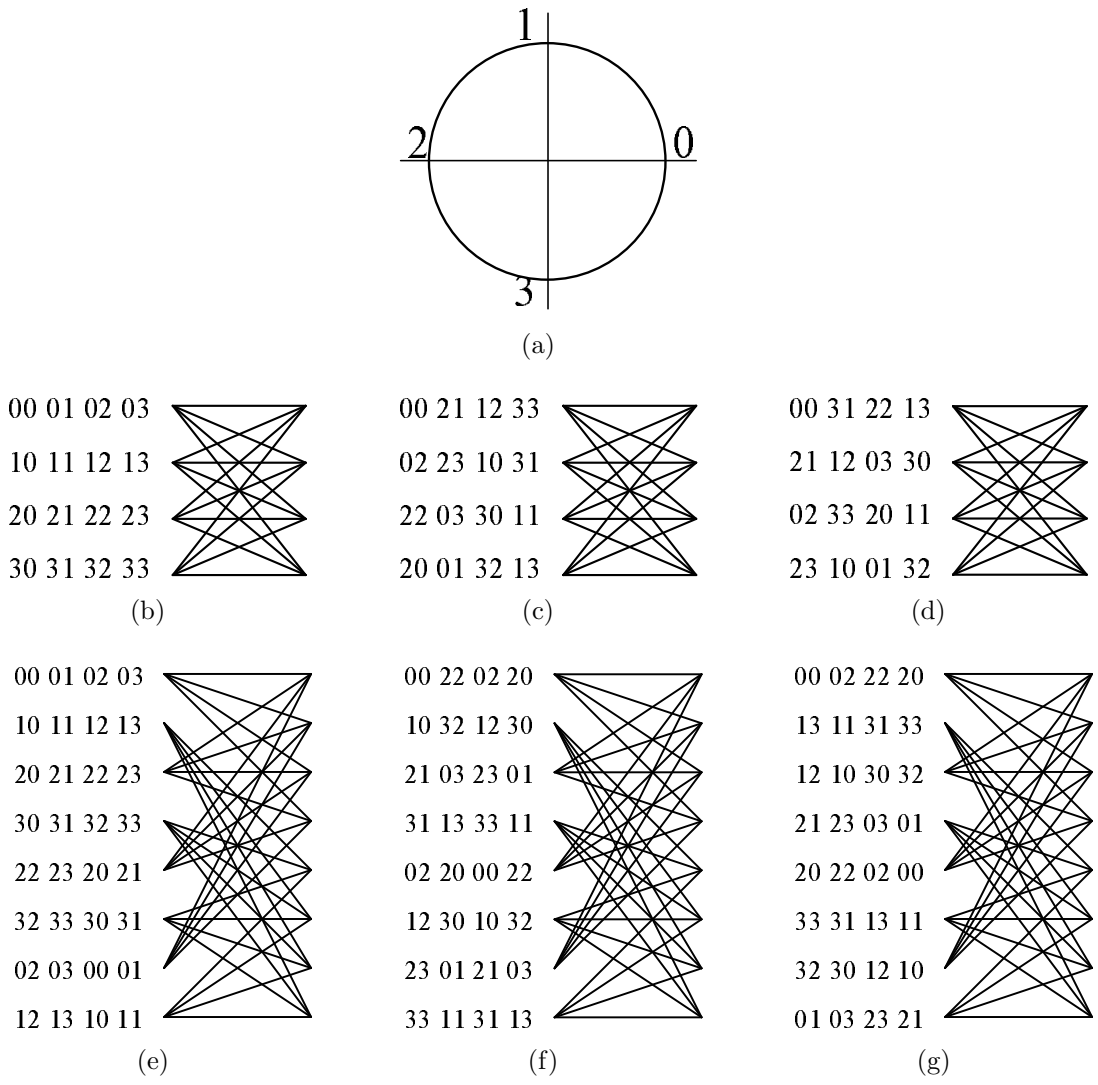


Figure 1.2: (a) QPSK signal constellation (b) 4-state ST code [1] (c) 4-state ST code [4] (d) 4-state ST code [5] (e) 8-state ST code [1] (f) 8-state ST code [4] (g) 8-state ST code [5]

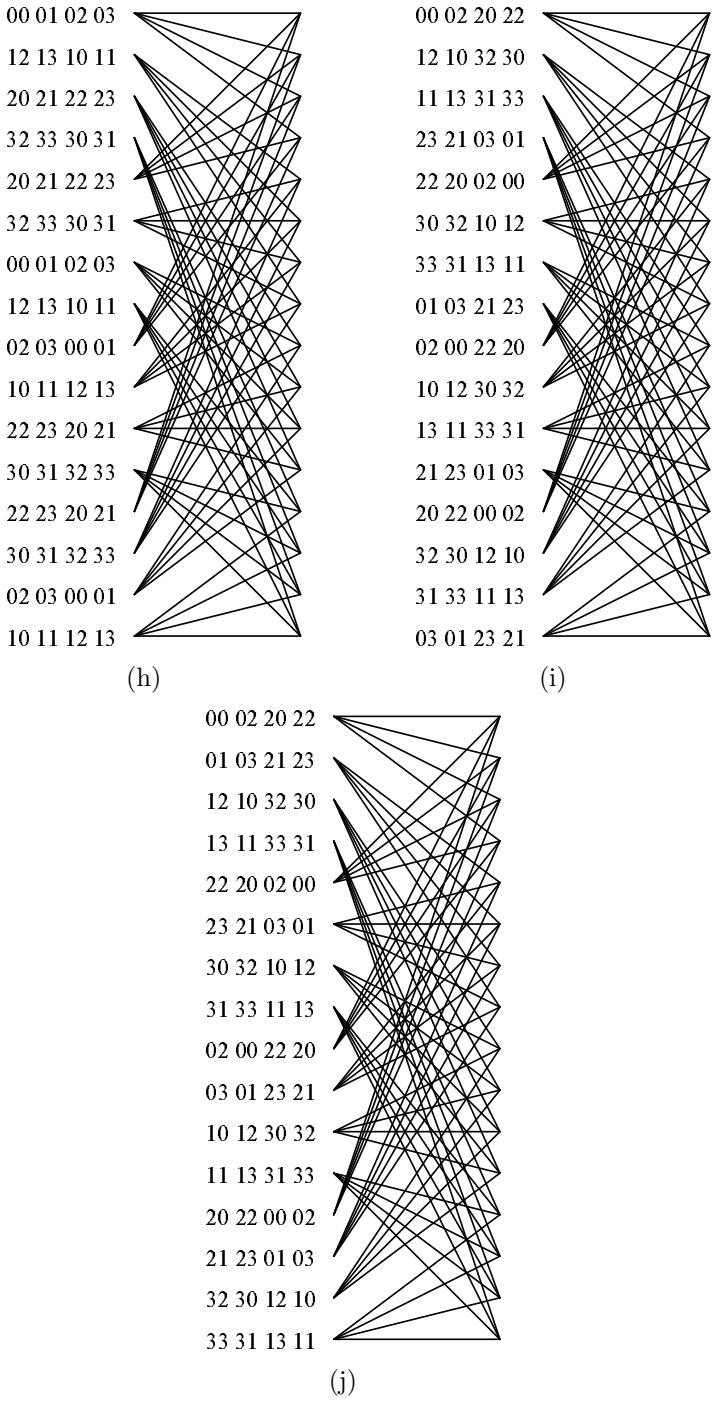


Figure 1.2: (continued) (h) 16-state ST code [1] (i) 16-state ST code [4] (j) 16-state ST code [5]

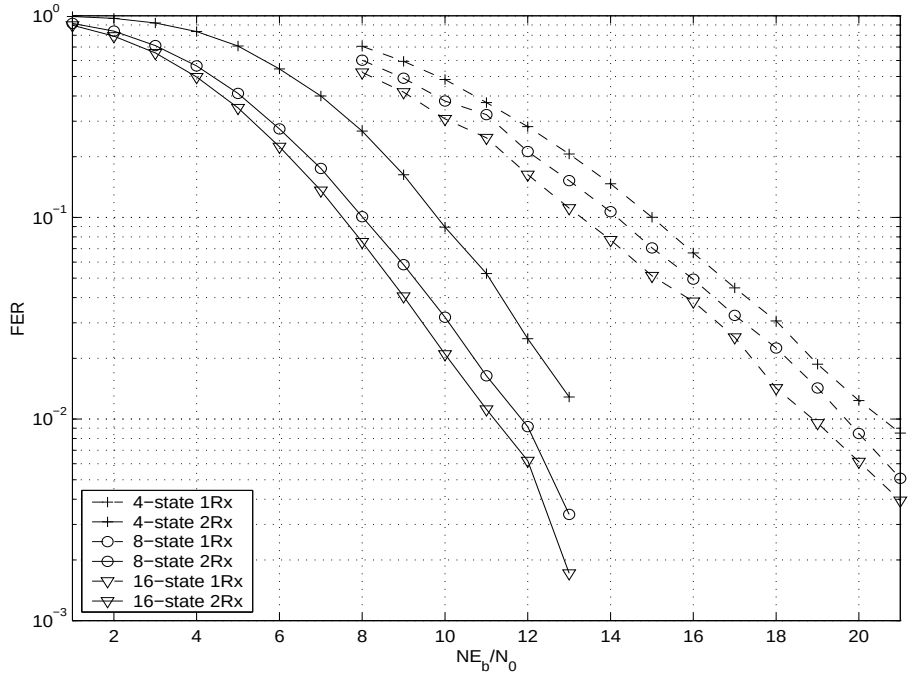


Figure 1.3: Performance of 4-, 8-, and 16-state codes from [1] in quasi-static fading channel

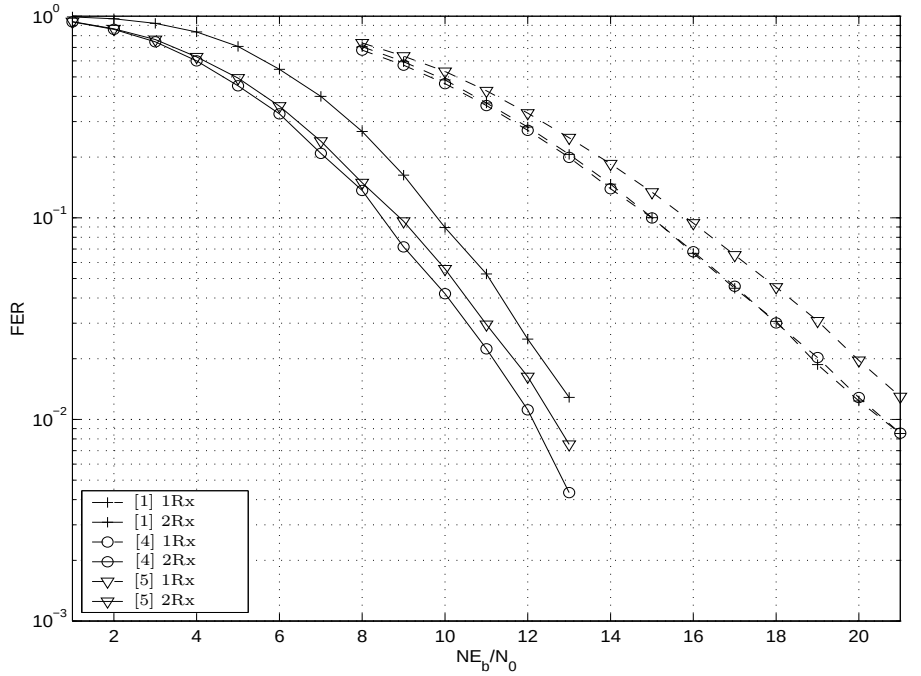


Figure 1.4: Performance of 4-state codes from Figure 1.2 in quasi-static fading channel

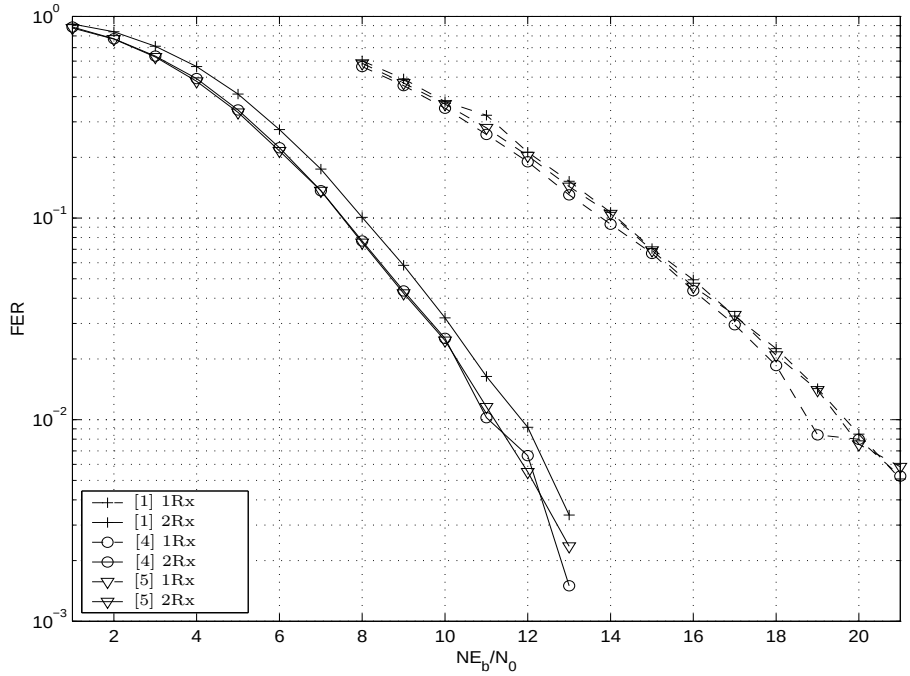


Figure 1.5: Performance of 8-state codes from Figure 1.2 in quasi-static fading channel

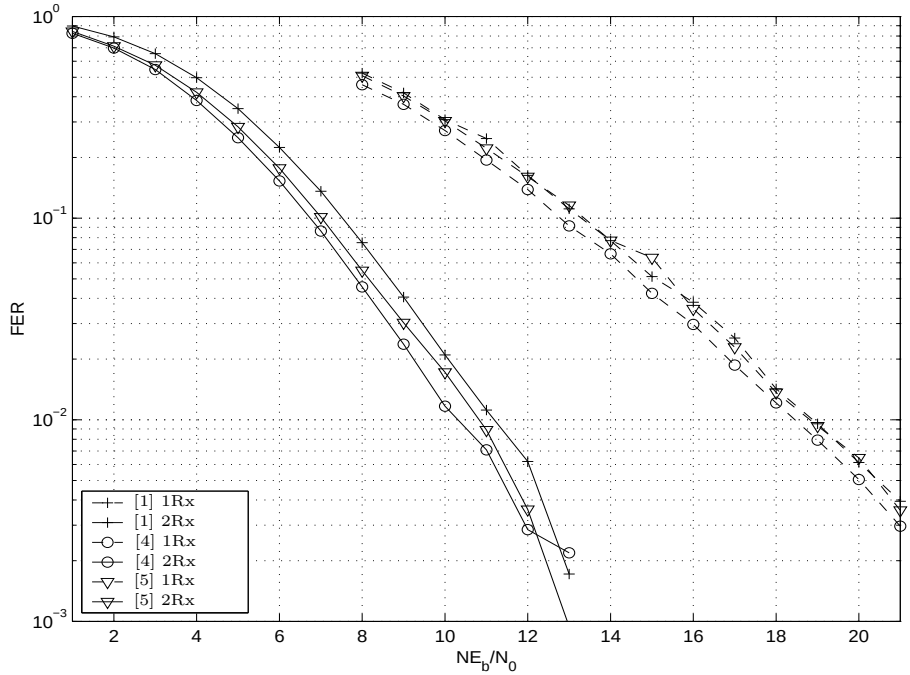


Figure 1.6: Performance of 16-state codes from Figure 1.2 in quasi-static fading channel

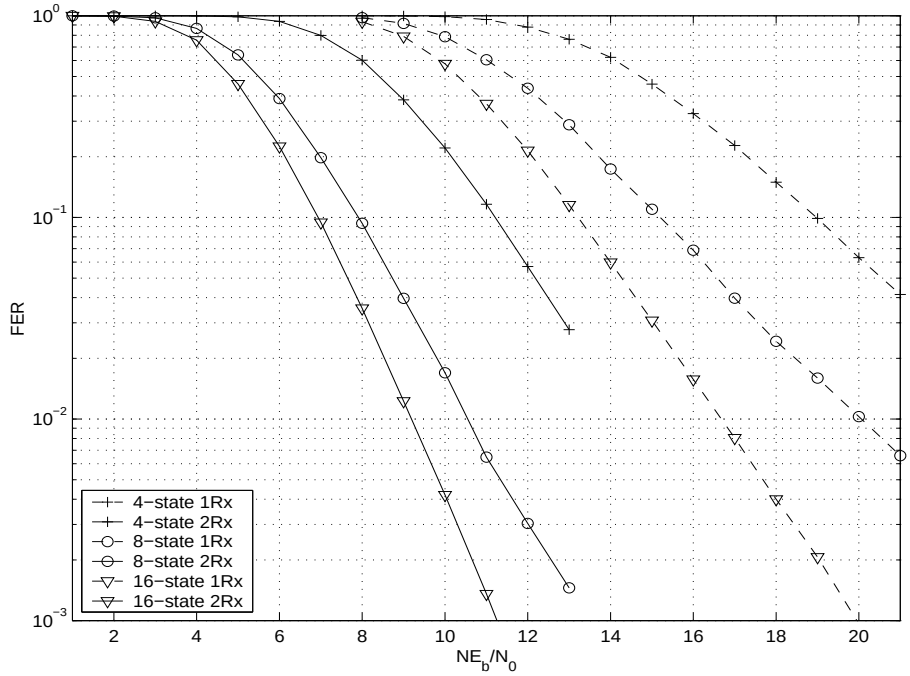


Figure 1.7: Performance of 4-, 8-, and 16-state codes from [1] in rapid fading channel

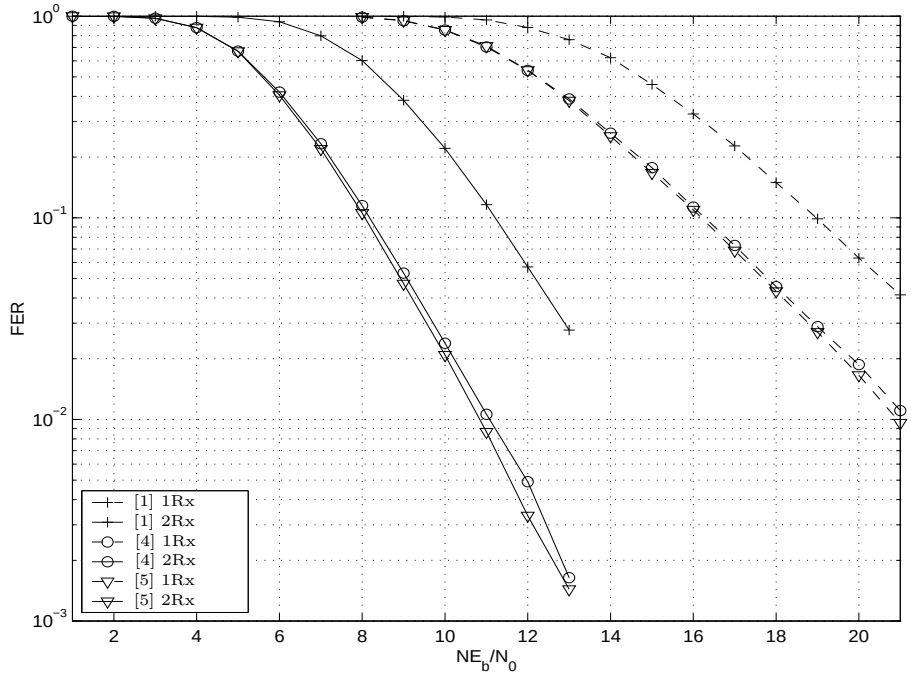


Figure 1.8: Performance of 4-state codes from Figure 1.2 in rapid fading channel

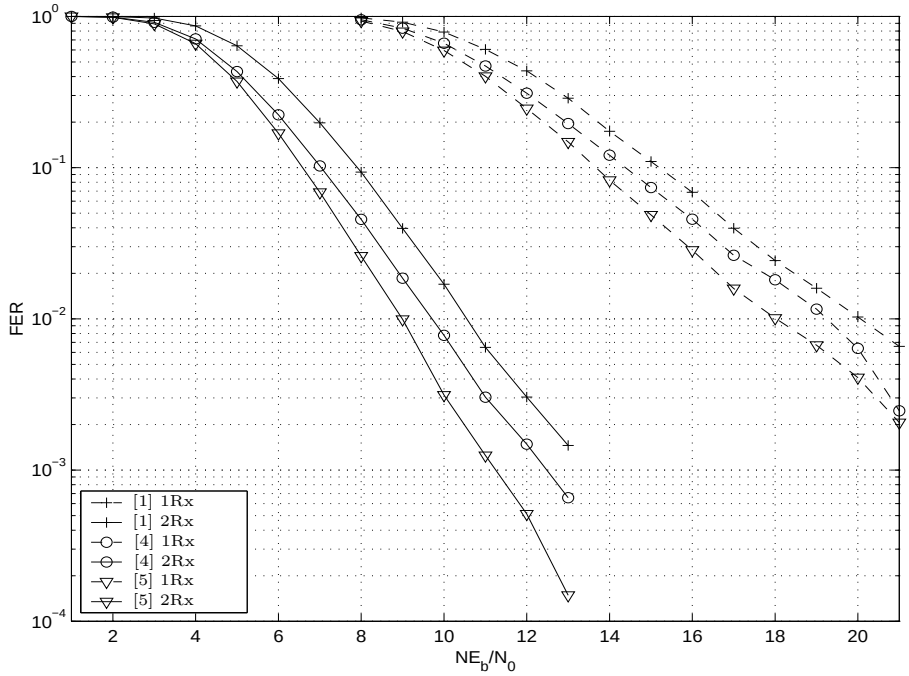


Figure 1.9: Performance of 8-state codes from Figure 1.2 in rapid fading channel

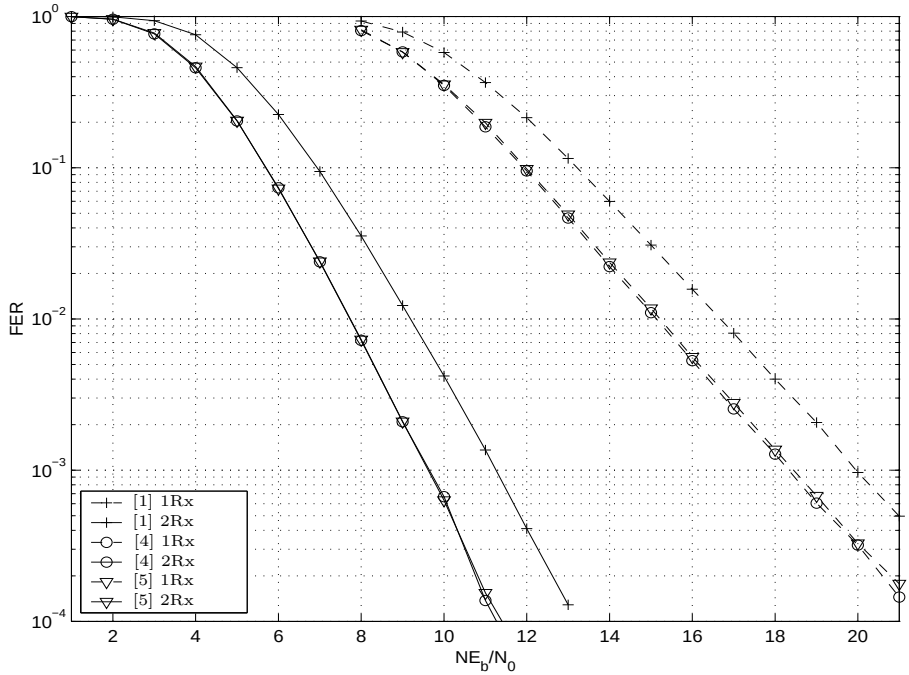


Figure 1.10: Performance of 16-state codes from Figure 1.2 in rapid fading channel

code without leaving space for the improvement of coding advantage. The design rules proposed in [6] have been reformulated and simplified in [7]. In [8], design criteria for full spacial diversity for QAM ST codes are proposed. The full spacial diversity is ensured by sufficient conditions on the codewords or generator matrices instead of on every codeword pair.

An alternative systematic method of designing ST trellis codes for full spatial diversity and any number of transmit antennas, any number of state and arbitrary signal constellations, is proposed in [9]. This method was developed from observing the group/subgroup of the state transitions on the code trellis and it leaves a space for optimization of coding advantage. Optimum space-time convolutional codes that provide maximum diversity and coding gains are presented in [4].

In [3], design criteria of ST codes have been proposed for high and low diversity orders in both quasi-static and rapid fading channels. The design criteria found in [3] for low diversity orders are the same design criteria found earlier in [1].

Tighter design criteria of ST codes ware derived in [10] for low and moderate signal to noise ratio (SNR) ranges. They used these criteria, throw computer search, to get new improved codes at low SNR ranges with two transmit antennas, and even these codes outperform some of the existing codes at their designed SNR ranges. The worst-case pairwise codeword error probability analysis under arbitrary quasi-static fading is presented in [11]. In [12], the code design criteria were optimized for coding gain. Space-time code design for single carrier transmission

over frequency selective fading channels has been studied in [13] and design criteria for this wireless communication channel model have been derived.

In [14], orthogonal designs of space-time block codes has been proposed. Orthogonally constructed space-time codes have been proposed by many researchers where in one of them [15] the proposed method simplifies the design of ST codes for more than two transmit antennas and the symmetry found on the constructed codes trellises simplifies the decoding. In [16], the use of multidimensional codes is proposed for ST codes instead of TCM codes, namely spherical codes. This technique had been tested on orthogonal frequency division multiplexing (OFDM) and showed superior performance over the current IEEE 802.11a specifications for 24-Mbits/s data rate over slow fading and AWGN channels. In [17], unitary ST modulation for multiple-antenna communications has been proposed and in [18] differential ST modulation is proposed where both modulations use a set of unitary code matrices.

In [19] and [20], turbo ST coded-modulation and recursive ST trellis codes for turbo modulation were proposed respectively with design analysis, codes performance and a designed example codes, while in [21], the performance of parallel concatenated ST codes was studied.

In addition to the performance analysis of ST codes, error performance in the mean of pairwise error probability (PEP), bit error rate (BER), and Frame Error Rate (FER) are investigated in [22][3][23][24][25][26][27]. Some of these propose

upper bounds on error rates such as [22] and [27], while others propose exact forms for PEP and use these expressions to compute bit and/or frame error rates [24][25][26][23]. Since computation of exact PEP expressions involve the calculation of the transfer function, the state reduction techniques of the error state diagram could be utilized to simplify the calculations of the transfer function. The error state diagram has $2^{2v}$ states which makes the computation difficult and time consuming as the number of states increases. The reduced state diagram has the same number of states as the code trellis. To use the reduction techniques, the code must have some uniformity properties. In [25] it is stated that ST codes in general are not geometrically uniform [28] as claimed in [1]. However, ST codes satisfy encoder linearity and other conditions are proved to be quasi-regular codes in [29]. This allows the use of the reduction techniques of the error diagram. Quasi-regularity property allows the assumption that the transmitted codeword is the all zero codeword and the other codewords are error events. The transfer function is calculated by making the zero state as the input and the output of system.

The Chernoff bound was used for the calculation of the upper bound on PEP in rapid fading environment in [1]. The same Chernoff bound approach with the transfer function derived from the code error diagram was used in calculating the upper bound on PEP in [27]. A tighter bound on the PEP and BER was presented in [30]. However, these three bounds, including the tighter one [30], are still upper bounds and not the exact expressions. The exact PEP proposed in [26]

was derived using residues, while in [24] a numerical technique with any degree of accuracy for the derivation of the exact PEP was proposed. The proposed method uses the Gauss-Chebyshev quadrature and the moment generating function (MGF) approach. Both of these methods are not in a product form, so that they can not utilize the transfer function bounding techniques. A simpler exact PEP expression is presented in [23] using Craig's formula for the Gaussian Q-function. The PEP is expressed in the form of a single finite-range integral where the integrand involves the MGF of a nonnegative random variable.

Many performance improved ST codes designed for different environments are proposed in [30],[31],[32],[5], [33], [34], [3], and others.

Joachim Hagenauer [2] proposed the concept of using punctured convolutional codes to generate a family of rate compatible punctured convolutional (RCPC) codes. A low rate $1/N$ convolutional code is punctured periodically with period $P$ to obtain a family of codes with rate $P/(P+L)$ where $L$ can vary from 1 to $(N-1)P$. The code rate could be changed depending on the channel state. These codes generated from the same mother code use a trellis similar to that of the low rate mother code, which reduces the decoding complexity of the obtained high-rate codes with a comparable performance.

The concept of puncturing techniques was applied to trellis-coded modulation (TCM) codes and analyzed in [35] and [36]. In both convolutional codes and TCM codes, bits are punctured then the transmitted symbols are generated. In [37]

puncturing was performed to bits and symbols for convolutional codes. A punctured convolutional code was used with ST block codes to achieve higher data rates [38]. Puncturing the convolutional code as an outer code and then applying space-time block coded modulation for two transmit antennas could increase the data rate by 50 or 100 percent, without increasing the transmitted power, depending on the number of receive antennas used.

In [39] and [40] a special puncturing method is proposed for BPSK space-time trellis codes with small frame length. A rate one ST code with constraint length five and frame size 16 is punctured to achieve two diversity order with rates 4/3 and 8/7. The cost of rate improvement is performance degradation.

In [41], an MTCM hybrid automatic repeat request scheme employing symbol puncturing was proposed. This scheme can adapt itself depending on the channel state by a direct feedback from the receiver. A punctured multiplicity 2 MTCM code was generated from a mother MTCM code with multiplicity 3. The code rate varies between 1.67 of the mother code and 2.5 of the punctured code depending on the redundancy needed by the receiver. In [42], performance of ST codes in pure ARQ (ST-ARQ) protocol was studied and two ST hybrid ARQ protocols were proposed. The first one is a ST hybrid ARQ (ST-HARQ) protocol and the other is turbo ST hybrid ARQ (TST-HARQ) protocol. Another space-time hybrid ARQ scheme has been proposed in [43] where different ST trellis codes are employed for retransmissions. In [44], Maximum Likelihood (ML) detection and decoding of ST

codes were analyzed and studied.

## 1.5 Thesis Contribution and Organization

### 1.5.1 Thesis Contributions

The main objective of this research is to improve the space-time coding systems throughput and reliability. There are two methods presented in this work to improve the system throughput. The first one is using higher rate channel encoder, which has a rate grater than 1/2. Using the same signal constellation, more information bits are accepted by the encoder each time slot, which increases the number of branches diverging from each trellis state. Consequently, the minimum inter-branch Euclidean distance will decrease that in general results in a degradation in the communication system performance. However, applying design criteria proposed in [1] and [3] in an exclusive search program implemented in C Language, good performing high-rate ST code that satisfies both criteria is found. Simulation results show that the designed code outperforms some of the existing normal rate ST codes. Searching the literature, the use of such high-rate codes in a two transmit antennas system is not pointed out.

The second method is based on puncturing, where a symbol puncturing technique is proposed for space-time codes. A lower transmitted power per source bit and an increase in the system throughput is encountered but with a small degra-

dation on the frame error rate performance. No general bit or symbol puncturing technique for space-time trellis codes is found in the literature except the recently proposed special method for BPSK ST codes with small frame size in [39] and [40]. The proposed technique in this research is a general one with normal frame size and it can be applied to ST codes with any number of trellis states. On the new technique, puncturing is performed to the space-time encoder output symbols before modulation and transmission. Design criteria to get good performing QSK ST codes without and with symbol puncturing are derived for quasi-static and rapid fading channels. The derived design criteria are implemented in an exhaustive search C language program. Simulation results without puncturing show that the new codes have comparable performance to the best codes in the literature. The designed codes outperform the best known ST codes under symbol puncturing. Since symbol puncturing on space-time trellis codes is not like symbol puncturing on single antenna trellis codes, the transmitted ST symbols generally are different from the encoder output ST symbols because of the symbol shifting at the puncturing circuit. A decoding technique using maximum likelihood decoder with modified puncturing patterns is presented for the decoder of punctured space-time codes where it can also be used with the un-punctured space-time codes.

Punctured space-time codes can not be presented using normal trellis diagrams since normal trellis diagrams describe only one transition at a time while puncturing is performed on $P$ successive transitions. A $P$-transition trellis diagram

representation of punctured space-time codes is presented. This representation is also valid for un-punctured space-time codes.

System reliability is improved by using hybrid forward error correction and automatic repeat request schemes. Three type-I and three type-II HAQR protocols that use normal rate, high-rate and punctured space-time codes are proposed. Both type-I and type-II HARQ schemes have the same reliability, however the type-II HARQ protocols have better throughput performance than the corresponding type-I HARQ. The presented protocols show good performance via simulation.

### 1.5.2 Thesis Organization

This thesis is organized as follows. This Chapter is started with a general overview, followed by description of the wireless communication channel models used in this research. A detail review of ST coding systems performance and design criteria is given and simulation of some of the existing codes are reproduced. This Chapter is concluded with literature survey and thesis contributions.

In the next Chapter, the design criteria studied in detail in this Chapter are used in exhaustive search approach to find high-rate space-time code. The designed code is simulated and compared to some of the existing normal rate space-time codes. In the same Chapter, the idea of symbol puncturing on space-time codes is introduced. The symbol puncturing and the extraction of the modified puncturing patterns from the original puncturing patterns are illustrated with some examples.

The Chapter is concluded with the alternative representation of punctured space-time codes. Performance analysis of symbol punctured space-time codes and the design criteria are given in Chapter three. The derived design criteria are used to design ST codes that have a good performance with and without puncturing. The designed codes are tested via simulation and compared to some of the existing codes.

Chapter four begins with an introduction followed by a review of pure and hybrid automatic repeat request schemes. The type-I and type-II HARQ protocols used in this work are presented. The presented protocols are simulated and compared to each other. A summary of main conclusions and extension of this work is given in Chapter five.

# CHAPTER 2

# HIGH-RATE AND SYMBOL PUNCTURED ST CODES

## 2.1 INTRODUCTION

As mentioned in Chapter one, there are two ways to improve the spectral efficiency of ST codes; the first way is by using a high-rate channel encoder and the second one is by puncturing. Each of these ways has its advantages and disadvantages. These ways are studied in detail with some examples in this Chapter.

This Chapter is organized as follows. In the first section, the use of high-rate encoder in ST coding systems is illustrated with a designed high-rate QPSK ST code. The designed code is simulated and compared to the 4- and 8-state QPSK ST codes from [1] in both quasi-static and rapid fading environments. In

the second section and its subsections, encoder and decoder systems of the symbol PST coding system are demonstrated. Then, effects of Puncturing Patterns (PP's) length (puncturing period) and structure on the coding system rate, frame length, and decoding complexity are studied. The Chapter is concluded with an alternative ST trellis cods representation that can be used to represent PST trellis codes.

## 2.2 High Rate Space-Time Codes

Since they first introduced by Trarokh [1] in 1998, space-time trellis codes normally employ a rate 1/2 (2/4 and 3/6 with maximum spectral efficiency 2 b/s/Hz and 3 b/s/Hz for QPSK and 8PSK ST codes respectively) channel codes. No attempt to use a higher rate channel codes, because it has been stated in [1] that it is not possible to have a code that achieves full spacial diversity (full rank) and at the same time has a higher spectral efficiency than 2 b/s/Hz (3 b/s/Hz) for QPSK (8PSK) ST codes. That implies a traditional trade-off between diversity and rate. So the most important question to answer is which is more significant on the system performance a higher rate with lower diversity order or a lower rate with higher diversity order? This question is mainly dependent on the application and the operational SNR's.

However, it had been shown in [45] that codes with higher rates and lower diversity orders (at least 4) outperform codes with lower rates and higher diversity orders at high SNR ranges. Similar results were found in [3] for high product (more

than or equals to 4) of the minimum rank by the number of receive antennas ($r \cdot M$) and ST symbol-wise Hamming distance by the number of receive antennas ($\delta_H \cdot M$) for quasi-static and rapid fading channels respectively. Since for high products, the number of independent sub channels is high so the channel converges to Gaussian channel and thus the system performance is dominated by the minimum Euclidean distance. It is observed in [3] that ST codes with lower rank (one) and higher trace (ten) outperform codes with full rank (two) and lower trace (four) at reasonable diversity advantages. This observation suggests the use of higher rate channel encoders to improve the spectral efficiency of ST coding systems.

### 2.2.1 Search Criteria

Fortunately, the analysis in Chapter one for normal rate ST codes is valid for high-rate ST codes. Thus the same design criteria are used to design a high-rate QPSK 8-state ST code.

The design criteria sets I-IV in Chapter one were implemented using a C program. In addition to the design criteria sets, the search program excludes codes that do not satisfy the following conditions.

- The code must span all possible ST symbols for $N$ transmit antennas, which means it should contain all possible $N$ QPSK symbols concatenations. Since in this analysis there are two transmit antennas, the number of possible two QPSK symbols concatenations (QPSK symbol pairs) equals $4^2 = 16$. Codes

does not satisfy this condition does not have full rank and maximum $\delta_H$ [1]. In addition, they have a lower distance between codewords which increase probability of errors.

- No QPSK pair (ST symbol) appears more than once in the branches diverging from or merging into the same state. Codes does not satisfy this conditions does not have maximum $\delta_H$.

- The encoder of the code must be linear, thus the encoder diagram contains only memory elements and exclusive ors (modulo-2 adders). This research is restricted to linear encoders only.

The search program procedure is:

- Code generation: ST codes are generated using generating matrix.

- Testing conditions: the above conditions are tested.

- Metric computations: the new code metrics such as rank, determinant and product distance are calculated.

- Comparing and selecting: the generated code metrics are compared and the code with best metric depending on the implemented design criterion is selected.

These conditions are included in the search program to minimize the searching time because condition testing does not take long time while metric computations

take most of the searching time.

Fortunately, the search results for the 8-state high-rate ST code show that it is possible to have 8-state high-rate ST codes that satisfy the four design criteria sets and the above conditions. One of these codes is shown in Figure 2.1.

### 2.2.2 Numerical Results

New high-rate 8-state QPSK code metrics are given in Table 2.1. For the sake of comparison, the metrics of the 4- and 8-state QPSK ST codes from [1] are also given in the table. The new code does not have a full rank (two) as expected. However, it has the same trace, $\delta_H$, and minimum product distance as the 8-state code from [1] and even better minimum Euclidean distance.

The performance of the obtained 8-state code from the search criteria is simulated in quasi-static and rapid fading environments. The new code is compared with the QPSK 4- and 8-state ST codes designed in [1] in the mean of FER (frame error rate) vs. transmitted power per information bit $NE_b/N_0$. Because of rate difference and for fair comparison between the codes, the computer simulations were not performed in the mean of FER vs. SNR $NE_S/N_0$. For existing QPSK ST trellis codes, the SNR equals the transmitted power per information bit. Where as for the designed high-rate QPSK ST trellis code the transmitted power per information bit equals the SNR plus 1.7609 dB, since $E_b = 2E_s/3$.

The simulation results are given in Figure 2.2 and 2.3 for quasi-static and rapid

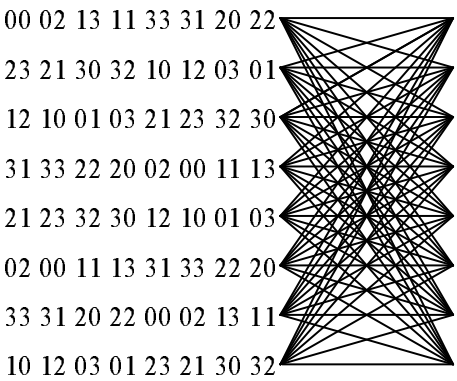


Figure 2.1: Search result for 8-state high-rate QPSK ST code

TABLE 2.1: New high-rate ST code metrics

| Number of states | Source | Rank | Determinant | Trace | $\delta_H$ | Minimum product distance | Minimum Euclidean distance |
|---|---|---|---|---|---|---|---|
| 4 | [1] | 2 | 4 | 4 | 2 | 4 | 2.828427 |
| 8 | [1] | 2 | 12 | 8 | 2 | 16 | 4.000000 |
| | high-rate | 1 | 4 | 8 | 2 | 16 | 4.828427 |

fading channels respectively. From Figure 2.2, it is clearly seen that the 4-state code from [1] outperforms the 8-state high-rate code in quasi-static environment for one receive antenna. Where as for two receive antennas, the new code outperforms the code from [1] for low and moderate $NE_b/N_0$ ranges while for high $NE_b/N_0$ the code from [1] has a better performance. It is expected that the new high-rate code will not have good performance in quasi-static fading channel since the code matrix does not have a full rank and there are few diversity antennas ($r \times M < 4$). However, the new 8-state high-rate code outperforms the 4-state code from [1] by about one dB for one receive antenna and two dB's for two receive antennas in rapid fading environment, which is also expected since the new code has better minimum product distance than the 4-state code from [1] and also for the new code $\delta_H \times M \geq 4$ for two receive antennas. The 8-state code from [1] outperforms the new high-rate code for both environments and receive antenna cases.

## 2.3 Symbol Punctured ST Codes

Puncturing generally means deleting one or more bits (systematic or parity) before transmission. It is usually used to increase the spectral efficiency of communication systems and reduce the high-rate codes decoding complexity. Puncturing is performed periodically on the output bits of the encoder. The puncturing pattern is represented by a $N$-row and $P$-column matrix with ones where no bits (symbols) are punctured and zeros otherwise, where $P$ is the puncturing period and $N$ is the

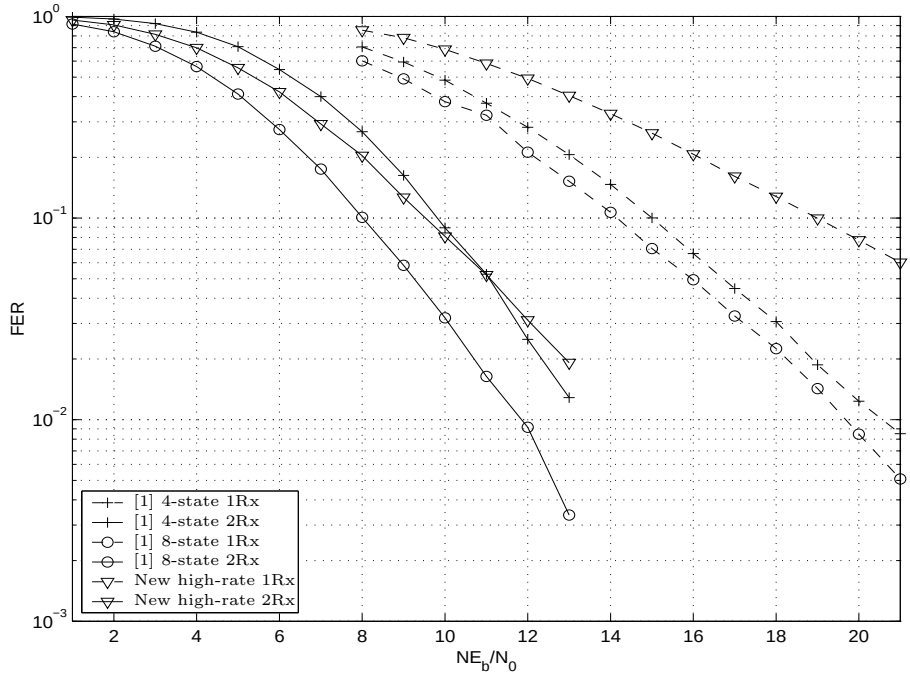


Figure 2.2: Performance of 8-state high-rate code in quasi-static fading channel

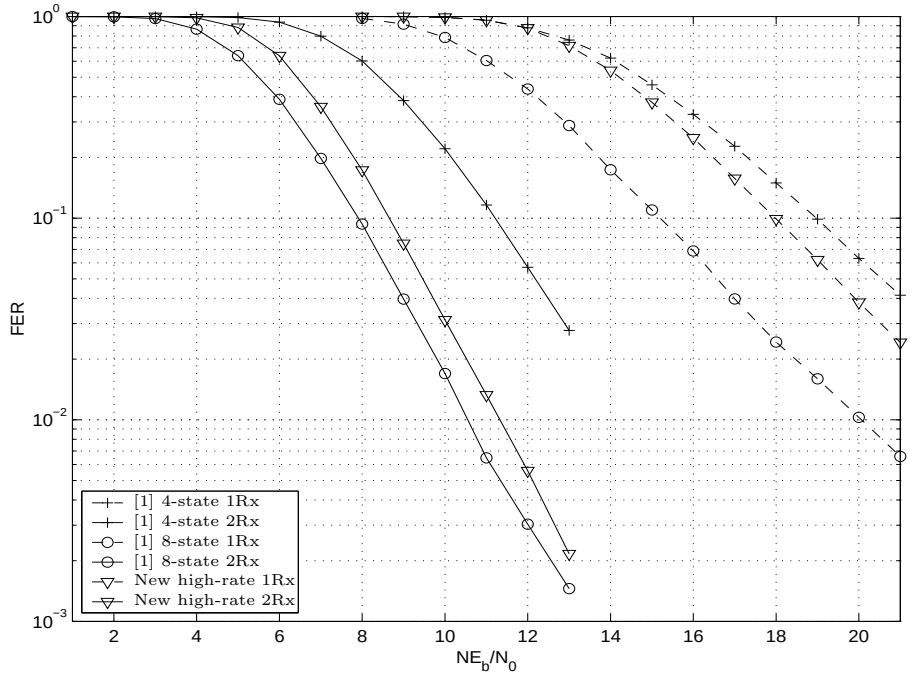


Figure 2.3: Performance of 8-state high-rate code in rapid fading channel

number of encoder output bits (symbols) at each time slot.

General symbol puncturing technique has not yet been used with ST trellis codes (except the recently presented special puncturing method for BPSK ST codes with small frame size [39][40]). Moreover, no puncturing technique has been proposed for application on ST trellis codes in the literature. In this section the idea of applying periodic symbol puncturing on QPSK ST trellis coded modulation is introduced and studied.

### 2.3.1 ENCODER/DECODER

The encoder and decoder of the symbol PST coding system shown in Figure 2.4 are generally similar to the encoder and decoder of the un-punctured ST coding system. In fact, the encoder and decoder of the symbol PST coding system essentially can be used with the un-punctured ST coding system. The differences between the two systems are illustrated in the following subsections.

#### Encoder

The new symbol PST system encoder is shown in Figure 2.4(a). For QPSK signaling, two ($k = 2$) input bits ($y_t^1$ and $y_t^2$) are passed to a channel encoder with rate $2/4$ to generate four output bits $n = 4$, two groups $N = 2$ where each group contains two encoder output bits $m = 2$. These four output bits are passed to a QPSK signal constellation mapper (size $2^m$) to produce two QPSK symbols ($x_t^1$ and $x_t^2$).

The main difference between the new ST encoder and the original (un-punctured) one is the puncturing block, which consists of a puncturing pattern circuit and a buffer. The output symbols of the puncturing block ($c_t^1$ and $c_t^2$) are modulated and transmitted each via a transmit antenna simultaneously at the same transmission time and frequency.

In the puncturing pattern circuit, the symbols that have to be punctured are removed, while the remaining symbols are rearranged and then buffered for transmission. In the buffer, the symbols, which had to be transmitted using the same transmit antenna, following a punctured symbol are shifted up to fill the empty position of the punctured symbol. Thus each of the $N$ transmit antennas has a symbol to transmit at all transmission time instances. If the puncturing pattern circuit has no zeros, then this encoder operates exactly like the original ST encoder system.

**Decoder**

The receivers of both the un-punctured and the punctured systems employ the Viterbi soft decoding algorithm with maximal-ration combining method. The main difference between the two receiver systems is that in the un-punctured receiver systems, branch metrics are calculated and survivor paths are selected each reception time (each time the receiver receives a transmitted symbol). This metric is

given for one transition by:

$$\sum_{j=1}^{M}\left|r_t^j-\sum_{i=1}^{N}\alpha_{i,j}\left(t\right)c_t^i\right|^2 \tag{2.1}$$

where $r_t^j$ is the received signal at the $j^{th}$ antenna at time $t$. The cumulative path metric equals to:

$$\sum_{t=1}^{l}\sum_{j=1}^{M}\left|r_t^j-\sum_{i=1}^{N}\alpha_{i,j}\left(t\right)c_t^i\right|^2 \tag{2.2}$$

where $l$ is the un-punctured transmitted frame length. However, in the symbol PST receiver systems, branch metrics are calculated and survivor paths are selected periodically each $(P-N_z/2)$ reception times such that a stage ($P$ successive transition on the code trellis) cumulative path metric is:

$$\sum_{t=(m-1)\left(P-\frac{N_z}{2}\right)+1}^{m\left(P-\frac{N_z}{2}\right)}\sum_{j=1}^{M}\left|r_t^j-\sum_{i=1}^{N}\alpha_{i,j}\left(t\right)c_t^i\right|^2 \tag{2.3}$$

where $P$ is the puncturing period, and $N_z$ is the number of zero elements in the PP as will be explained in the following section. The decoder applies the PP on the code trellis and compares the resulting symbols with the received signals each $(P-N_z/2)$ times. The cumulative path metric calculated for each trellis state in the punctured ST decoder is given by:

$$\sum_{m=1}^{k_p}\sum_{t=(m-1)\left(P-\frac{N_z}{2}\right)+1}^{m\left(P-\frac{N_z}{2}\right)}\sum_{j=1}^{M}\left|r_t^j-\sum_{i=1}^{N}\alpha_{i,j}\left(t\right)c_t^i\right|^2=\sum_{t=1}^{l_p}\sum_{j=1}^{M}\left|r_t^j-\sum_{i=1}^{N}\alpha_{i,j}\left(t\right)c_t^i\right|^2 \tag{2.4}$$

where $l_p = k_p\,(P - N_z/2)$ is the transmitted punctured frame length, and $k_p$ is the number of periodic application of the PP on a single frame of encoder output symbols (un-punctured frame) of length $l$. From equations (2.2) and (2.4), it is easily seen that the normal ST decoder makes decision on survivor paths $l$ times while the PST decoder makes decision on survivor paths $K_p$ times. The decoder of the symbol PST coding system is shown in Figure 2.4(b).

### 2.3.2 PUNCTURING PATTERN, CODE RATE AND FRAME LENGTH

In this section the puncturing pattern is defined and the effects of the puncturing period on the symbol PST code rate, transmitted frame length, and decoding complexity are analyzed. PP's of periods two, three four, five and six are studied for illustration throughout this section.

#### Puncturing Pattern

In symbol PST coding system, a puncturing pattern is a $N$ by $P$ matrix (Figure 2.5), where $N$ is the number of transmit antennas and $P$ is the puncturing period. Each row of the puncturing pattern corresponds to a transmit antenna and the columns correspond to time instances. The puncturing pattern is periodically applied to the encoder-mapper output symbols. The PP elements are zeros and ones, where a zero corresponds to a punctured symbol while a one corresponds to a transmitted symbol. For puncturing patters with the same size, there could be

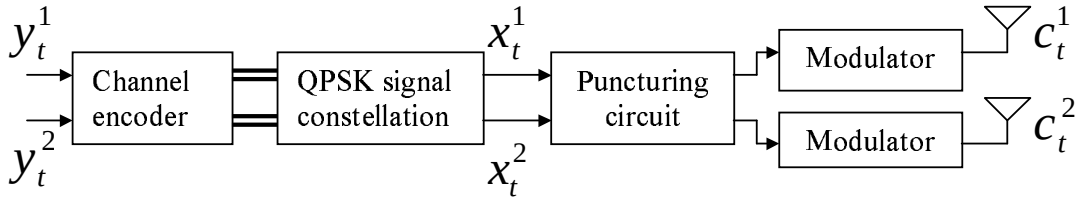


(a)

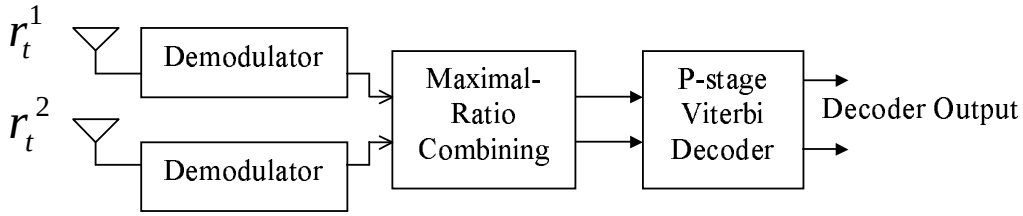


(b)

Figure 2.4: Block diagram of QPSK symbol PST coding system (a) Encoder (b) Decoder

many puncturing rates. These puncturing rates could start with the un-punctured code where all the PP elements are ones (maximum redundancy) and end with a punctured code where half the PP elements are zeros and half of PP elements are ones (zero redundancy).

For puncturing period two, the PP's are of size 2 by 2. In this case there is only one possible puncturing rate in addition to the mother code. All possible PP's of period two are shown in Figure 2.6. In this case, PP-(1) in Figure 2.6(1) is the un-punctured rate with maximum redundancy. PP-(2) and PP-(3) represent the only possible puncturing rate with zero redundancy where two symbols are punctured (one symbol is removed from encoder-mapper output symbols corresponding to each transmit antenna each time the PP is applied) out of four symbols. Therefore for a block of four input bits only two QPSK symbols are transmitted instead of four QPSK symbols on the un-punctured codes. This puncturing rate is similar to the un-coded system with the same diversity order. PP-(4) to PP-(7) are not valid PP's, because in the first two PP's symbols are punctured from both transmit antennas at the same time, which will result in a complete lose of a trellis transition, while in the last two PP's, symbols are punctured only from one of the transmit antennas, which means only one of the transmit antennas has a symbol to transmit while the other transmit antenna has no symbol to transmit. The equation of the transmitted ST symbol in terms of the encoder output symbols is given in Figure 2.7(a), and an example of applying PP-(2) to the encoder output symbols

is shown in Figure 2.7(b). As can be seen from Figure 2.7 $c_1^1$ is either $x_1^1$ or $x_2^1$, and $c_1^2$ is either $x_1^2$ or $x_2^2$.

For puncturing period three, the PP's are of size 2 by 3. In this case there is also one puncturing rate in addition to the un-punctured one. Each row of the PP's has a single zero element. Therefore only two columns contain a zero element while the remaining column contains two one elements with no two zero elements at the same column. All possible valid PP's (except the un-punctured) of period three are shown in Figure 2.8. In this case, PP-(1) throw PP-(6) represents the only possible puncturing rate with some redundancy where two symbols are punctured (one symbol is punctured from the output symbols corresponding to each transmit antenna each time the PP is applied) out of six symbols. So for a block of six input bits only four QPSK symbols are transmitted instead of six QPSK symbols on the un-punctured codes. An example of applying PP-(5) to the encoder output symbols is shown in Figure 2.9. There are more freedom in the selection of the punctured symbols on PP's of period there than that of period two. Therefor, it is expected that code punctured with PP's of period three would perform better than that punctured with PP's of period two, because in PP's of period three there is some redundancy available to the decoder while in PP's of period two there is no redundancy available to the decoder.

It is observed that $c_1^1$ is either $x_1^1$ or $x_2^1$, $c_1^2$ is either $x_1^2$ or $x_2^2$, $c_2^1$ is either $x_2^1$ or $x_3^1$, and $c_2^2$ is either $x_2^2$ or $x_3^2$. This observation suggests a modified (expanded)

$$\begin{bmatrix} P_{1,1} & P_{1,2} & \cdots & P_{1,P} \\ P_{2,1} & P_{2,2} & \cdots & P_{2,P} \\ \vdots & \vdots & \ddots & \vdots \\ P_{N,1} & P_{N,2} & \cdots & P_{N,P} \end{bmatrix}$$

Figure 2.5: Puncturing pattern

$$\begin{bmatrix} 1 & 1 \\ 1 & 1 \end{bmatrix} \quad \begin{bmatrix} 0 & 1 \\ 1 & 0 \end{bmatrix} \quad \begin{bmatrix} 1 & 0 \\ 0 & 1 \end{bmatrix} \quad \begin{bmatrix} 0 & 1 \\ 0 & 1 \end{bmatrix} \quad \begin{bmatrix} 1 & 0 \\ 1 & 0 \end{bmatrix} \quad \begin{bmatrix} 0 & 0 \\ 1 & 1 \end{bmatrix} \quad \begin{bmatrix} 1 & 1 \\ 0 & 0 \end{bmatrix}$$

(1) (2) (3) (4) (5) (6) (7)

Figure 2.6: All possible 2 by 2 PP's

$$c_1^1 = P_{1,1} \cdot x_1^1 + P_{2,1} \cdot x_2^1 \qquad c_1^2 = P_{1,2} \cdot x_1^2 + P_{2,2} \cdot x_2^2$$

(a)

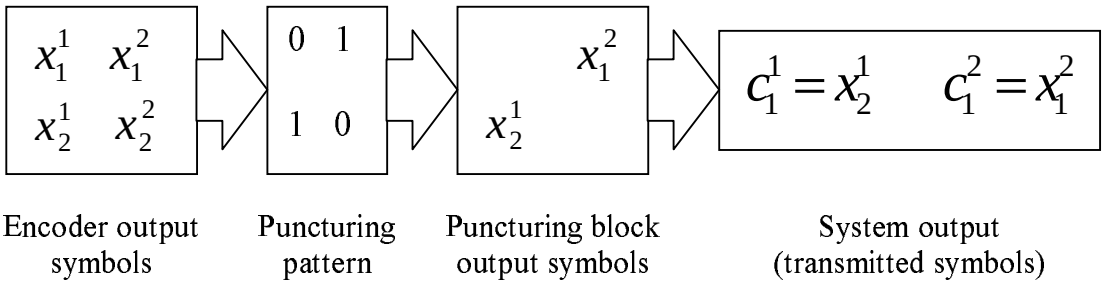


(b)

Figure 2.7: Symbol PST codes with period 2 (a) Equation of the transmitted ST symbol in terms of encoder output symbols (b) Example of applying period 2 PP-(2) shown in Figure 2.6(2) on the encoder output symbols

puncturing pattern (MPP) that could be used instead of the PP in the encoding and decoding of symbol PST codes. The MPP has the same number of ones as the original PP, the same number of rows but it has $(P - N_z/2)(1 + N_z/2)$ columns ($N_z$ number of zero elements on PP). The use of MPP would simplify the decoding of symbol PST codes. MPP's for PP's of period two are special case where MPP's and PP's are exactly the same in elements and size. For PP's of period three, MPP's are of size 2 by 4. Figure 2.10(a) shows how to extract the MPP's from the original PP's of period three where $\overline{P} = NOT(P)$. The equations of the two transmitted ST symbols in terms of the encoder output symbols using MPP's are given in Figure 2.10(b).

For puncturing period four, the PP's are of size 2 by 4. In this case there are two puncturing rates that could be applied to the ST code. The first rate (rate-one puncturing), where only two symbols out of eight are removed each time the PP is applied. Each row of the PP's has a single zero element. Therefore only two columns contain a zero element while the other two columns contain two one elements with no two zero elements at the same column. Thus only one symbol is punctured from the output of the encoder corresponding to a transmit antenna from a block of four symbols each time the PP is applied. Therefor, for a block of eight input bits only six QPSK symbols are transmitted instead of eight QPSK symbols on the un-punctured codes. In this puncturing rate there is more redundancy available to the decoder than that available to the decoder with PP's

$$\begin{bmatrix} 0 & 1 & 1 \\ 1 & 0 & 1 \end{bmatrix} \quad \begin{bmatrix} 0 & 1 & 1 \\ 1 & 1 & 0 \end{bmatrix} \quad \begin{bmatrix} 1 & 0 & 1 \\ 1 & 1 & 0 \end{bmatrix}$$

(1) (2) (3)

$$\begin{bmatrix} 1 & 0 & 1 \\ 0 & 1 & 1 \end{bmatrix} \quad \begin{bmatrix} 1 & 1 & 0 \\ 0 & 1 & 1 \end{bmatrix} \quad \begin{bmatrix} 1 & 1 & 0 \\ 1 & 0 & 1 \end{bmatrix}$$

(4) (5) (6)

Figure 2.8: All possible valid 2 by 3 puncturing pattens

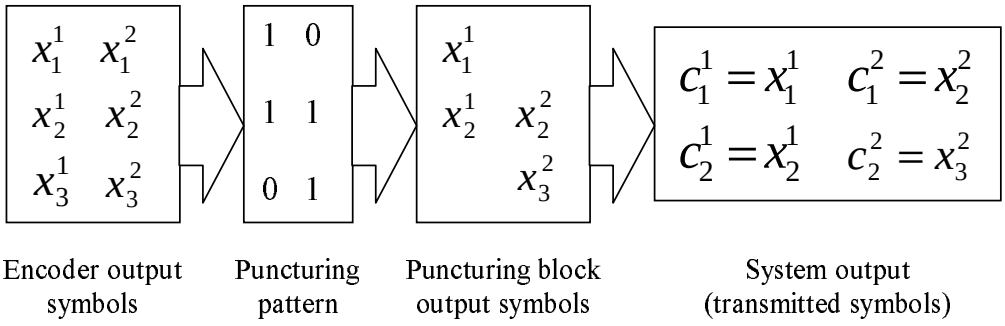


Figure 2.9: Example of applying period 3 PP-(5) shown in Figure 2.8(5) on ST encoder output symbols

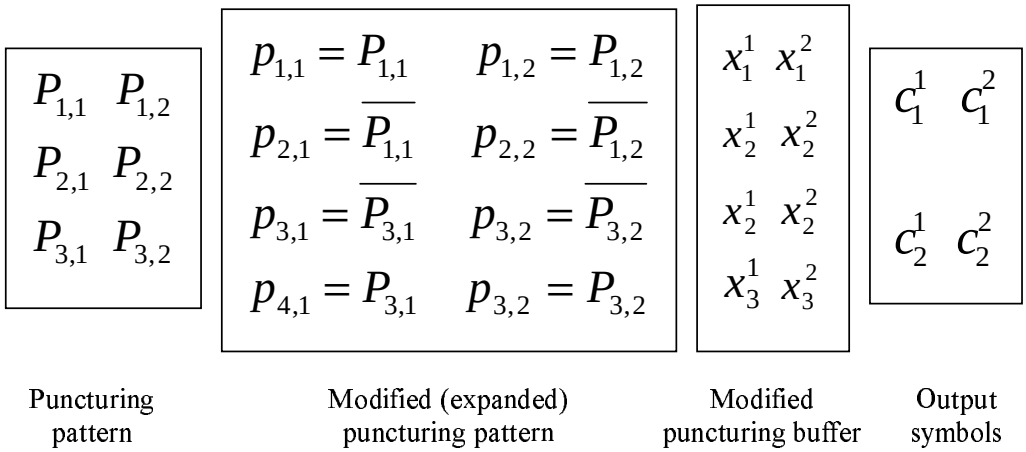


(a)

$$c_1^1 = p_{1,1} \cdot x_1^1 + p_{2,1} \cdot x_2^1 \qquad c_1^2 = p_{1,2} \cdot x_1^2 + p_{2,2} \cdot x_2^2$$
$$c_2^1 = p_{3,1} \cdot x_2^1 + p_{4,1} \cdot x_3^1 \qquad c_2^2 = p_{3,2} \cdot x_2^2 + p_{4,2} \cdot x_3^2$$

(b)

Figure 2.10: Symbol PST codes with period 3 (a) Extraction of MPP from PP (b) Equations of the two transmitted ST symbols in terms of the encoder output symbols

of periods two and three. So it is expected that codes punctured using rate-one period four PP's would outperform codes punctured using PP's of period two or three. All possible valid rate-one PP's of period four and two transmit antennas are shown in Figure 2.11. Figure 2.12 shows an example of applying period four rate-one PP-(6) (shown in Figure 2.11(6)) on the encoder output symbols. The MPP for this case are of size 2 by 6. As in period three, rate-one MPP's could be extracted from rate-one PP's of period four as explained in Figure 2.13(a). In Figure 2.13(b) equations of the three transmitted ST symbols for rate-one PST in terms of the encoder output symbols using the MPP's are given.

ST codes can be further punctured using PP's of period four, but in this case more symbols are punctured. This is the second rate (rate-two puncturing), where four symbols are removed out of eight symbols each time the PP is applied. It is clear that each row of the PP contains two zero elements, therefore each column has a zero element with no two zero elements at the same column. In other words, a symbol is punctured each time instance so that two transmissions occur for each application of the PP. These (rate-two) PP's are generated by replacing a one element by a zero element in the columns containing two one elements of the rate-one PP's.

This puncturing rate removes all the available redundancy and it is like that of period two PP's with more freedom. Therefore for a block of eight input bits, four QPSK symbols are transmitted instead of eight QPSK symbols in the un-punctured

$$\begin{bmatrix} 0 & 1 & 1 & 1 \\ 1 & 0 & 1 & 1 \end{bmatrix} \quad \begin{bmatrix} 0 & 1 & 1 & 1 \\ 1 & 1 & 0 & 1 \end{bmatrix} \quad \begin{bmatrix} 0 & 1 & 1 & 1 \\ 1 & 1 & 1 & 0 \end{bmatrix} \quad \begin{bmatrix} 1 & 0 & 1 & 1 \\ 0 & 1 & 1 & 1 \end{bmatrix}$$

(1) (2) (3) (4)

$$\begin{bmatrix} 1 & 1 & 0 & 1 \\ 0 & 1 & 1 & 1 \end{bmatrix} \quad \begin{bmatrix} 1 & 1 & 1 & 0 \\ 0 & 1 & 1 & 1 \end{bmatrix} \quad \begin{bmatrix} 1 & 0 & 1 & 1 \\ 1 & 1 & 0 & 1 \end{bmatrix} \quad \begin{bmatrix} 1 & 0 & 1 & 1 \\ 1 & 1 & 1 & 0 \end{bmatrix}$$

(5) (6) (7) (8)

$$\begin{bmatrix} 1 & 1 & 0 & 1 \\ 1 & 0 & 1 & 1 \end{bmatrix} \quad \begin{bmatrix} 1 & 1 & 1 & 0 \\ 1 & 0 & 1 & 1 \end{bmatrix} \quad \begin{bmatrix} 1 & 1 & 0 & 1 \\ 1 & 1 & 1 & 0 \end{bmatrix} \quad \begin{bmatrix} 1 & 1 & 1 & 0 \\ 1 & 1 & 0 & 1 \end{bmatrix}$$

(9) (10) (11) (12)

Figure 2.11: All possible valid rate-one 2 by 4 puncturing pattens

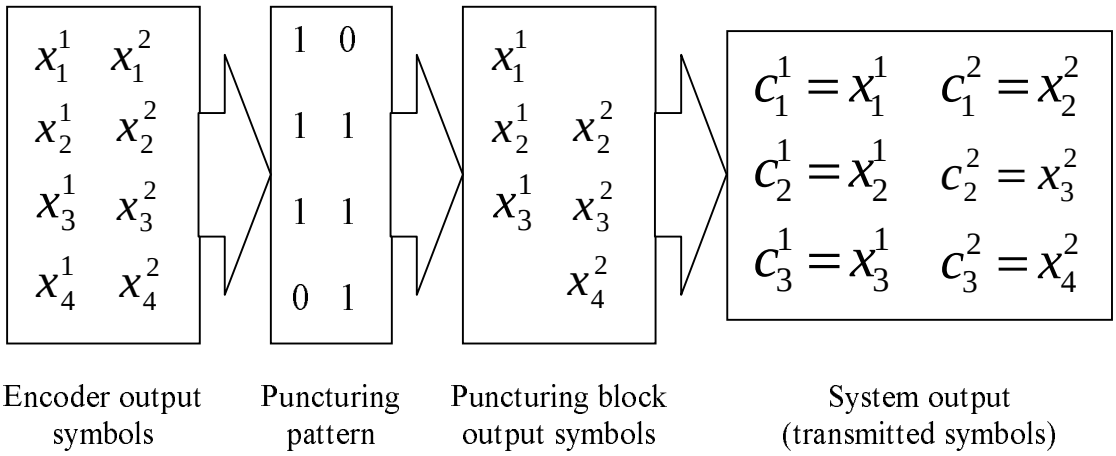


Figure 2.12: Example of applying period 4 rate-one PP (6) shown in Figure 2.11(6) on ST encoder output

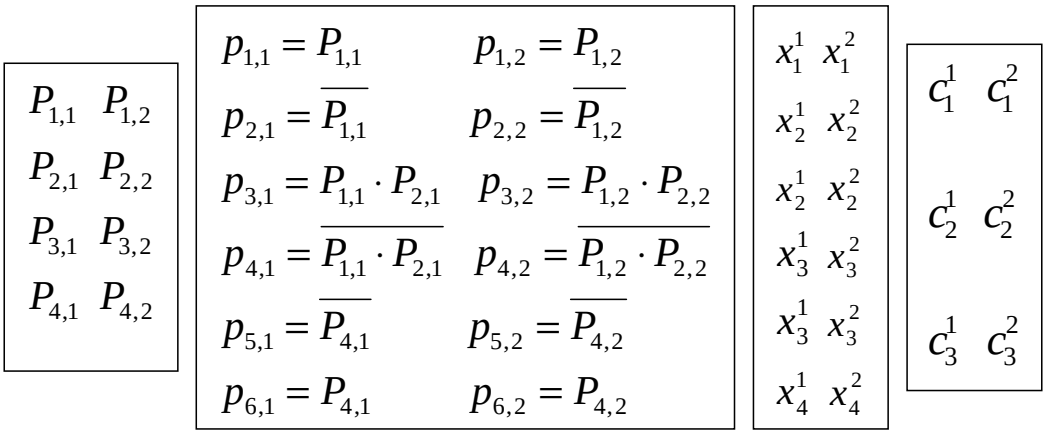


(a)

$$c_1^1 = p_{1,1} \cdot x_1^1 + p_{2,1} \cdot x_2^1 \qquad c_1^2 = p_{1,2} \cdot x_1^2 + p_{2,2} \cdot x_2^2$$
$$c_2^1 = p_{3,1} \cdot x_2^1 + p_{4,1} \cdot x_3^1 \qquad c_2^2 = p_{3,2} \cdot x_2^2 + p_{4,2} \cdot x_3^2$$
$$c_3^1 = p_{5,1} \cdot x_3^1 + p_{6,1} \cdot x_4^1 \qquad c_3^2 = p_{5,2} \cdot x_3^2 + p_{6,2} \cdot x_4^2$$

(b)

Figure 2.13: Symbol PST codes with period 4 rate-one (a) Extraction of MPP from PP (b) Equation of the three transmitted ST symbols in terms of the encoder output symbols using the MPP

ST code. All possible valid rate-two PP of period four and two transmit antennas are shown in Figure 2.14. Puncturing process is illustrated by an example in Figure 2.15, where the rate-two PP(5) shown in 2.14(5) is used. Like in rate-one puncturing, it is possible to generate the MPP's for PP's to simplify the decoding process. Figure 2.16(a) illustrates how to extract the MPP from the original PP, and Figure 2.16(b) gives the equations of the two transmitted ST symbols in terms of the encoder output symbols using the MPP.

Symbol punctured ST codes are not like symbol punctured TCM codes since puncturing in ST codes is not performed to the whole ST symbol as in TCM codes, but at most one of its component constellation symbols is punctured at a time. Thus the symbol shift process described above is required so that each transmit antenna has a modulated constellation symbol to transmit at all transmission times. The following example illustrate puncturing and shifting in ST codes using different periods and puncturing rates.

**Example 2.1** *Consider the 4-state QPSK ST code designed in [1] shown in Figure 1.2(b). The un-punctured system encoder accepts 2 input bits each time instance. The two encoder-mapper output symbols are modulated and transmitted via the two transmit antennas. If this code is punctured using PP with period $P$, then due to $2P$ input bits each $P$ successive time instances, the two encoder-mapper output streams each with $P$ symbols are passed to the puncturing circuit. In the puncturing circuit, each row of the PP is applied to the corresponding stream such*

$$\begin{bmatrix} 0 & 0 & 1 & 1 \\ 1 & 1 & 0 & 0 \end{bmatrix} \quad \begin{bmatrix} 0 & 1 & 0 & 1 \\ 1 & 0 & 1 & 0 \end{bmatrix} \quad \begin{bmatrix} 1 & 1 & 0 & 0 \\ 0 & 0 & 1 & 1 \end{bmatrix}$$

(1) (2) (3)

$$\begin{bmatrix} 1 & 0 & 1 & 0 \\ 0 & 1 & 0 & 1 \end{bmatrix} \quad \begin{bmatrix} 0 & 1 & 1 & 0 \\ 1 & 0 & 0 & 1 \end{bmatrix} \quad \begin{bmatrix} 1 & 0 & 0 & 1 \\ 0 & 1 & 1 & 0 \end{bmatrix}$$

(4) (5) (6)

Figure 2.14: All possible valid rate-two 2 by 4 puncturing pattens

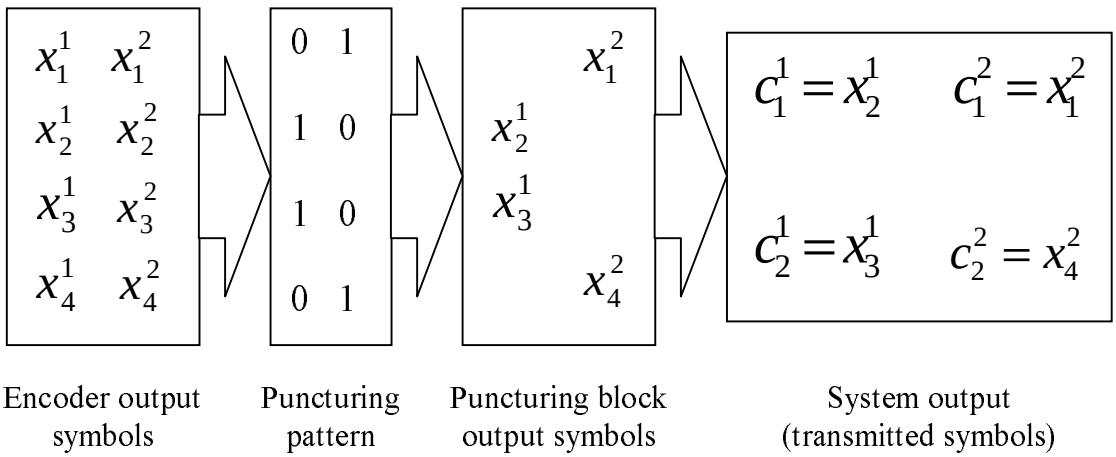


Figure 2.15: Example of applying period 4 rate-one PP-(5) shown in Figure 2.14(5) on ST encoder output

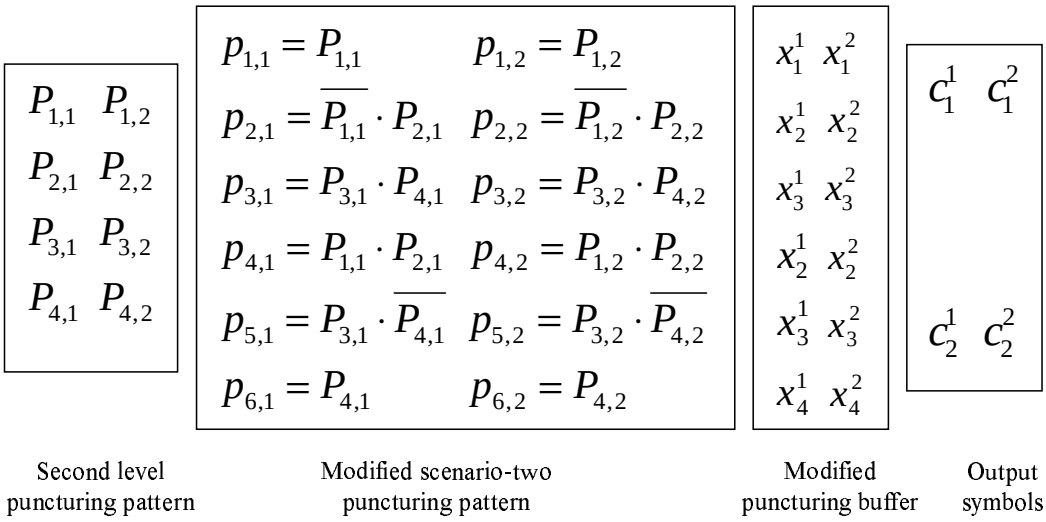


(a)

$$c_1^1 = p_{1,1} \cdot x_1^1 + p_{2,1} \cdot x_2^1 + p_{3,1} \cdot x_3^1 \quad c_1^2 = p_{1,2} \cdot x_1^2 + p_{2,2} \cdot x_2^2 + p_{3,2} \cdot x_3^2$$

$$c_2^1 = p_{4,1} \cdot x_2^1 + p_{5,1} \cdot x_3^1 + p_{6,1} \cdot x_4^1 \quad c_2^2 = p_{4,2} \cdot x_2^2 + p_{5,2} \cdot x_3^2 + p_{6,2} \cdot x_4^2$$

(b)

Figure 2.16: Symbol PST codes with period 4 rate-two (a) Extraction of MPP from PP (b) Equations of the two transmitted ST symbols in terms of the encoder output symbols using MPP's

*that each symbol in a stream is multiplied by one or zero. The remaining* $P - N_z/2$ *symbols in each stream are buffered in a buffer of size* $P - N_z/2$*. After filling both buffer the stored symbol streams are modulated and transmitted via the two transmit antennas in* $P - N_z/2$ *time instances. This process is illustrated in Table 2.2 for five cases in addition to the original (un-punctured) system: period two PP-(1), period two PP-(3), period three PP-(5), period four rate-one PP-(6), and period four rate-two PP-(3) where these PP's are shown in Figure 2.6(1), Figure 2.6(3), Figure 2.8(5), Figure 2.11(6), and Figure 2.14(3) respectively, and the input bits are assumed to be (011111011010001110110110). In the table, P-S-PP is puncturing period - puncturing rate - puncturing pattern, E-M stream i is the encoder/mapper P symbols output stream corresponding to transmit antenna i, and P-B stream i is the puncturing circuit/buffer* $P - N_z/2$ *symbols output stream corresponding to transmit antenna i. The P-B* $P - N_z/2$ *symbols output stream i is given by*

$$P_{i,1} \cdot x_1^i \; P_{i,2} \cdot x_2^i \; \cdots \; P_{i,P} \cdot x_P^i \tag{2.5}$$

*where* $(x_1^i \; x_2^i \; \cdots \; x_P^i)$ *is the* $i^{th}$ *encoder-mapper P symbols output stream, and* $[P_{i,1} \; P_{i,2} \; \cdots \; P_{i,P}]$ *is the* $i^{th}$ *row of the PP. There are exactly* $N_z/2$ *symbols that are deleted in 2.5. The* $t^{th}$ *transmitted ST symbol is the concatenation of the* $t^{th}$ *symbols in the two P-B output streams where* $t = 1, 2, \cdots P - N_z/2$*. Period two PP-(1) is given in the table to show that if the PP has no zero element, then the system output is exactly like the un-punctured system output.*

For PP's of period five, there are two puncturing rates. The first rate (rate-one) where two symbols are punctured out of ten symbols, there are twenty possible valid PP's. The second rate (rate-two) where four symbols are punctured out of ten symbols, there are thirty possible valid PP's. While for PP's of period six, there are three puncturing rates. The first rate (rate-one) where two symbols are punctured out of twelve symbols, there are thirty possible valid PP's. The second rate (rate-two) where four symbols are punctured out of twelve symbols, there are ninety possible valid PP's. The third rate (rate-three) where six symbols are punctured out of twelve symbols, there are ninety possible valid PP's. This last puncturing rate is similar to that of period two and period four rate-two, where all the available redundancy in the code is removed. Possible valid PP's of period five and six are not shown because of brevity of discussion.

As the puncturing period increases, the number of possible valid PP's increases and the number of possible puncturing rates increase. Moreover the freedom of selecting the punctured symbols increase. Unfortunately, the decoder complexity and decoding time increase too.

### Code Rate

The rate ($R$) of the QPSK symbol PST code depends on the puncturing period ($P$) and on the number of zero elements ($N_z$) in the PP (or equivalently the number

TABLE 2.2: Example 2.1

| P-R-pp | output | MSB (011111011010001110110110) LSB | | | | | | | | | | | |
|---|---|---|---|---|---|---|---|---|---|---|---|---|---|
| | input bits | 10 | 01 | 11 | 10 | 11 | 00 | 10 | 10 | 01 | 11 | 11 | 01 |
| | current state | 0 | 2 | 1 | 3 | 2 | 3 | 0 | 2 | 2 | 1 | 3 | 3 |
| | next state | 2 | 1 | 3 | 2 | 3 | 0 | 2 | 2 | 1 | 3 | 3 | 1 |
| Normal | E-M stream 1 | 0 | 2 | 1 | 3 | 2 | 3 | 0 | 2 | 2 | 1 | 3 | 3 |
| | E-M stream 2 | 2 | 1 | 3 | 2 | 3 | 0 | 2 | 2 | 1 | 3 | 3 | 1 |
| | ST ($c_t^1 c_t^2$) | 02 | 21 | 13 | 32 | 23 | 30 | 02 | 22 | 21 | 13 | 33 | 31 |
| 2-un-1 | E-M stream 1 | 0 2 | | 1 3 | | 2 3 | | 0 2 | | 2 1 | | 3 3 | |
| | P-B stream 1 | 0 2 | | 1 3 | | 2 3 | | 0 2 | | 2 1 | | 3 3 | |
| | E-M stream 2 | 2 1 | | 3 2 | | 3 0 | | 2 2 | | 1 3 | | 3 1 | |
| | P-B stream 2 | 2 1 | | 3 2 | | 3 0 | | 2 2 | | 1 3 | | 3 1 | |
| | ST ($c_t^1 c_t^2$) | 02 21 | | 13 32 | | 23 30 | | 02 22 | | 21 13 | | 33 31 | |
| 2-one-3 | E-M stream 1 | 0 2 | | 1 3 | | 2 3 | | 0 2 | | 2 1 | | 3 3 | |
| | P-B stream 1 | 0 | | 1 | | 2 | | 0 | | 2 | | 3 | |
| | E-M stream 2 | 2 1 | | 3 2 | | 3 0 | | 2 2 | | 1 3 | | 3 1 | |
| | P-B stream 2 | 1 | | 2 | | 0 | | 2 | | 3 | | 1 | |
| | ST ($c_t^1 c_t^2$) | 01 | | 12 | | 20 | | 02 | | 23 | | 31 | |
| 3-one-5 | E-M stream 1 | 0 2 1 | | | 3 2 3 | | | 0 2 2 | | | 1 3 3 | | |
| | P-B stream 1 | 0 2 | | | 3 2 | | | 0 2 | | | 1 3 | | |
| | E-M stream 2 | 2 1 3 | | | 2 3 0 | | | 2 2 1 | | | 3 3 1 | | |
| | P-B stream 2 | 1 3 | | | 3 0 | | | 2 1 | | | 3 1 | | |
| | ST ($c_t^1 c_t^2$) | 01 23 | | | 33 20 | | | 02 21 | | | 13 31 | | |
| 4-one-6 | E-M stream 1 | 0 2 1 3 | | | | 2 3 0 2 | | | | 2 1 3 3 | | | |
| | P-B stream 1 | 0 2 1 | | | | 2 3 0 | | | | 2 1 3 | | | |
| | E-M stream 2 | 2 1 3 2 | | | | 3 0 2 2 | | | | 1 3 3 1 | | | |
| | P-B stream 2 | 1 3 2 | | | | 0 2 2 | | | | 3 3 1 | | | |
| | ST ($c_t^1 c_t^2$) | 01 23 12 | | | | 20 32 02 | | | | 23 13 31 | | | |
| 4-two-3 | E-M stream 1 | 0 2 1 3 | | | | 2 3 0 2 | | | | 2 1 3 3 | | | |
| | P-B stream 1 | 0 2 | | | | 2 3 | | | | 2 1 | | | |
| | E-M stream 2 | 2 1 3 2 | | | | 3 0 2 2 | | | | 1 3 3 1 | | | |
| | P-B stream 2 | 3 2 | | | | 2 2 | | | | 3 1 | | | |
| | ST ($c_t^1 c_t^2$) | 03 22 | | | | 22 32 | | | | 23 11 | | | |

of punctured symbols each application of the PP) as follows:

$$R = \frac{4P}{2P - N_z} \tag{2.6}$$

This equation is also valid for the un-punctured QPSK ST codes decoded using the $P$-stage decoder. The rates of QPSK symbol PST codes using different puncturing periods and puncturing rates are listed in Table 2.3.

The symbol punctured QPSK ST codes have a lower transmitted power per information bit than that of the un-punctured QPSK ST codes. Therefore, for a fair comparison between the un-punctured and punctured QPSK ST codes from power point of view, frame error rate (FER) vs. signal to noise ratio (SNR $NE_s/N_0$) carve should be sifted to the left by a constant amount of dB's to get FER vs. transmitted power per information bit to noise ratio (BNR $NE_b/N_0$) carve. This constant value ($k_c$) depends on the code rate as shown in the following equation:

$$k_c = -10 \log \left( \frac{2}{R} \right) \tag{2.7}$$

For example, the FER vs. SNR carves should be shifted to the left by zero dB for the un-punctured QPSK ST code, 1.2494 dB for rate-one, and 3.0103 dB for rate-two QPSK symbol PST codes with period four PP's, to get the FER vs. BNR carves.

If a ST code is punctured with a specific rate-one PP to get rate-one PST

code and the same (mother) ST code is punctured with a rate-two PP, extracted from that rate-one pattern, to get a rate-two PST code, then a family of the unpunctured ST code and the two PST codes is produced with different rates depending on the signal constellation, puncturing period and number of zero elements on the PP. For example if the rate-one PP-(6) of period four shown in Figure 2.11(6) is used to puncture a QPSK ST code, and the same ST code is punctured using rate-two period four PP extracted from rate-one PP-(6) (either period four rate-two PP-(3) or PP-(4) shown in Figure 2.14(3) and 2.14(4) respectively) a family of three codes is generated with rates 2, 2.667, and 4 b/s/Hz respectively. This family of codes can be used in a variable rate ST codes application such as Automatic Repeat Request (ARQ) protocols.

To generate families of QPSK symbol PST codes with members more than three, the puncturing period must be an integer greater than five. If the puncturing period is set to five, then a family of three codes is produced with rates 2, 2.5 and 3.333 b/s/Hz. However, if the puncturing period is set to six, then the resulting families would have four members with rates 2, 2.4, 3, and 4 b/s/Hz.

As the puncturing period increases, the compatibility and flexibility of the PST codes family's increase. Which result in more adaptability and reliability in the rates of codes family's. However, as mention earlier the decoding time and complexity increases significantly.

**Transmitted Frame Length**

The normal (un-punctured) transmitted frames length $l$ must be a multiple of the puncturing period $P$. Because the puncturing periods used here are two, three four, five and six, a frame length, which is a multiple of these periods, is selected to be $l = 120$. The punctured transmitted frame length ($l_p$) is a function of the puncturing period as given by the following equation:

$$l_p = l \cdot \frac{(P - N_z/2)}{P} = k_p \cdot P \cdot \frac{2}{R} \tag{2.8}$$

Where

$$k_p = \frac{l}{P} = \frac{l_p}{(P - N_z/2)} \tag{2.9}$$

is a constant integer equals the number of applications of the PP on a single encoder output symbols frame of length $l$. As it is shown above, $R$ depends on the puncturing period. It should be noticed here that the trellis should arrive (terminate) to its initial zero state at the end of each frame, so that a specific number of zeros is added (concatenated) to the input bits of the encoder. This number of zeros depends on the number of input bits to the encoder $k$ and the number of encoder memory elements $v$. For example if the puncturing period three is used to puncture a 4-state QPSK code, there are 238 source input bits plus two zeros (padded zeros) passed to the encoder to form a frame of 120 ST symbols containing 240 QPSK symbols (120 QPSK symbols corresponding to each

transmit antenna) for the un-punctured system or a transmitted frame of 80 ST symbols containing 160 QPSK symbols (80 QPSK symbols corresponding to each transmit antenna) for the PST system. In this case $k_p$ equals 40 applications of the PP on a single frame and $k_c = 1.7609$ dB. The transmitted frame length, $k_c$ and $k_p$ are listed in Table 2.3 for different puncturing periods.

## 2.4 Alternative ST Trellis Codes Representation

An alternative representation of ST codes that is valid for high-rate, normal and punctured ST codes is illustrated in this section. This representation is similar to the representation of MTCM in the sense that the branch labels in both representations describe the transmitted symbols in more than one time instance. That makes the similarities and deferences between PST codes and punctured MTCM codes easily seen.

Consider a ST code, the code trellis shows all branches connecting state $\sigma_g$ and state $\sigma_h$ where $g, h \in \{0, 1, \cdots, 2^v - 1\}$ for one transition (one trellis stage). The branch label $s^i_{g,h}$ is the signal transmitted via transmit antenna $i$, $i = 1, 2, \cdots, N$, when a transition from state $\sigma_g$ to state $\sigma_h$ $g, h = 0, 1, \cdots, 2^v - 1$ occurs. The code trellis can represent $P$ trellis transitions by concatenating $P$ successive transitions. If only the initial and the final states are considered, then there will be $n_p =$

TABLE 2.3: Rate, frame length and power factor for PST codes with different puncturing period

| Puncturing Period | Puncturing rate | Code Rate (b/s) | Transmitted frame length | $k_c$ dB | $k_p$ applications |
|---|---|---|---|---|---|
| uncoded | | 4 | 120 | 3.0103 | - |
| un-punctured | | 2 | 120 | 0.0 | - |
| two | one | 4 | 60 | 3.0103 | 60 |
| three | one | 3 | 80 | 1.7609 | 40 |
| four | one | 2.667 | 90 | 1.2494 | 30 |
| | two | 4 | 60 | 3.0103 | 30 |
| five | one | 2.5 | 96 | 0.9691 | 24 |
| | two | 3.333 | 72 | 2.2185 | 24 |
| six | one | 2.4 | 100 | 0.7918 | 20 |
| | two | 3 | 80 | 1.7609 | 20 |
| | three | 4 | 60 | 3.0103 | 20 |

$B^{P-1}$ paths connecting each initial and final state pair, and each path is formed by $P$ successive transitions, where $B = 2^k$ is the number of branches diverging from each state in the original trellis diagram and $k$ is the number of source bit entering the encoder each time instance. In this case the intermediate transitions forming the connecting paths could be represented by $n_p$ parallel branches. The new trellis diagram has the same number of states as the original one but with parallel branches. Any state pair ($\sigma_g$,$\sigma_h$) is connected with $n_p$ parallel branches with branch label bundle $\mathbf{A}_{g,h}$ consists of $n_p$ parallel branch labels, where $\mathbf{A}_{g,h}$ is given by:

$$\mathbf{A}_{g,h} = \begin{bmatrix} \left(x^1_{g,h}x^2_{g,h}\cdots x^N_{g,h}\right)^1_1 \left(x^1_{g,h}x^2_{g,h}\cdots x^N_{g,h}\right)^1_2 \cdots \left(x^1_{g,h}x^2_{g,h}\cdots x^N_{g,h}\right)^1_P \\ \left(x^1_{g,h}x^2_{g,h}\cdots x^N_{g,h}\right)^2_1 \left(x^1_{g,h}x^2_{g,h}\cdots x^N_{g,h}\right)^2_2 \cdots \left(x^1_{g,h}x^2_{g,h}\cdots x^N_{g,h}\right)^2_P \\ \vdots \\ \left(x^1_{g,h}x^2_{g,h}\cdots x^N_{g,h}\right)^{n_p}_1 \left(x^1_{g,h}x^2_{g,h}\cdots x^N_{g,h}\right)^{n_p}_2 \cdots \left(x^1_{g,h}x^2_{g,h}\cdots x^N_{g,h}\right)^{n_p}_P \end{bmatrix} \tag{2.10}$$

where $\left(x^i_{g,h}\right)^m_t$ is the transmitted channel symbol via transmit antenna $i$ at time instance $t$, $t = 1, 2, \cdots, P$ associated with the parallel branch $m$, $m = 1, 2, \cdots, n_p$ when a transition from state $\sigma_g$ to state $\sigma_h$ occurs. This new representation accepts $\overline{k} = kP$ input bits, where the last $2^v$ input bits are used to select the parallel branch label bundle within the current encoder state and the first $kP - 2^v$ input bits are used to select parallel branch label within the bundle. The alternative representation is equivalent to the MTCM code presentation with multiplicity $P$

and $N$ transmit antennas.

**Example 2.2** *Figure 2.17(a) shows the trellis diagram of a 4-state QPSK ST code. There are two input bits to the encoder each time instance $k = 2$ and thus there are $B = 4$ branches diverging from each state in the original trellis as shown in Figure 2.17(a). This trellis diagram describes one transition only. If $P$ such a diagram are concatenated then the resulting trellis diagram will describe $P$ successive transitions as in Figure 2.17(b). In other words the new trellis describes the transmitted symbols for $P$ successive time instances. There are $4^{P-1}$ paths connecting any initial and final state pairs ($\sigma_g$,$\sigma_h$) $g, h \in \{0, 1, 2, 3\}$. For illustration the paths connecting initial state $\sigma_1$ and final state $\sigma_2$ are marked by dark lines in Figure 2.17(b). Let $P = 2$ as shown in Figure 2.17(c), then there will be 4 paths connecting each initial and final state pairs, thus there are $n_p = 4$ parallel branches in each bundle connecting each state pair of the 16 possible state pairs. There are $\overline{k} = 4$ input bits where the last two input bits are used to select a parallel branch bundle out of the four bundles diverging from the current state and the firs two input bits are used to select a parallel branch within the selected bundle. The selected branch labels are the channel symbols that will be transmitted during two successive time instances.*

For this representation to be a true (valid) representation, the output channel symbols must be identical to the same input bits, which is the case for the alternative representation. The next example proves that the transmitted symbols are

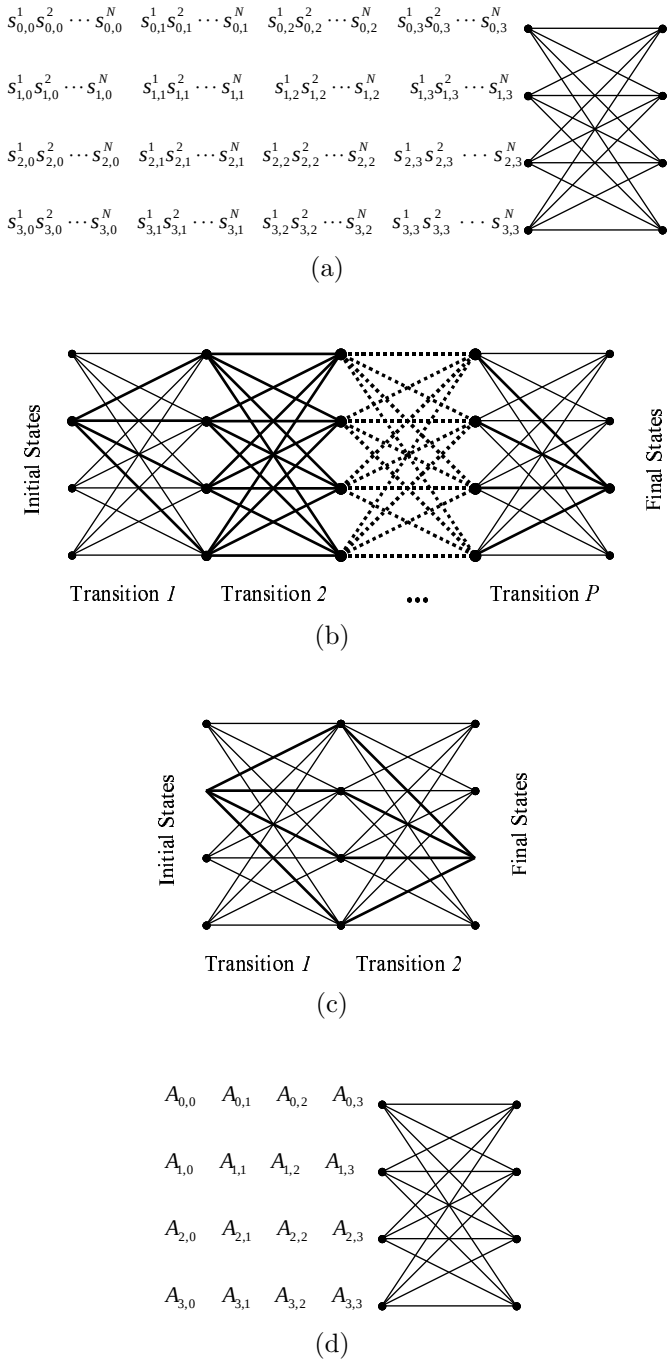


Figure 2.17: Example of the alternative representation (a) Original QPSK 4-state ST trellis diagram (b) Concatenated P stage trellis diagram (c) Two stage trellis diagram (d) Alternative trellis diagram

identical to the same input bits.

**Example 2.3** *Consider the 4-state ST code designed in [1] shown in Figure 1.2(b), the two- and three-transition representations are shown in Figure 2.18(a) and Figure 2.18(b) respectively. For the normal representation, the system accepts 2 input bits each time instance and the selected branch and the next system state are dependent on these two input bits. Where as for the two-transition representation, the system accepts four input bits each time instance, so that the next state is only dependent on the most significant two bits and the selected parallel branch depends on the least significant two input bits. The three-transition system accepts six input bits each time instance such that the most significant two input bits are used to select the next state and the least significant four input bits are used to select between the parallel branches connecting the current and the next states. Let the input bits be (011111011010001110110110), the input to each of the three systems, the output symbols from each system and the encoder states are shown in Table 2.4. The input bits are organized such that the right most bit is the firs input bit entering the system and it is the least significant one. From the rows of the output symbols in the Table it is clearly seen that these three systems have identical output for the same input bits.*

Period $P$ PP's can be applied directly to the branch label of the $P$-transition representation. The PST code is easily represented by this alternative trellis rep-

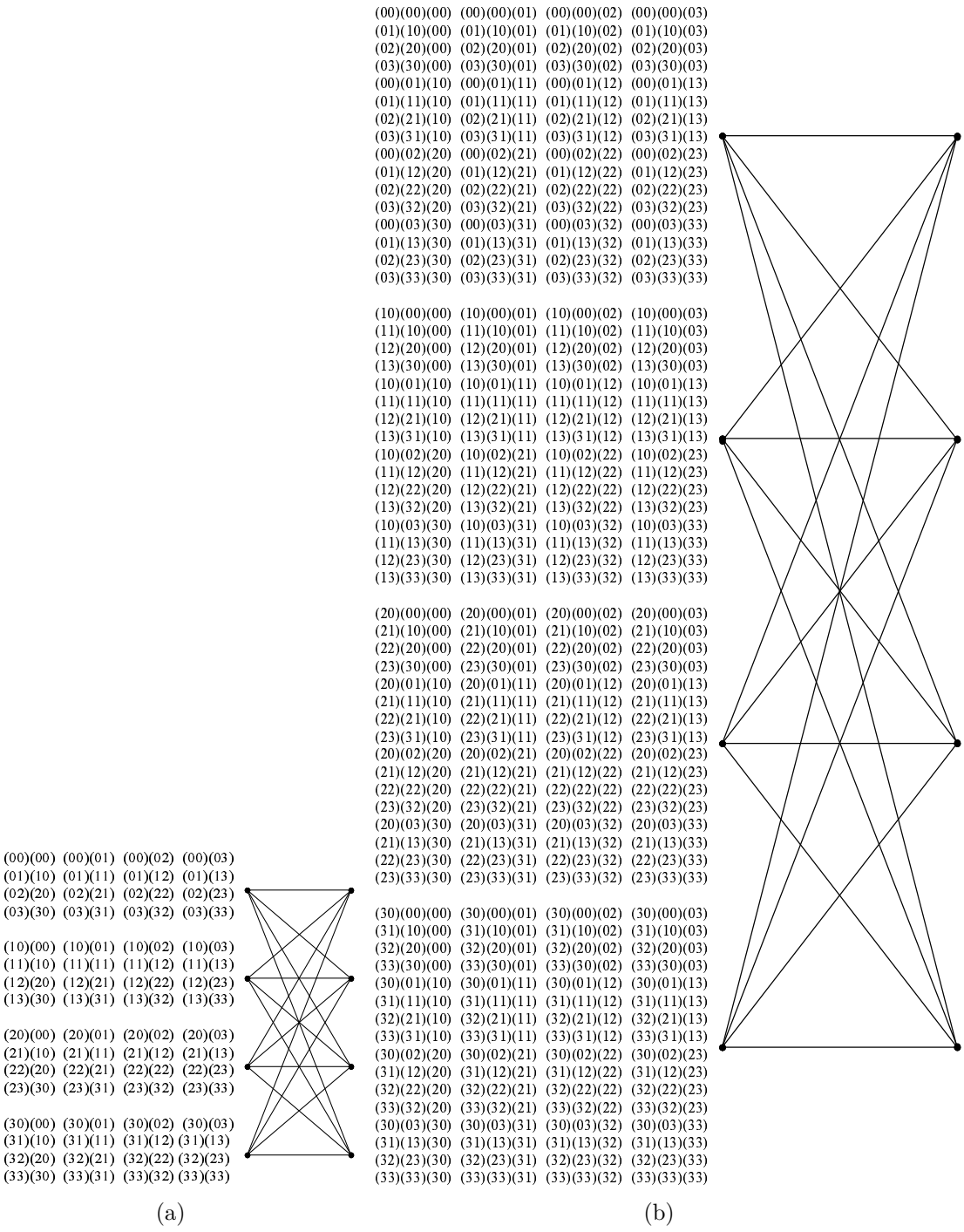


Figure 2.18: New representation of the 4-state QPSK ST code designed in [1] (a) Two-transition representation (b) Three-transition representation

TABLE 2.4: Example 2.3

| Rep | MSB (011111011010001110110110) LSB | | | | | | | | | | | |
|---|---|---|---|---|---|---|---|---|---|---|---|---|
| Normal | time | 0 | 1 | 2 | 3 | 4 | 5 | 6 | 7 | 8 | 9 | 10 | 11 |
| | input | 10 | 01 | 11 | 10 | 11 | 00 | 10 | 10 | 01 | 11 | 11 | 01 |
| | current | 0 | 2 | 1 | 3 | 2 | 3 | 0 | 2 | 2 | 1 | 3 | 3 |
| | next | 2 | 1 | 3 | 2 | 3 | 0 | 2 | 2 | 1 | 3 | 3 | 1 |
| | output | 02 | 21 | 13 | 32 | 23 | 30 | 02 | 22 | 21 | 13 | 33 | 31 |
| Two | time | 0 | | 1 | | 2 | | 3 | | 4 | | 5 | |
| | input | 0110 | | 1011 | | 0011 | | 1010 | | 1101 | | 0111 | |
| | current | 0 | | 1 | | 2 | | 0 | | 2 | | 3 | |
| | next | 1 | | 2 | | 0 | | 2 | | 3 | | 1 | |
| | output | 02 21 | | 13 32 | | 23 30 | | 02 22 | | 21 13 | | 33 31 | |
| Three | time | 0 | | | 1 | | | 2 | | | 3 | | |
| | input | 110110 | | | 001110 | | | 011010 | | | 011111 | | |
| | current | 0 | | | 3 | | | 0 | | | 1 | | |
| | next | 3 | | | 0 | | | 1 | | | 1 | | |
| | output | 02 21 13 | | | 32 23 30 | | | 02 22 21 | | | 13 33 31 | | |

resentation, with parallel branch labels bundle given by:

$$\mathbf{A}_{g,h} = \begin{bmatrix} \left(s^1_{g,h}s^2_{g,h}\cdots s^N_{g,h}\right)^1_1 \left(s^1_{g,h}s^2_{g,h}\cdots s^N_{g,h}\right)^1_2 \cdots \left(s^1_{g,h}s^2_{g,h}\cdots s^N_{g,h}\right)^1_{P-\frac{N_z}{2}} \\ \left(s^1_{g,h}s^2_{g,h}\cdots s^N_{g,h}\right)^2_1 \left(s^1_{g,h}s^2_{g,h}\cdots s^N_{g,h}\right)^2_2 \cdots \left(s^1_{g,h}s^2_{g,h}\cdots s^N_{g,h}\right)^2_{P-\frac{N_z}{2}} \\ \vdots \\ \left(s^1_{g,h}s^2_{g,h}\cdots s^N_{g,h}\right)^{n_p}_1 \left(s^1_{g,h}s^2_{g,h}\cdots s^N_{g,h}\right)^{n_p}_2 \cdots \left(s^1_{g,h}s^2_{g,h}\cdots s^N_{g,h}\right)^{n_p}_{P-\frac{N_z}{2}} \end{bmatrix} \quad (2.11)$$

where $\left(s^i_{g,h}\right)^m_t$ is the transmitted channel symbol via transmit antenna $i$ at time instance $t$, $t = 1, 2, \cdots, P - N_z/2$ associated with the parallel branch $m$, $m = 1, 2, \cdots, n_p$ when a transition from state $\sigma_g$ to state $\sigma_h$ occurs. For a given $P$, $\left(s^i_{g,h}\right)^m_t$ can be expressed in terms of the MPP's and un-punctured $P$-transition representation such that:

$$\left(s^i_{g,h}\right)^m_t = \sum_{n=1}^{\frac{N_z}{2}+1} p_{i,(N_z/2+1)(t-1)+n} \left(x^i_{g,h}\right)^m_{(t-1)+n} \quad (2.12)$$

where $p_{i,n}$ is the $i^{th}$ row $n^{th}$ column element of the MPP. There is only one non zero product in the summation in equation (2.12). For the PST systems each branch is labeled with only $(P - N_z/2)$ ST symbols that are transmitted in $(P - N_z/2)$ time instances.

**Example 2.4** *Consider the two- and three-transition representation of the code designed in [1] shown in Figure 2.18(a) and 2.18(b) respectively. If for example period two PP(3) shown in Figure 2.6(3) is applied to the branches in the two-*

*transition representation, the resulting PST code is shown in Figure 2.19(a). Applying period three PP(5) shown in Figure 2.8(5) to the three-transition representation of the punctured code will produce the trellis diagram shown in Figure 2.19(b). The response of the PST systems with the two- and three-transition representations to the input bits (011111011010001110110110) are given in Table 2.5. Comparing the output ST symbols of the two-transition alternative punctured system representation with the corresponding period two punctured ST output symbols in Table 2.2, the output of both representations is identical for the same input bits. Also comparing the output ST symbols of the three-transition alternative punctured system representation with the corresponding period three punctured ST output symbols in Table 2.2, both systems also has identical output for the same input bits. That means the alternative $P$-transition representation is also valid for punctured ST codes with period $P$.*

From the alternative representation of the ST and the PST codes, it is noticed that the complexity of the $P$-stage decoder of the PST is less than that of the ST decoder using the same $P$-transition representation, since each branch in the PST $P$-transition trellis consists of $P - N_z/2$ ST symbols while each branch in the ST $P$-transition trellis consists of $P$ ST symbols. This property was not clear in the original trellis representation of ST codes. However, if the normal decoder of ST codes is used, the PST decoder will be more complex as mentioned earlier.

This representation clearly demonstrates the rate-compatibility property of

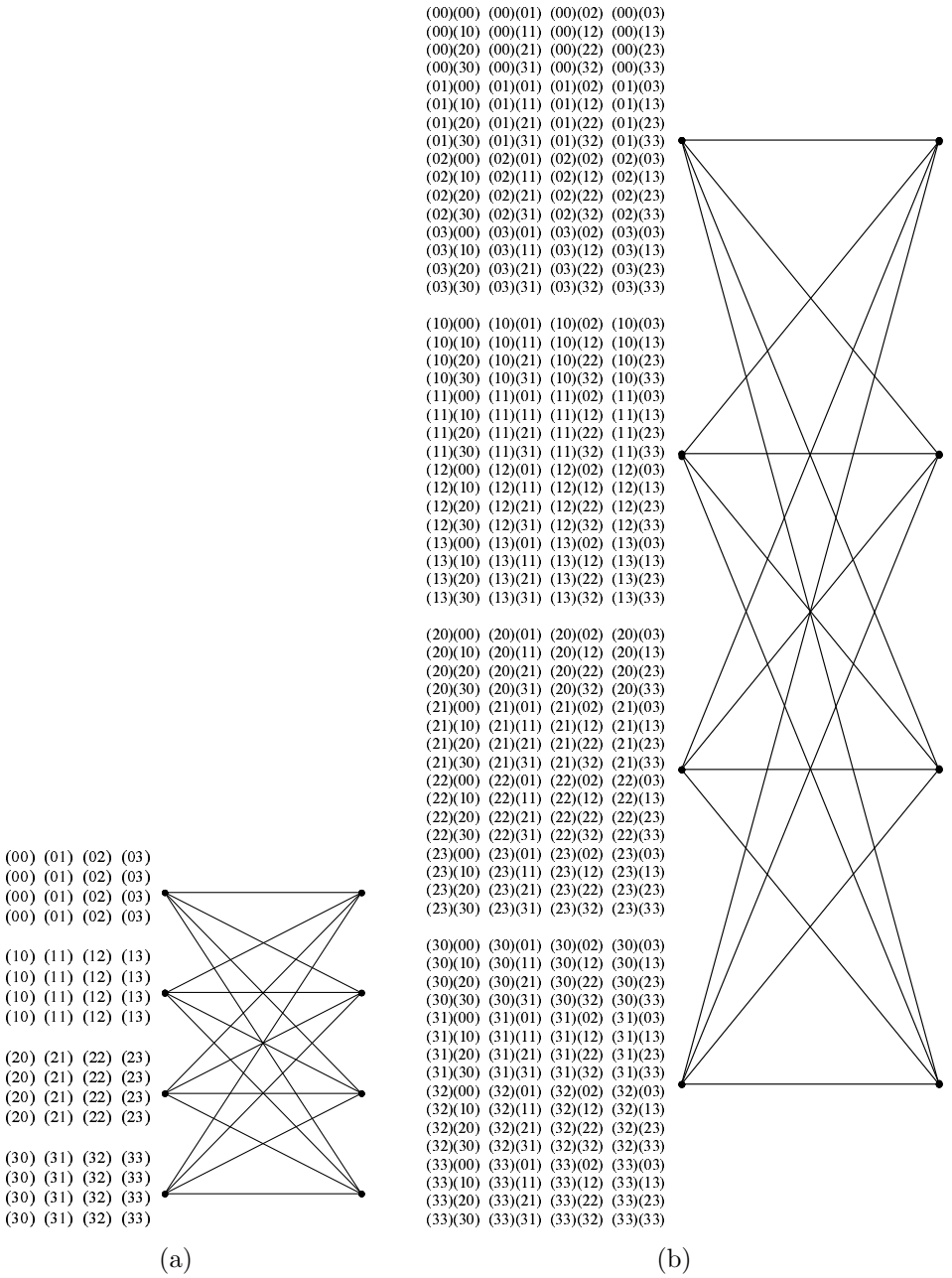


Figure 2.19: Alternative punctured code trellis representation of the 4-state QPSK ST code designed in [1] (a) PST code by period 2 PP-(3) shown in Figure 2.6(3) (b) PST code by period 3 PP-(5) shown in Figure 2.8(5)

.

TABLE 2.5: Example 2.4

| Rep | MSB (011111011010001110110110) LSB | | | | | | |
|---|---|---|---|---|---|---|---|
| Two | time | 0 | 1 | 2 | 3 | 4 | 5 |
| | input | 0110 | 1011 | 0011 | 1010 | 1101 | 0111 |
| | current | 0 | 1 | 2 | 0 | 2 | 3 |
| | next | 1 | 2 | 0 | 2 | 3 | 1 |
| | output | 02 21 | 13 32 | 23 30 | 02 22 | 21 13 | 33 31 |
| | pnc output | 01 | 12 | 20 | 02 | 23 | 31 |
| Three | time | 0 | | 1 | 2 | 3 | |
| | input | 110110 | | 001110 | 011010 | 011111 | |
| | current | 0 | | 3 | 0 | 1 | |
| | next | 3 | | 0 | 1 | 1 | |
| | output | 02 21 13 | | 32 23 30 | 02 22 21 | 13 33 31 | |
| | pnc output | 01 23 | | 33 20 | 02 21 | 13 31 | |

PST codes family, since each member of a family of PST codes has the same $P$-transition alternative trellis representation structure and essentially the same decoder. However, rate-compatible ST (RC-ST) codes are unlike rate-compatible trellis (RC-TCM) codes [46] because of the following reasons. In a RC-TCM codes family, only the last $P - m_p$ symbols of the branch labels in the mother (unpunctured) TCM code are deleted and the first $m_p$ symbols of the branch labels of both the punctured and the mother TCM codes are the same where $P$ and $m_p$ are the multiplicities of the mother and the punctured TCM codes respectively. While in a RC-ST codes family, the $P - N_z/2$ ST symbols of branch labels of the punctured ST code and the first $P - N_z/2$ ST symbols of branch labels of the mother ST code are deferent at least in one ST symbol depending on the PP structure. This is because of the symbol shit process and the restriction on the columns of the PP's explained earlier, and the fact that a ST symbol is a concatenation of the $N$ constellation symbols where each symbol corresponds to one of the $N$ transmit antennas ($\mathbf{s}_t = s_t^1 s_t^2 \cdots s_t^N$).

# CHAPTER 3

# PERFORMANCE ANALYSIS AND DESIGN CRITERIA OF SYMBOL PUNCTURED SPACE-TIME CODES

## 3.1 INTRODUCTION

Performance criteria of ST codes given in Chapter one have been implemented by applying the performance criteria of MTCM codes in fading channels to multiple transmit antennas. Unfortunately, performance criteria of symbol punctured MTCM codes [46] are not applicable to symbol PST codes, because of the symbol shifting process described in Chapter two. However, the performance criteria of ST codes in fading channels studied in Chapter one can be applied to symbol PST

codes but by taking the effects of puncturing in the computation of the PST code metrics. From the resulting bounds on the PEP, design criteria of symbol PST codes are obtained.

In this Chapter, performance of symbol PST coding systems are analyzed for two fading channel models; quasi-static and rapid fading channels described in Chapter one. The effects of puncturing on the code performance especially on the PEP bounds and code metrics are studied. Then symbol PST codes design criteria for both channel models are established. This Chapter is concluded with designed codes and numerical results.

## 3.2 Performance Analysis and Design Criteria

As in Chapter one, this analysis starts by stating notations. Let the encoder-mapper output symbols matrix denoted by $\mathbf{x}$ be:

$$\mathbf{x} = \begin{bmatrix} x_1^1 & x_2^1 & \cdots & x_l^1 \\ x_1^2 & x_2^2 & \cdots & x_l^2 \\ \vdots & \vdots & \ddots & \vdots \\ x_1^N & x_2^N & \cdots & x_l^N \end{bmatrix} \tag{3.1}$$

where $l$ is the un-punctured frame length, the $i^{th}$ row $\mathbf{x}^i = [x_1^i, x_2^i, \cdots, x_l^i]$ is the encoder-mapper output symbols sequence corresponding to the $i^{th}$ transmit antenna ($i = 1, 2, \cdots, N$), and the $n^{th}$ column $\mathbf{x}_n = \left[x_n^1, x_n^2, \cdots, x_n^N\right]^T$ is the $N$ encoder-mapper output symbols, due to the $n^{th}$ $k$-tuple input bits, that are passed to the puncturing circuit ($n = 1, 2, \cdots, l$). The transmitted codeword matrix $\mathbf{c}$ after the puncturing circuit is given by:

$$\mathbf{c} = \begin{bmatrix} c_1^1 & c_2^1 & \cdots & c_{l_p}^1 \\ c_1^2 & c_2^2 & \cdots & c_{l_p}^2 \\ \vdots & \vdots & \ddots & \vdots \\ c_1^N & c_2^N & \cdots & c_{l_p}^N \end{bmatrix} \tag{3.2}$$

where $l_p$ is the punctured transmitted frame length, the $i^{th}$ row $\mathbf{c}^i = \left[c_1^i, c_2^i, \cdots, c_{l_p}^i\right]$ is the puncturing circuit output symbols sequence transmitted via the $i^{th}$ transmit antenna ($i = 1, 2, \cdots, N$), and the $t^{th}$ column $\mathbf{c}_t = \left[c_t^1, c_t^2, \cdots, c_t^N\right]^T$ is the transmitted ST symbol at time instance $t$ ($t = 1, 2, \cdots, l_p$). In [1] ,[3], and others, each column $\mathbf{c}_t$ of the codeword matrix $\mathbf{c}$ is considered as a single ST symbol, while in this analysis each element $c_t^i$, $t = 1, 2, \cdots, l_p$ $i = 1, 2, \cdots, N$, of the codeword matrix $\mathbf{c}$ is considered as a single symbol. So each ST symbol consists of $N$ symbols and when using the word symbol it refers to an element $c_t^i$ in the codeword matrix $\mathbf{c}$ unless stated otherwise. The elements of the codeword matrix $\mathbf{c}$ are given in

terms of the elements of the matrix $\mathbf{x}$ and the MPP as:

$$c_t^i = \sum_{n=t+\frac{N_z}{2}}^{t+\frac{N_z}{2}+\left[\frac{t-1}{P-\frac{N_z}{2}}\right]} p_{i,g} \cdot x_n^i \tag{3.3}$$

where $[\cdot]$ is $integer\,(\cdot)$, $g$ is a function of $t$ and $n$:

$$g = \left(n - 1 + \frac{N_z}{2}\left(t - \left[\frac{t-1}{P-\frac{N_z}{2}}\right] - 1\right)\right)\ modulo - \left(\left(P - \frac{N_z}{2}\right)\left(\frac{N_z}{2} + 1\right)\right) + 1 \tag{3.4}$$

and $p_{i,g}$ is the $i^{th}$ element in the $g^{th}$ column of the MPP, $g = 1, 2, \cdots, (P - N_z/2)(N_z/2+1)$, $i = 1, 2, \cdots, N$, $t = 1, 2, \cdots, l_p$, and $1 \leq n \leq l$. There is only one non zero element in the summation in (3.3).

At the receiver, the received signal at the $j^{th}$ receive antenna ($j = 1, 2, \cdots, M$) is a noisy superposition of the $N$ transmitted symbols corrupted by channel fading. The received signal matrix $\mathbf{r}$ equals:

$$\mathbf{r} = \begin{bmatrix} r_1^1 & r_2^1 & \cdots & r_{l_p}^1 \\ r_1^2 & r_2^2 & \cdots & r_{l_p}^2 \\ \vdots & \vdots & \ddots & \vdots \\ r_1^M & r_2^M & \cdots & r_{l_p}^M \end{bmatrix} \tag{3.5}$$

and $\mathbf{r}_t = \left[r_t^1, r_t^2, \cdots, r_t^M, \right]^T$ is the received sequence at the $M$ receive antennas at reception time $t$, thus the signal at the $j^{th}$ receive antenna after the match filter is

given by:

$$r_t^j = \sum_{i=1}^{N} \alpha_{i,j}(t)\, c_t^i + n_t^j \tag{3.6}$$

where $n_t^j$ is the noise component of the $j^{th}$ receive antenna at time $t$, and it is modeled as independent complex Gaussian random variable with zero mean and variance $N_0/2$ per dimension. The fade coefficients $\alpha_{i,j}(t)$, $t = 1, 2, \cdots, l_p$ $i = 1, 2, \cdots, N$ $j = 1, 2, \cdots, M$, are modeled as complex Gaussian random variables with zero mean and variance $1/2$ per dimension, and vary independently from one symbol interval to other in rapid fading channels and from one frame interval to other in quasi-static fading channels. Moreover, the fade coefficients for paths from the $N$ transmit antennas to the $M$ receive antennas at time $t$ are uncorrelated. Hence, the received signals at time $t$ can be written in terms of the transmitted symbols as:

$$\mathbf{r}_t = \mathbf{a}(t)\, \mathbf{c}_t + \mathbf{n}_t \tag{3.7}$$

where $\mathbf{a}(t)$ is the fade coefficients matrix at time $t$, which equals:

$$\mathbf{a}(t) = \begin{bmatrix} \alpha_{1,1}(t) & \alpha_{2,1}(t) & \cdots & \alpha_{N,1}(t) \\ \alpha_{1,2}(t) & \alpha_{2,2}(t) & \cdots & \alpha_{N,2}(t) \\ \vdots & \vdots & \ddots & \vdots \\ \alpha_{1,M}(t) & \alpha_{2,M}(t) & \cdots & \alpha_{N,M}(t) \end{bmatrix} \tag{3.8}$$

and $\mathbf{n}_t = \left[n_t^1, n_t^2, \cdots, n_t^M\right]^T$ is the noise vector at time $t$. The row $\mathbf{a}_j(t)$ of the fade

matrix is the channel path gains from the $N$ transmit antennas to the $j^{th}$ receive antenna at time $t$.

$$\mathbf{a}_j(t) = [\alpha_{1,j}(t) \quad \alpha_{2,j}(t) \quad \cdots \quad \alpha_{N,j}(t)] \tag{3.9}$$

The maximum-likelihood decoder selects the path with the minimum cumulative branch metric, which is given by:

$$\sum_{t=1}^{l_p}\sum_{j=1}^{M}\left|r_t^j - \sum_{i=1}^{N}\alpha_{i,j}(t)\,c_t^i\right|^2 \tag{3.10}$$

Substituting (3.3) in (3.10), results in:

$$\sum_{t=1}^{l_p}\sum_{j=1}^{M}\left|r_t^j - \sum_{i=1}^{N}\alpha_{i,j}(t)\sum_{n=t+\frac{N_z}{2}\left[\frac{t-1}{P-\frac{N_z}{2}}\right]}^{t+\frac{N_z}{2}+\frac{N_z}{2}\left[\frac{t-1}{P-\frac{N_z}{2}}\right]} p_{i,g}\cdot x_n^i\right|^2 \tag{3.11}$$

The decoder will decides on the sequence (codeword matrix) $\mathbf{e}$ in favor of the transmitted sequence $\mathbf{c}$ when:

$$\sum_{t=1}^{l_p}\sum_{j=1}^{M}\left|r_t^j - \sum_{i=1}^{N}\alpha_{i,j}(t)\,c_t^i\right|^2 \geq \sum_{t=1}^{l_p}\sum_{j=1}^{M}\left|r_t^j - \sum_{i=1}^{N}\alpha_{i,j}(t)\,e_t^i\right|^2 \tag{3.12}$$

The probability of this event is the conditional pairwise error probability and it is

well approximated by [1]:

$$P\left(\mathbf{c}\rightarrow\mathbf{e}|\alpha_{i,j}\left(t\right),i,j,t\right)\leq\exp\left(-d^{2}\left(\mathbf{c},\mathbf{e}\right)\frac{E_{b}}{4N_{0}}\right) \tag{3.13}$$

which is the standard approximation to the Gaussian tail function. $E_s$ is replaced by $E_b$ since they are equal for un-punctured QPSK ST codes and differ by $k_c$ for punctured QPSK codes. The expression $d^2(\mathbf{c},\mathbf{e})$ is the square (modified) Euclidean distance and it is given by:

$$d^{2}\left(\mathbf{c},\mathbf{e}\right)=\sum_{t=1}^{l_{p}}\sum_{j=1}^{M}\left|\sum_{i=1}^{N}\alpha_{i,j}\left(t\right)\left(c_{t}^{i}-e_{t}^{i}\right)\right|^{2} \tag{3.14}$$

Let $\hat{\mathbf{x}}$ be the encoder-mapper output symbols sequence that after puncturing produce the sequence $\mathbf{e}$. Substituting the value of $e_t^i$ in terms of $\widehat{x_n^i}$ and (3.3) in equation (3.14) results in:

$$d^{2}\left(\mathbf{c},\mathbf{e}\right)=\sum_{t=1}^{l_{p}}\sum_{j=1}^{M}\left|\sum_{i=1}^{N}\alpha_{i,j}\left(t\right)\left(\sum_{n=t+\frac{N_{z}}{2}\left[\frac{t-1}{P-\frac{N_{z}}{2}}\right]}^{t+\frac{N_{z}}{2}+\frac{N_{z}}{2}\left[\frac{t-1}{P-\frac{N_{z}}{2}}\right]}p_{i,g}\cdot\left(x_{n}^{i}-\widehat{x_{n}^{i}}\right)\right)\right|^{2} \tag{3.15}$$

### 3.2.1 Common Design criterion and Puncturing Patten Structure

Before continuing the analysis in fading channels, a common design criterion on the mother ST code is obtained and the effects of the PP structure are studied.

To minimize the effects of puncturing on the PST system performance, the square Euclidean distance of the PST code (3.15) between all codeword pairs should be maximized. For symbol PST codes, the square Euclidean distance is mainly dependent on the mother ST code, puncturing period and the PP structure. To maximize the square Euclidean distance of the PST codes for any puncturing period and PP structure, there should be a design criterion on the mother ST code that is valid for both quasi-static and rapid fading channels.

In the original ST systems, the encoder-mapper output symbols $N$ streams are modulated and transmitted via the $N$ transmit antennas. Thus the square Euclidean distance of the un-punctured ST code (1.12) could be written directly in terms of the encoder-mapper output ST symbols as:

$$d^2(\mathbf{c},\mathbf{e}) = \sum_{n=1}^{l}\sum_{j=1}^{M}\left|\sum_{i=1}^{N}\alpha_{i,j}(n)\left(x_n^i - \widehat{x_n^i}\right)\right|^2 \tag{3.16}$$

It is clear that the square Euclidean distance between the two codewords $\mathbf{c}$ and $\mathbf{e}$ equals the summation of the square Euclidean distance between the encoder-mapper output ST symbols $x_n^1 x_n^2 \cdots x_n^N$ and $\widehat{x_n^1}\widehat{x_n^2}\cdots\widehat{x_n^N}$ $(n = 1, 2, \cdots, l)$ multiplied by the channel gains. Thus to maximize the square Euclidean distance of the mother ST code, the square Euclidean distance between the encoder-mapper output ST symbols $x_n^1 x_n^2 \cdots x_n^N$ and $\widehat{x_n^1}\widehat{x_n^2}\cdots\widehat{x_n^N}$ $(n = 1, 2, \cdots, l)$ should be maximized.

However, this is not valid for PST codes because of the shift of symbols such

that the encoder-mapper output ST symbol is not the transmitted ST symbol. Consequently, for the QPSK symbol PST code, to maximize the square Euclidean distance between all codeword pairs $(\mathbf{c}, \mathbf{e})$, the square Euclidean distance between the encoder-mapper output symbols $x_n^i$ and $\widehat{x_n^i}$ $(n = 1, 2, \cdots, l \; i = 1, 2, \cdots, N)$ should be maximized. This is equivalent to maximize the symbol-wise Hamming distance $(\Delta_H)$ between the encoder-mapper output ST symbols $x_n^1 x_n^2 \cdots x_n^N$ and $\widehat{x_n^1}\widehat{x_n^2} \cdots \widehat{x_n^N}$ $(n = 1, 2, \cdots, l)$.

**Definition 3.1** *The symbol-wise Hamming distance $\Delta_H$ between two ST symbols $x_n^1 x_n^2 \cdots x_n^N$ and $\widehat{x_n^1}\widehat{x_n^2} \cdots \widehat{x_n^N}$ equals the number of places where $x_n^i \neq \widehat{x_n^i}$ for $i = 1, 2, \cdots, N$*

The symbol-wise Hamming distance $\Delta_H$ does not necessarily equal the ST symbol-wise Hamming distance $\delta_H$. The following example illustrates the deference between $\Delta_H$ and $\delta_H$.

**Example 3.1** *Consider the two ST symbols (00) and (01) or (000) and (010), then in this case both $\Delta_H$ and $\delta_H$ equal one. However, for the two ST symbols (00) and (12) or (102) and (113), $\Delta_H$ equals two while $\delta_H$ equals one.*

By looking at the definition of $\Delta_H$, it is observed that maximizing $\Delta_H$ between two ST symbols, will maximize $\delta_H$. The maximum value of $\Delta_H$ between two ST symbols is $N$, which corresponds to the maximum value of $\delta_H$ between the two ST symbols that is one. For a ST code, the maximum value of the symbol-wise

Hamming distance $\Delta_H$ between two codewords with the ST symbol-wise Hamming distance $\delta_h$, is $N \cdot \delta_H$. The symbol-wise Hamming distance $\Delta_H$ could easily be maximized for a ST code by maximizing the symbol-wise Hamming distance between branches diverging from and merging into the same state.

The selection of appropriate puncturing period is application dependent since it affects the data rate, the decoder complexity, and the reliability of PST codes family. However, for a given period, the PP structure design is mainly dependent on the mother ST code. Maximizing $\Delta_H$ simplify the design of PP's for best performance in both quasi-static and rapid fading channels. ST codes with maximum $\Delta_H$, would perform better as the zeros in the PP are far from each other. That means, for a given puncturing period, all the remaining $P - N_z/2$ symbols from the encoder-mapper output $P$ symbols corresponding to one of the $N$ transmit antennas are shifted such that the effect of the punctured symbols are distributed over the transmitted $P - N_z/2$ ST symbols. For example, ST code punctured using period three PP-(5) shown in Figure 2.8(5) is expected to outperform the same mother ST code but punctured using period three PP-(1) shown in Figure 2.8(1).

From the above analysis, two design criteria are derived, the first is the maximization of symbol-wise Hamming distance $\Delta_H$ and it is related to the design of the mother ST code. The second one is for ST code with maximum $\Delta_H = N \cdot \delta_h$ and a given puncturing period, the design of the PP for best performance is simply by separating the punctured symbol in the PP as far as possible.

### 3.2.2 QUASI-STATIC RAYLEIGH FADING CHANNELS

For quasi-static fading channels, the fade coefficients remain constant during frame transmission time $l_p$ and vary independently from one frame to another. Therefore

$$\alpha_{i,j}(1) = \alpha_{i,j}(2) = \cdots = \alpha_{i,j}(l_p) = \alpha_{i,j}$$

and the $j^{th}$ row of the coefficients matrix will be:

$$\mathbf{a}_j = [\alpha_{1,j} \quad \alpha_{2,j} \quad \cdots \quad \alpha_{N,j}] \tag{3.17}$$

Thus, the square Euclidean distance (3.15) can be written as:

$$d^2(\mathbf{c},\mathbf{e}) = \sum_{j=1}^{M}\sum_{i=1}^{N}\sum_{i'=1}^{N}\alpha_{i,j}\overline{\alpha_{i',j}}\sum_{t=1}^{l_p}\sum_{n=t+\frac{N_z}{2}\left[\frac{t-1}{P-\frac{N_z}{2}}\right]}^{t+\frac{N_z}{2}+\frac{N_z}{2}\left[\frac{t-1}{P-\frac{N_z}{2}}\right]} p_{i,g}\left(x_n^i - \widehat{x_n^i}\right)\overline{p_{i',g}\left(x_n^{i'} - \widehat{x_n^{i'}}\right)} \tag{3.18}$$

that could be manipulated to arrive at:

$$d^2(\mathbf{c},\mathbf{e}) = \sum_{j=1}^{M}\mathbf{a}_j\mathbf{A}(\mathbf{c},\mathbf{e})\,\mathbf{a}_j^H \tag{3.19}$$

where

$$A_{i,i'}(\mathbf{c},\mathbf{e}) = \sum_{t=1}^{l_p} \sum_{n=t+\frac{N_z}{2}}^{t+\frac{N_z}{2}+\frac{N_z}{2}\left[\frac{t-1}{P-\frac{N_z}{2}}\right]} p_{i,g}\left(x_n^i - \widehat{x_n^i}\right)\overline{p_{i',g}\left(x_n^{i'} - \widehat{x_n^{i'}}\right)} \tag{3.20}$$

By construction, $\mathbf{A}(\mathbf{c},\mathbf{e})$ has a square root $\mathbf{B}(\mathbf{c},\mathbf{e})$ (codeword difference matrix) that equals:

$$\mathbf{B}(\mathbf{c},\mathbf{e}) = \begin{bmatrix} c_1^1 - e_1^1 & c_2^1 - e_2^1 & \cdots & c_{l_p}^1 - e_{l_p}^1 \\ c_1^2 - e_1^2 & c_2^2 - e_2^2 & \cdots & c_{l_p}^2 - e_{l_p}^2 \\ \vdots & \vdots & \ddots & \vdots \\ c_1^N - e_1^N & c_2^N - e_2^N & \cdots & c_{l_p}^N - e_{l_p}^N \end{bmatrix} \tag{3.21}$$

and clearly

$$\mathbf{A}(\mathbf{c},\mathbf{e}) = \mathbf{B}(\mathbf{c},\mathbf{e}) \cdot \mathbf{B}^H(\mathbf{c},\mathbf{e}) \tag{3.22}$$

Hence $\mathbf{A}(\mathbf{c},\mathbf{e})$ is a nonnegative definite Hermitian matrix with real nonnegative eigenvalues [1]. So, there exist a unitary matrix $\mathbf{V}$ such that:

$$\mathbf{V}\mathbf{A}(\mathbf{c},\mathbf{e})\mathbf{V}^H = \mathbf{D} \tag{3.23}$$

where $\mathbf{D}$ is a real diagonal matrix of the eigenvalues of the matrix $\mathbf{A}(\mathbf{c},\mathbf{e})$, with diagonal elements $\lambda_i$, $i = 1, 2, \cdots, N$ counting multiplicity and $\lambda_1 \geq \lambda_2 \geq \cdots \geq \lambda_n \geq 0$. The rows $[\mathbf{v}_1, \mathbf{v}_2, \cdots, \mathbf{v}_N]$, (eigenvectors of $\mathbf{A}(\mathbf{c},\mathbf{e})$) of $\mathbf{V}$ form a complete orthonormal basis of the $N$-dimensional vector space.

Using the above results,(3.19) can be written as:

$$d^2(\mathbf{c},\mathbf{e}) = \sum_{j=1}^{M}\sum_{i=1}^{N} \lambda_i \left|\beta_{i,j}\right|^2 \tag{3.24}$$

where $\beta_{i,j} = \mathbf{a}_j \cdot \mathbf{v}_i$. Substituting (3.24) in (3.13) leads to:

$$P(\mathbf{c} \to \mathbf{e}|\alpha_{i,j}, i, j) \leq \exp\left(-\frac{E_b}{4N_0}\sum_{j=1}^{M}\sum_{i=1}^{N} \lambda_i \left|\beta_{i,j}\right|^2\right) \tag{3.25}$$

The $\beta_{i,j}$ are independent complex Gaussian random variables with variance 1/2 per dimension and mean value $E[\mathbf{a}_j \cdot \mathbf{v}_i]$. Letting

$$K_{i,j} = \left|E[\beta_{i,j}]\right|^2 = \left|E[\mathbf{a}_j] \cdot E[\mathbf{v}_i]\right|^2 = \left|[E[a_{1,j}] \quad E[a_{2,j}] \quad \cdots \quad E[a_{N,j}]] \cdot \mathbf{v}_i\right|^2 \tag{3.26}$$

thus $|\beta_{i,j}|$ are independent Rician distributions [1] with probability density function (pdf):

$$p(|\beta_{i,j}|) = 2\left|\beta_{i,j}\right| \exp\left(-\left|\beta_{i,j}\right|^2 - K_{i,j}\right) I_0\left(2\left|\beta_{i,j}\right|\sqrt{K_{i,j}}\right) \qquad |\beta_{i,j}| \geq 0 \tag{3.27}$$

where $I_0(\cdot)$ is the zero-order modified Bessel function of the first kind. Therefore the unconditioned upper bound on the probability of error is simply computed by averaging the right hand side of inequality (3.25) with respect to independent

Rician distribution of $|\beta_{i,j}|$ to arrive at [1]:

$$P(\mathbf{c} \to \mathbf{e}) \leq \prod_{j=1}^{M} \left( \prod_{i=1}^{N} \frac{1}{1 + \frac{E_b}{4N_0}\lambda_i} \exp\left( -\frac{K_{i,j}\frac{E_b}{4N_0}\lambda_i}{1 + \frac{E_b}{4N_0}\lambda_i} \right) \right) \tag{3.28}$$

A special case of Rayleigh fading where $E[\alpha_{i,j}] = 0$ and thus $K_{i,j} = 0$ results in an upper bound on PEP given by:

$$P(\mathbf{c} \to \mathbf{e}) \leq \left( \prod_{i=1}^{N} \left( 1 + \lambda_i \frac{E_b}{4N_0} \right) \right)^{-M} \tag{3.29}$$

Let $r$ denotes the rank of $\mathbf{A}(\mathbf{c}, \mathbf{e})$, then there are exactly $r$ nonzero eigenvalues of $\mathbf{A}(\mathbf{c}, \mathbf{e})$. Therefore, inequality (3.29) can be written as:

$$P(\mathbf{c} \to \mathbf{e}) \leq \left( \prod_{i=1}^{r} \lambda_i \right)^{-M} \left( \frac{E_b}{4N_0} \right)^{-rM} \tag{3.30}$$

From (3.30), a diversity advantage of $rM$ and a coding advantage of $(\lambda_1 \lambda_1 \cdot \lambda_r)^{1/r}$ are achieved.

From the above analysis, it is observed that the design criteria for un-punctured ST code in quasi-static are valid for PST codes but with one more criterion.

**Design Criteria for PST codes in Quasi-Static Fading Channels**

- Maximize the symbol-wise Hamming distance $\Delta_H$ for all distinct codeword pairs of the mother code.

- Maximize the minimum rank of the matrix $\mathbf{A}(\mathbf{c}, \mathbf{e})$ for all distinct codeword

pairs for both the mother and the punctured codes.

- Maximize the minimum determinant of $\mathbf{A}(\mathbf{c}, \mathbf{e})$ corresponding to distinct codeword pairs with the minimum rank for both the mother and the punctured ST codes.

The first design criterion is to insure the robustness of the ST code to the puncturing period and the PP structure. The second and the third criteria are the rank and determinant criteria respectively found in [1].

### 3.2.3 Rapid Rayleigh Fading Channels

In rapid fading channels, channel gains ($\alpha_{i,j}(t)$) vary independently form one symbol interval to another. Let $\mathbf{F}(\mathbf{c}_t, \mathbf{e}_t)$ denotes a ST symbols difference vector that is given by:

$$\mathbf{F}(\mathbf{c}_t, \mathbf{e}_t) = \begin{bmatrix} c_t^1 - e_t^1 & c_t^2 - e_t^2 & \cdots & c_t^N - e_t^N \end{bmatrix}^T \tag{3.31}$$

then, the $N$ by $N$ matrix $\mathbf{C}(\mathbf{c}_t, \mathbf{e}_t)$ defined by [1]:

$$\mathbf{C}(\mathbf{c}_t, \mathbf{e}_t) = \mathbf{F}(\mathbf{c}_t, \mathbf{e}_t) \cdot \mathbf{F}^H(\mathbf{c}_t, \mathbf{e}_t) \tag{3.32}$$

with the element at the $i^{th}$ row and the $i'^{th}$ column equals to:

$$\left(c_t^i - e_t^i\right)\overline{\left(c_t^{i'} - e_t^{i'}\right)} = \sum_{n=t+\frac{N_z}{2}\left\lfloor\frac{t-1}{P-\frac{N_z}{2}}\right\rfloor}^{t+\frac{N_z}{2}+\frac{N_z}{2}\left\lfloor\frac{t-1}{P-\frac{N_z}{2}}\right\rfloor} p_{i,g}\left(x_n^i - \widehat{x_n^i}\right)\overline{p_{i',g}\left(x_n^{i'} - \widehat{x_n^{i'}}\right)}$$

is a Hermitian matrix. So there exist a unitary matrix $\mathbf{V}(t)$ such that:

$$\mathbf{V}(t)\,\mathbf{C}(\mathbf{c}_t,\mathbf{e}_t)\,\mathbf{V}^H(t)=\mathbf{D}(t) \tag{3.33}$$

where $\mathbf{D}(t)$ is a real diagonal matrix with diagonal elements $D_{i,i}(t)$, $i=1,2,\cdots,N$ are the eigenvalues of $\mathbf{C}(\mathbf{c}_t,\mathbf{e}_t)$. The rows of $\mathbf{V}(t)$, $(\mathbf{v}_1(t),\mathbf{v}_2(t),\cdots,\mathbf{v}_N(t))$ eigenvectors of $\mathbf{C}(\mathbf{c}_t,\mathbf{e}_t)$ form a complete orthonormal basis of the $N$-dimensional vector space.

If $\mathbf{c}_t=\mathbf{e}_t$, then $\mathbf{C}(\mathbf{c}_t,\mathbf{e}_t)$ has all its eigenvalues equal zero. However, when $\mathbf{c}_t\neq\mathbf{e}_t$, then there is only one nonzero eigenvalue of $\mathbf{C}(\mathbf{c}_t,\mathbf{e}_t)$. Let this eigenvalue be denoted by $D_{1,1}(t)$ and let the eigenvector corresponding to $D_{1,1}(t)$ be denoted by $\mathbf{v}_1(t)$. The value of this nonzero element $D_{1,1}(t)$ is the squared Euclidean distance between $\mathbf{c}_t$ and $\mathbf{e}_t$.

$$D_{1,1}(t)=|\mathbf{c}_t-\mathbf{e}_t|^2=\sum_{i=1}^{N}\left|c_t^i-e_t^i\right|^2=\sum_{i=1}^{N}\left|\sum_{n=t+\frac{N_z}{2}}^{t+\frac{N_z}{2}+\left[\frac{t-1}{P-\frac{N_z}{2}}\right]}p_{i,g}\left(x_n^i-\widehat{x_n^i}\right)\right| \tag{3.34}$$

The square Euclidean distance $d^2(\mathbf{c},\mathbf{e})$ given in (3.15) could be expressed as:

$$d^2(\mathbf{c},\mathbf{e})=\sum_{t=1}^{l_p}\sum_{j=1}^{M}\sum_{i=1}^{N}|\beta_{i,j}(t)|^2\cdot D_{i,i}(t) \tag{3.35}$$

where $\beta_{i,j}(t)=\mathbf{a}_j(t)\cdot\mathbf{v}_i(t)$ are independent complex Gaussian variables with zero

mean and variance 1/2 per dimension, and $\mathbf{a}_j(t)$ is given by (3.9). While there is at most one nonzero eigenvalue $D_{1,1}(t)$ at each time $t$, equation (3.35) will be:

$$d^2(\mathbf{c},\mathbf{e}) = \sum_{t\in\gamma(\mathbf{c},\mathbf{e})}\sum_{j=1}^{M}|\beta_{1,j}(t)|^2 D_{1,1}(t) = \sum_{t\in\gamma(\mathbf{c},\mathbf{e})}\sum_{j=1}^{M}|\beta_{1,j}(t)|^2|\mathbf{c}_t-\mathbf{e}_t|^2 \tag{3.36}$$

where $\gamma(\mathbf{c},\mathbf{e})$ represents the set of time instances where $|\mathbf{c}_t-\mathbf{e}_t|\neq 0$ and $\delta_H$ equals the number of elements on $\gamma(\mathbf{c},\mathbf{e})$. Substituting the value of $d^2(\mathbf{c},\mathbf{e})$ from equation (3.36) into inequality (3.13), the conditional PEP upper bound will be:

$$P(\mathbf{c}\to\mathbf{e}|\alpha_{i,j}(t),i,j,t) \le \exp\left(-\sum_{t\in\gamma(\mathbf{c},\mathbf{e})}\sum_{j=1}^{M}|\beta_{1,j}(t)|^2|\mathbf{c}_t-\mathbf{e}_t|^2\frac{E_b}{4N_0}\right) \tag{3.37}$$

By noting that $D_{1,1}(t)$ given by (3.34) is the only nonzero eigenvalue, and averaging (3.37) with respect to the Rayleigh distribution of $|\beta_{1,j}(t)|$, the unconditional PEP upper bound will be [1]:

$$P(\mathbf{c}\to\mathbf{e}) \le \prod_{t\in\gamma(\mathbf{c},\mathbf{e})}\left(|\mathbf{c}_t-\mathbf{e}_t|^2\frac{E_b}{4N_0}\right)^{-M} = \prod_{t\in\gamma(\mathbf{c},\mathbf{e})}|\mathbf{c}_t-\mathbf{e}_t|^{-2M}\left(\frac{E_b}{4N_0}\right)^{-\delta_H M} \tag{3.38}$$

From this inequality, a diversity of $\delta_H M$ is achieved.

The design criteria for PST codes in rapid Rayleigh fading channels are also like that of un-punctured ST code.

**Design Criteria of PST codes in Rapid Fading Channels**

- Maximize the minimum symbol-wise Hamming distance $\Delta_H$ between all dis-

tinct codeword pairs of the mother ST code, thus the ST symbol-wise Hamming distance $\delta_H$ between all distinct codeword pairs will be maximized for both the un-punctured and the punctured ST codes.

- Maximize the product distance $d_p^2$ corresponding to the path with minimum $\delta_H$ of the mother ST code.

The first criterion, insure the maximization of $\delta_H$ of the mother code which is because of the maximization of $\Delta_H$. The second design criterion is the product distance criterion found in [1].

## 3.3 Search Criteria and Results

The design criteria for quasi-static and rapid fading channels were implemented using a C program. In addition to the design criteria, the search program excludes codes that do not satisfy the following conditions to minimize the searching time.

- The code must span all possible ST symbols for $N$ transmit antennas, which means it should contain all possible $N$ QPSK symbols concatenations. Since in this analysis there are two transmit antennas, the number of possible two QPSK symbols concatenations (QPSK symbol pairs) equals $4^2 = 16$. Codes does not satisfy this condition does not have full rank and maximum $\delta_H$ [1]. In addition, they have a lower distance between codewords which increase probability of errors.

- No QPSK pair (ST symbol) appears more than once in the branches diverging from or merging into the same state. Codes does not satisfy this conditions does not have maximum $\delta_H$.

- The encoder of the code must be linear, thus the encoder diagram contains only memory elements and exclusive ors (modulo-2 adders). This research is restricted to linear encoders only.

The search program procedure is:

- Code generation: ST codes are generated using generating matrix.

- Testing conditions: the above condtions are tested.

- Metric computations: the new code metrics such as rank, determinant and product distance are calculated.

- Comparing and selecting: the generated code metrics are compared and the code with best metric depending on the implemented design criterion is selected.

These conditions are included in the search program to minimize the searching time because condition testing does not take long time while metric computations take most of the searching time.

The search program spans all possible codes that satisfy the above conditions and the design criteria, and the codes with best metrics are selected. The search

results are shown in Figure 3.1, where five codes are found. One 4-state code that satisfy the design criteria for quasi-static and rapid fading channels is found, while it was not possible to find single 8- or 16-state code that satisfies both design criteria sets.

## 3.4 NUMERICAL RESULTS

Since the new codes satisfy the design criteria, they are excepted to have a comparable performance to the best codes in the literature. This can be shown via comparing new and best codes metrics, and performance by simulation. Metrics of the new codes are calculated and given in Table 3.1. In the same table, metrics of the best codes shown in Figure 1.2 are also given. To simplify referencing in the following section, each code is given a name in the third column.

From the table it is clearly seen that new and best codes have the same ST symbol-wise hamming distance ($\delta_H$) for the same number of states. However, the symbol-wise hamming distances ($\Delta_H$) for the new five codes are maximized. Since the maximization of $\Delta_H$ is the common criterion, it was not possible to find optimum 4- and 16-state codes that have maximum coding advantage or determinant. In contrast, the new 8-state code two (Nt8) and both 16-state codes (No16 and Nt16) have better minimum product distance than the best codes with the same number of states. These metrics does not completely describe the code performance so that the new and best codes are simulated to complete the comparison.

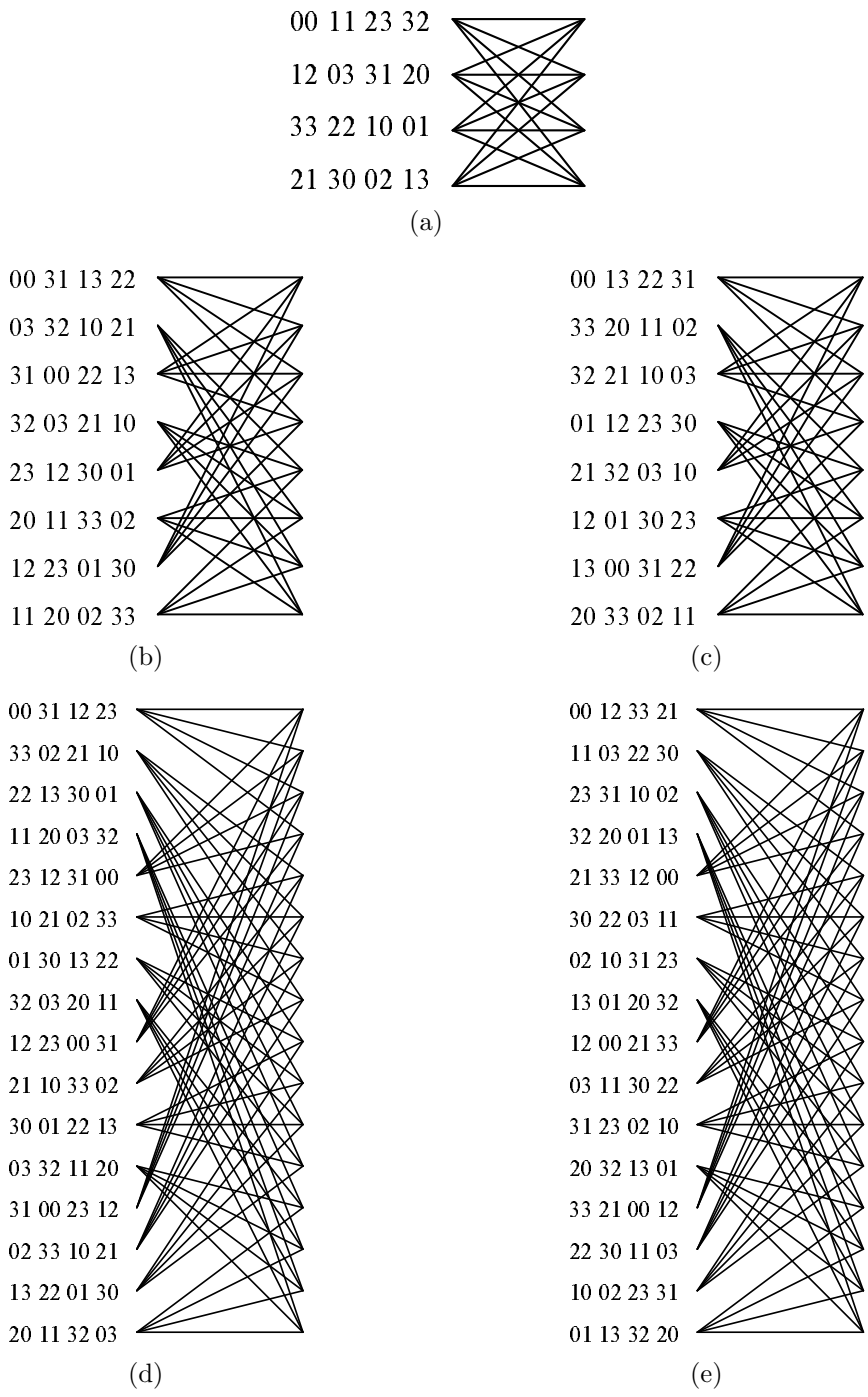


Figure 3.1: Search results for QPSK ST codes (a) 4-state QPSK (b) 8-state QPSK one (c) 8-state QPSK two (d) 16-state QPSK one (e) 16-state QPSK two

TABLE 3.1: Existing and new codes metrics

| Number of states | Source | Name | Rank | Determinant | $\Delta_H$ | $\delta_H$ | Product distance $pd_{min}$ |
|---|---|---|---|---|---|---|---|
| 4 | [1] | T4 | 2 | 4 | 2 | 2 | 4 |
| | [4] | B4 | 2 | 8 | 3 | 2 | 16 |
| | [5] | V4 | 2 | 4 | 3 | 2 | 24 |
| | new | N4 | 2 | 4 | 4 | 2 | 24 |
| 8 | [1] | T8 | 2 | 12 | 2 | 2 | 16 |
| | [4] | B8 | 2 | 16 | 3 | 2 | 24 |
| | [5] | V8 | 2 | 8 | 3 | 2 | 32 |
| | new one | No8 | 2 | 16 | 4 | 2 | 16 |
| | new two | Nt8 | 2 | 8 | 4 | 2 | 48 |
| | new high-rate | HR8 | 1 | 4 | 3 | 2 | 16 |
| 16 | [1] | T16 | 2 | 12 | 3 | 3 | 16 |
| | [4] | B16 | 2 | 32 | 4 | 3 | 64 |
| | [5] | V16 | 2 | 20 | 4 | 3 | 64 |
| | new one | No16 | 2 | 16 | 6 | 3 | 96 |
| | new two | Nt16 | 2 | 12 | 6 | 3 | 144 |

### 3.4.1 Performance in Quasi-Static Fading Channels

The new codes and the best ones have been simulated in quasi-static fading channels. The performance of the new five codes are shown in Figure 3.2. From Figure 3.3, it is seen that the optimum 4-state code B4 outperforms the V4 and N4 for one and two receive antennas by about 0.5 dB at frame error rate of $10^{-2}$, while both codes V4 and N4 outperform the reference code T4 for two receive antennas. All 8-state codes have almost identical performance for one and two receive antennas as shown in Figure 3.4. As can be seen from Figure 3.5, the 16-state codes almost have identical performance for one and two receive antennas too. The above results show that the new codes have a comparable performance in quasi-static fading channels to the existing codes. However, by construction the new codes are expected to outperform the existing codes under puncturing as will be shown next.

For puncturing period two, PP(2) is used to puncture the ST codes. In this case all the redundancy in the ST codes are deleted. For the 4-state codes as shown in Figure 3.6, N4 outperforms the optimum code B4 by about 0.5 dB and the code V4 by about one dB for one and two receive antennas. No8 and Nt8 have almost the same performance with a round 0.2 dB advantage for one receive antenna and around 0.1 dB advantage for two receive antennas to Nt8 over No8. Both code No8 and Nt8 outperform the optimum code B8 by a little more than one dB for both one and two receive antennas as shown in Figure 3.7. Figure 3.8 shows that

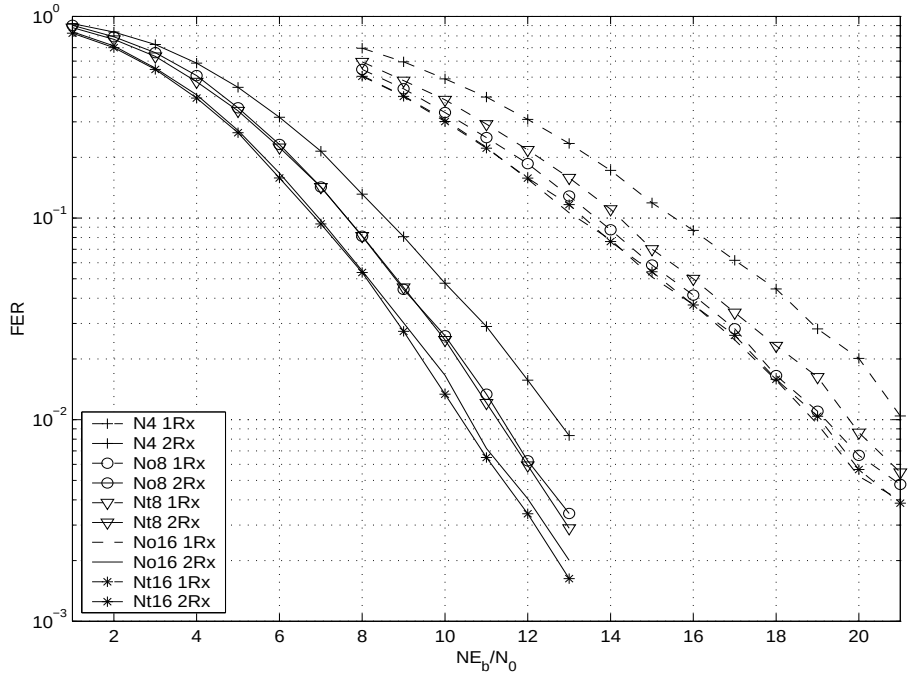


Figure 3.2: Performance of 4-, 8-, and 16-state codes in quasi-static fading channel

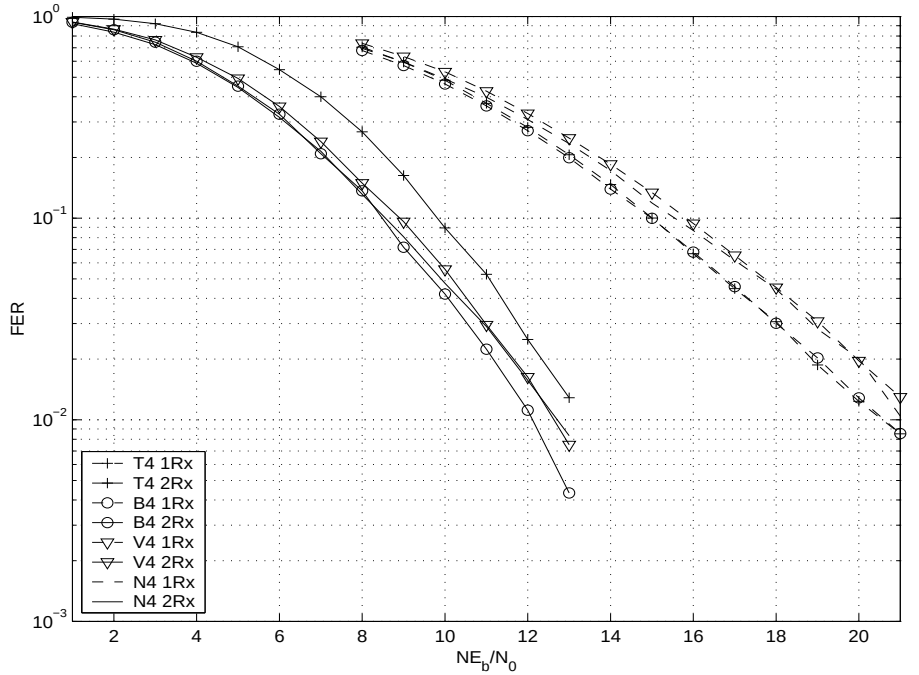


Figure 3.3: Performance comparison of 4-state codes in quasi-static fading channel

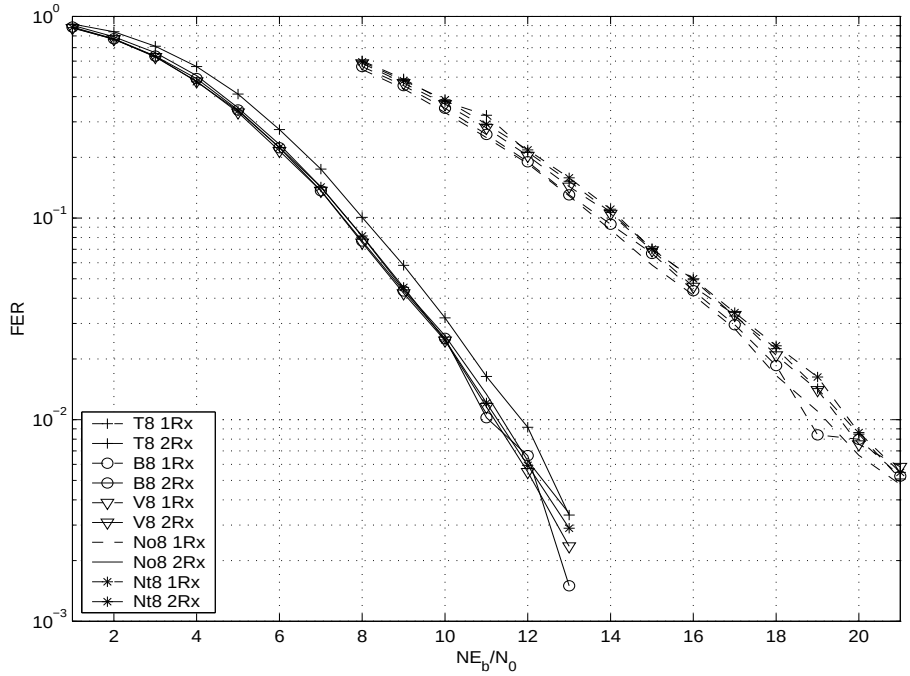


Figure 3.4: Performance comparison of 8-state codes in quasi-static fading channel

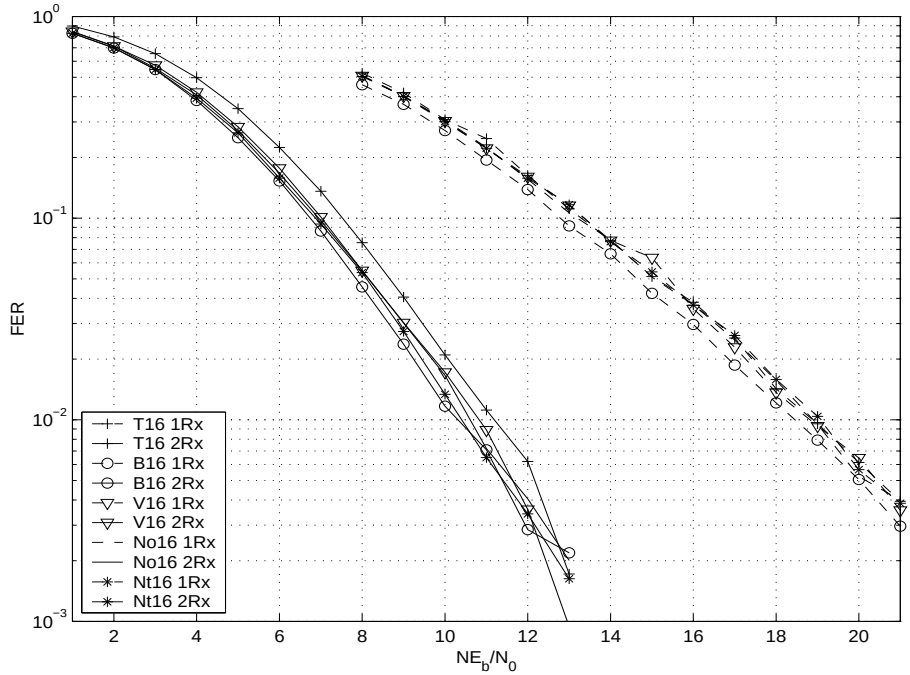


Figure 3.5: Performance comparison of 16-state codes in quasi-static fading channel

No16 and Nt16 have identical performance and also outperform V16 by more than one dB. However, the reference codes T4, T8, and T16, and the codes V8 and B16 (optimum 16-state code) have a zero performance for both one and two receive antennas. From the above results, although the new codes do not have a good performance under puncturing period two, they have a better performance than the existing codes under the same puncturing period.

Under puncturing with period three PP(5) there are some redundancy in the punctured codes. Since the codes punctured with period three have the same rate as that of the high-rate code HR8, the performance of the code HR8 found in Chapter two is compared to that of the 4- and 8-state punctured codes. The code N4 outperforms the optimum code B4 and the code V4 by about one dB and outperforms the reference code T4 by around two dB's for one receive antenna, while it outperforms the optimum code B4 by about two dB's and the codes V4 and T4 by more than three dB's for two receive antennas system (Figure 3.9). For the punctured 8-state codes with period three, the code Nt8 has an advantage of about 0.5 dB and more than one dB over No8 for one and two receive antennas respectively as it can be seen from Figure 3.10. In the other hand the code No8 outperforms V8 and T8 by two dB's and a little less than 0.5 dB for one and two receive antennas respectively, while in this case the optimum code B8 has the worst performance for both one and two receive antennas systems. The code HR8 outperforms N4 by 1.25 dB's for one receive antenna and 0.8 dB for two receive

antenna as can bee seen in Figure 3.9, while it has the same performance with around 0.2 dB advantage at high SNR and almost identical performance to Nt8 for one and two receive antennas respectively as shown in Figure 3.10. Unlike in period two where Nt16 and No16 have identical performance for one and two receive antennas, they have a similar performance only for one receive antenna and Nt16 has an advantage of 0.5 dB over No16 for two receive antennas (Figure 3.11). Both codes Nt16 and No16 outperforms all other 16-state codes by more than three dB's for one receive antenna and about 1.5 dB's for two receive antennas.

For period four, PP(6) is used. The code N4 also outperforms the other 4-state codes by about three dB's for one receive antenna and 2.5 dB's for two receive antennas as shown in Figure 3.12. Similarly, Nt8 has an advantage of about 1.25 dB's and about 0.75 dB over No8 for one and two receive antennas, where both codes outperform other 8-state codes by three dB's and two dB's for one and two receive antennas respectively (Figure 3.13). In contrast, No16 performs better than Nt16 by two dB's for one receive antenna and a little more than one dB for two receive antennas as it can be seen in Figure 3.14. This can be explained by the increasing redundancy and that No16 has a better deteminant than Nt16e. No16 outperforms other 16-state codes by about 2.5 dB's for both one and two receive antennas.

Since the decoding complexity and time increase as the puncturing period and number of state increase, only the new 4-state (N4) code is simulated with peri-

ods five and six. In Figure 3.15 shows the performance of N4 without and under puncturing with periods two, three, four, five and six. For the one receive antenna systems, most of the improvement in the performance (about four dB's) due to coding advantage (redundancy) is from period two where there is no redundancy in the punctured code to period three where there are still some redundancy available in the punctured code. N4 without puncturing has an advantage more than one dB over the punctured code with period six, while that code outperforms N4 when punctured with period five by only 0.2 dB. The performance deference increases to about one dB between punctured code with period five and punctured code with period four, and to three dB's between punctured code with period four and punctured code with period three. Similarly, for the two receive antennas systems, most of the improvement (three dB's) due to coding advantage is between punctured code with period two and that with period three. However, the performance deference between punctured code with period four and that with period three is only one dB, and between punctured code with period five and that with period four is about 0.5 dB. Punctured code with period six has identical performance to the normal (un-punctured) one, which means that the punctured code has enough redundancy to recover the transmitted frames as the normal code. Both codes outperforms that punctured with period five by about 0.25 dB. From the above results it can be seen that as the puncturing period increases, the performance of the punctured code improved and in the systems where there are enough diversity

advantage and large puncturing period, the punctured code would have identical performance to the un-punctured one.

### 3.4.2 Performance in Rapid Fading Channels

The new codes are also simulated in rapid fading channels as shown in Figure 3.16. From Figure 3.17, N4 and one of best codes in rapid fading channel V4 have identical performance and outperform B4 by about 0.1 dB and T4 the reference code by about three dB's for one receive antenna and outperform B4 by about 0.25 dB and T4 also by about three dB's for two receive antennas. For the 8-state codes as shown in Figure 3.18, the codes V8 and Nt8 have almost the same performance and outperform B8 by about one dB for one and two receive antennas, while the code B8 outperforms both No8 and T8 that have the same performance by around one dB for one and two receive antennas. The performance of No8 is expected since it is originally designed for quasi-static fading channels.

Since both new 16-state codes No16 and Nt16 have the minimum product distance better than other 16-state existing codes, it was expected that the codes No16 and Nt16 perform better than the remaining three codes in rapid fading channels. Simulation results given in Figure 3.19 show that the code Nt16 outperforms the clammed best existing code V16 and the code B16 by around 0.5 dB and the code No16 also outperforms the codes V16 and B16 by at least 0.18 dB for one and two receive antennas systems.

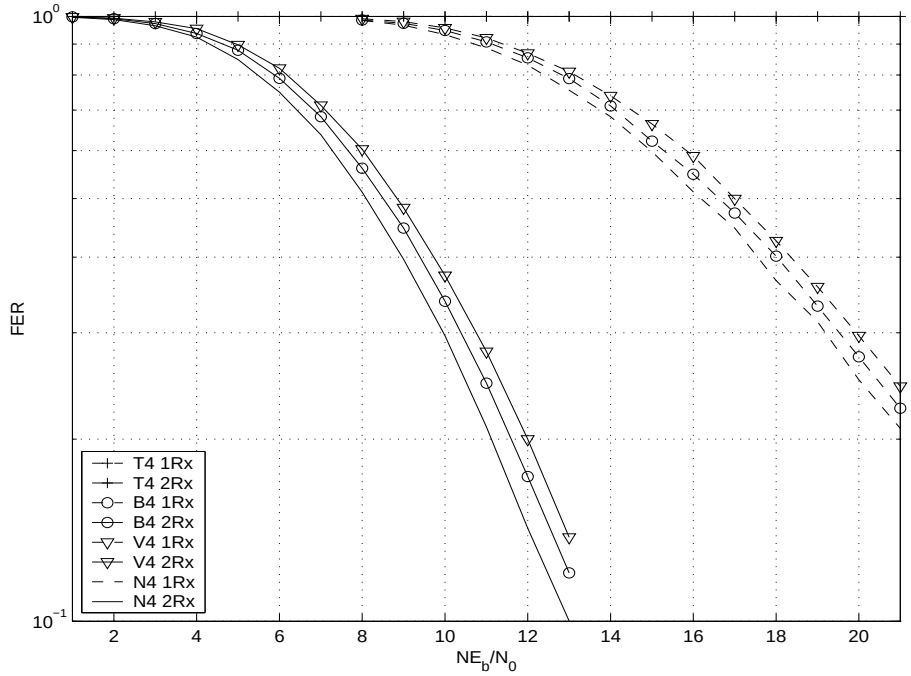


Figure 3.6: Performance of punctured 4-state codes with period 2 in quasi-static fading channel

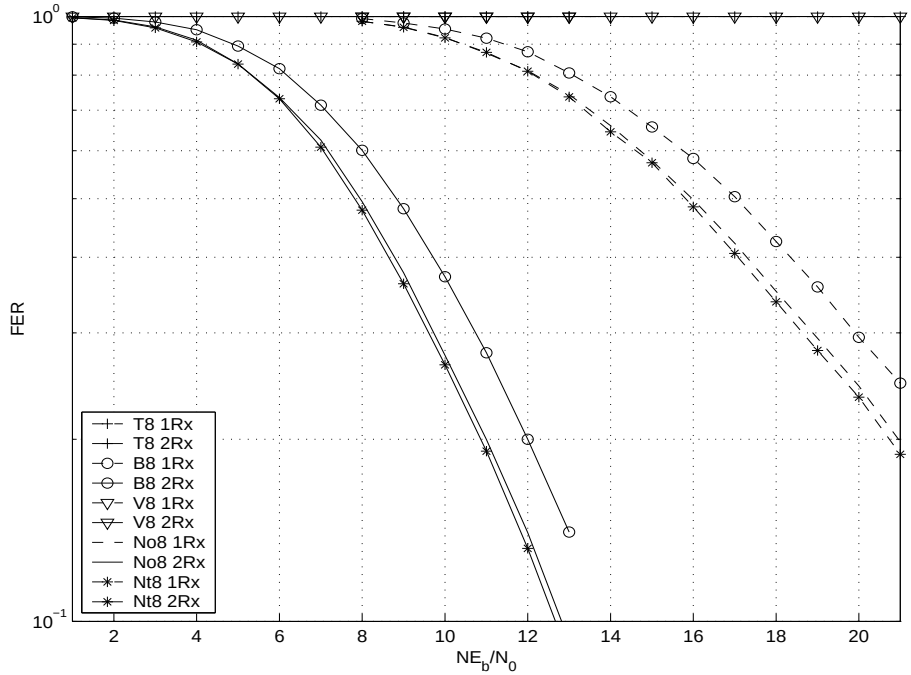


Figure 3.7: Performance of punctured 8-state codes with period 2 in quasi-static fading channel

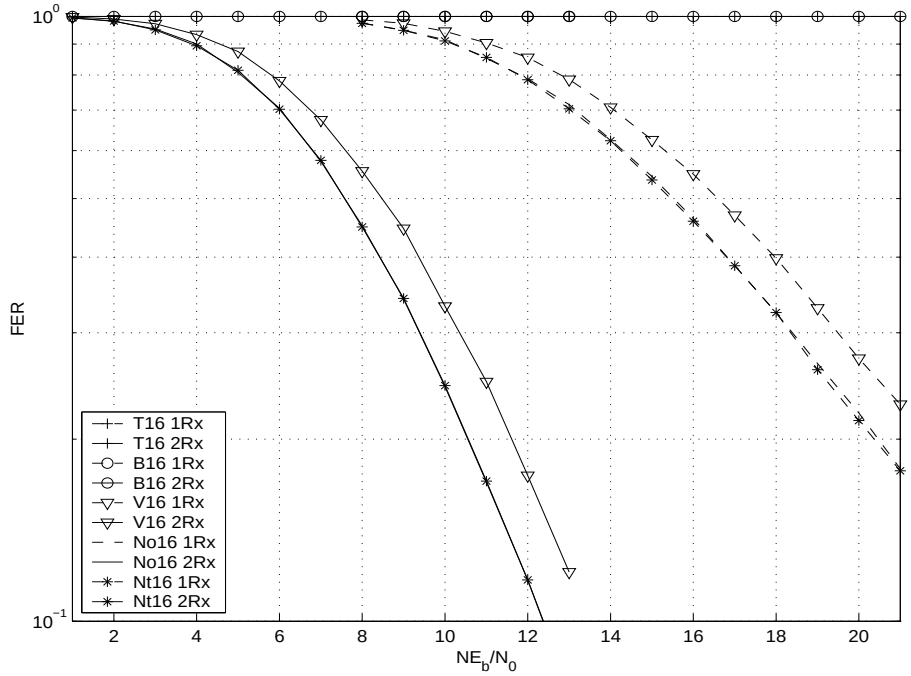


Figure 3.8: Performance of punctured 16-state codes with period 2 in quasi-static fading channel

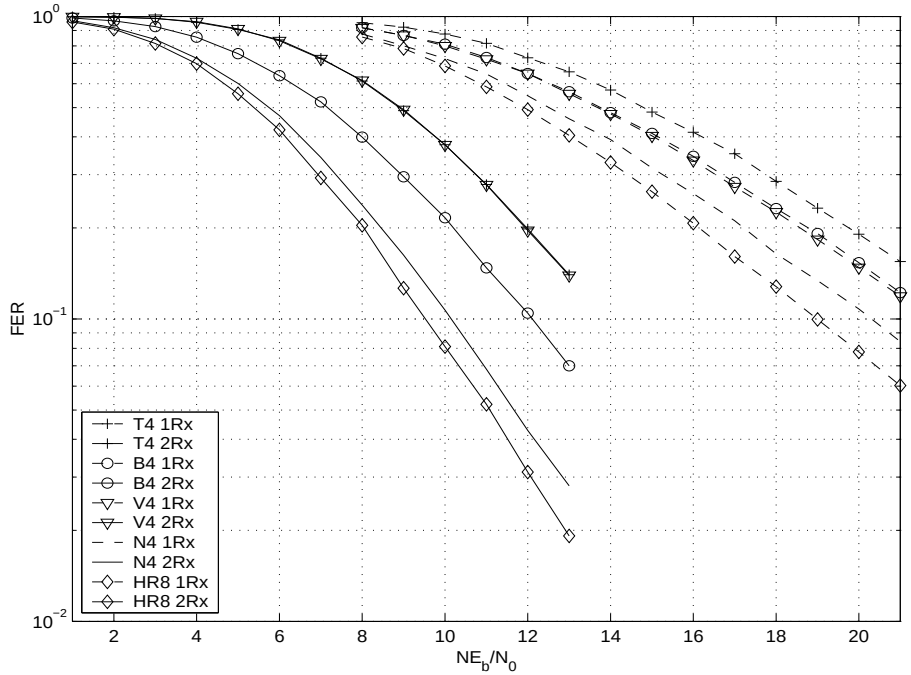


Figure 3.9: Performance of punctured 4-state codes with period 3 in quasi-static fading channel

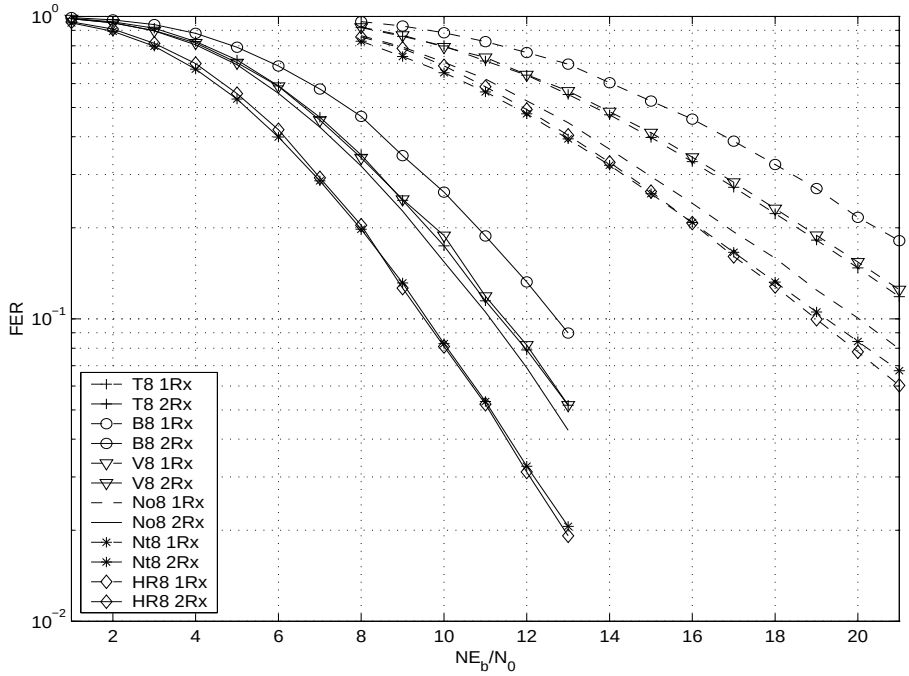


Figure 3.10: Performance of punctured 8-state codes with period 3 in quasi-static fading channel

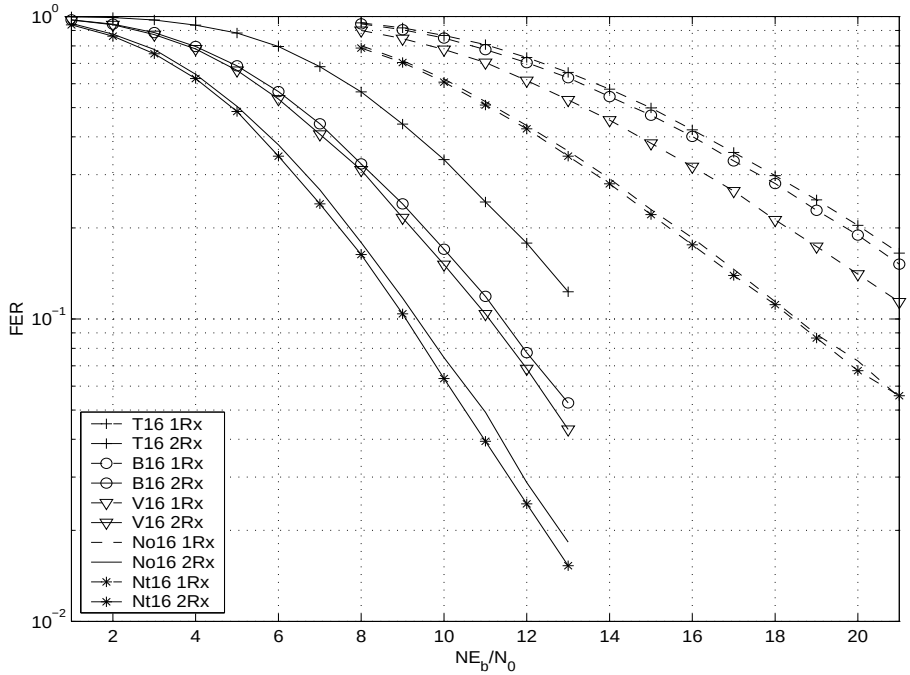


Figure 3.11: Performance of punctured 16-state codes with period 3 in quasi-static fading channel

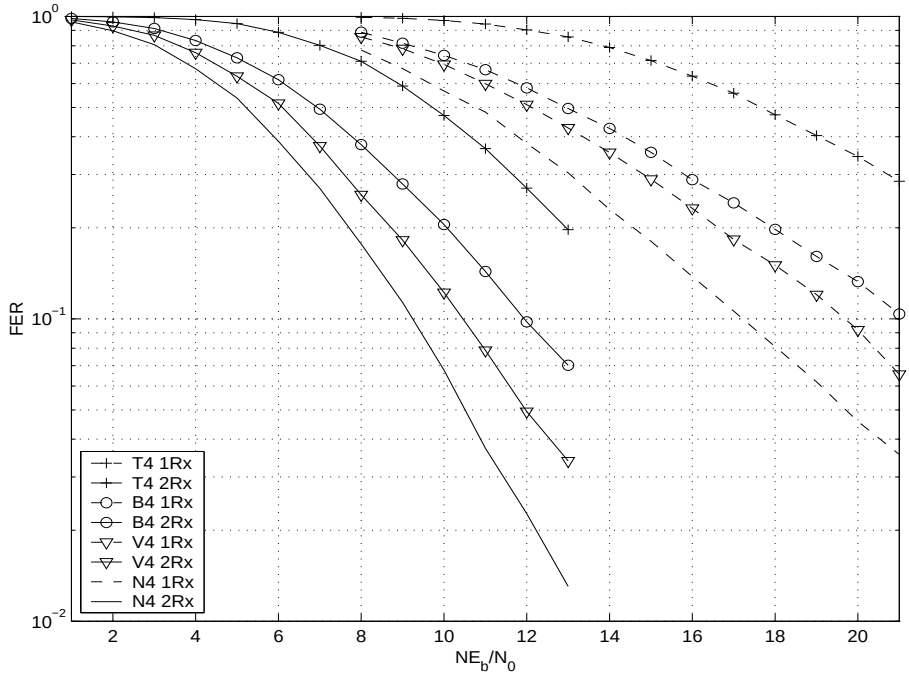


Figure 3.12: Performance of punctured 4-state codes with period 4 in quasi-static fading channel

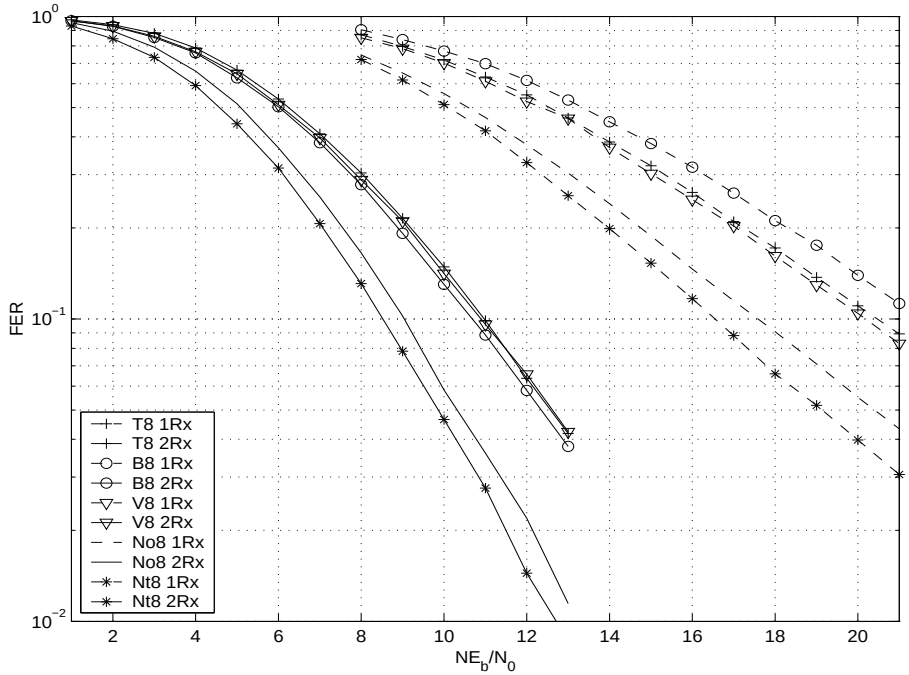


Figure 3.13: Performance of punctured 8-state codes with period 4 in quasi-static fading channel

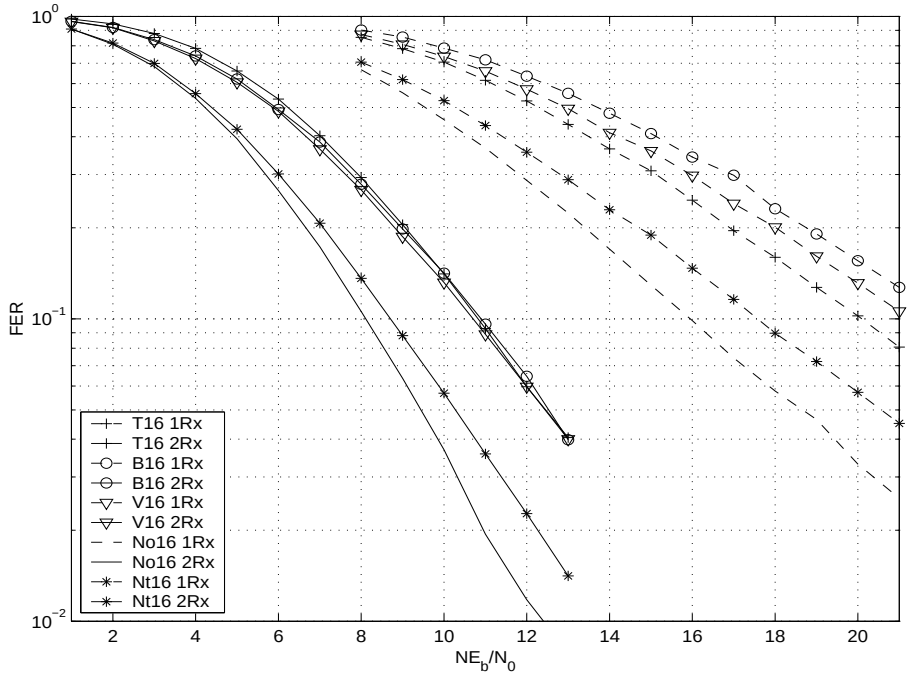


Figure 3.14: Performance of punctured 16-state codes with period 4 in quasi-static fading channel

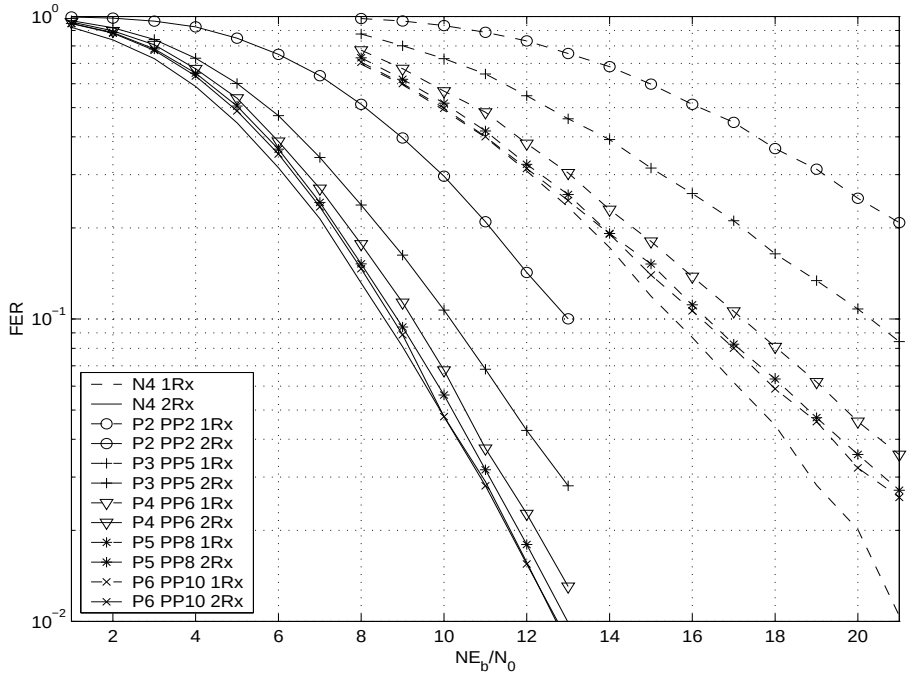


Figure 3.15: Performance of new 4-state code with deferent periods in quasi-static fading channel

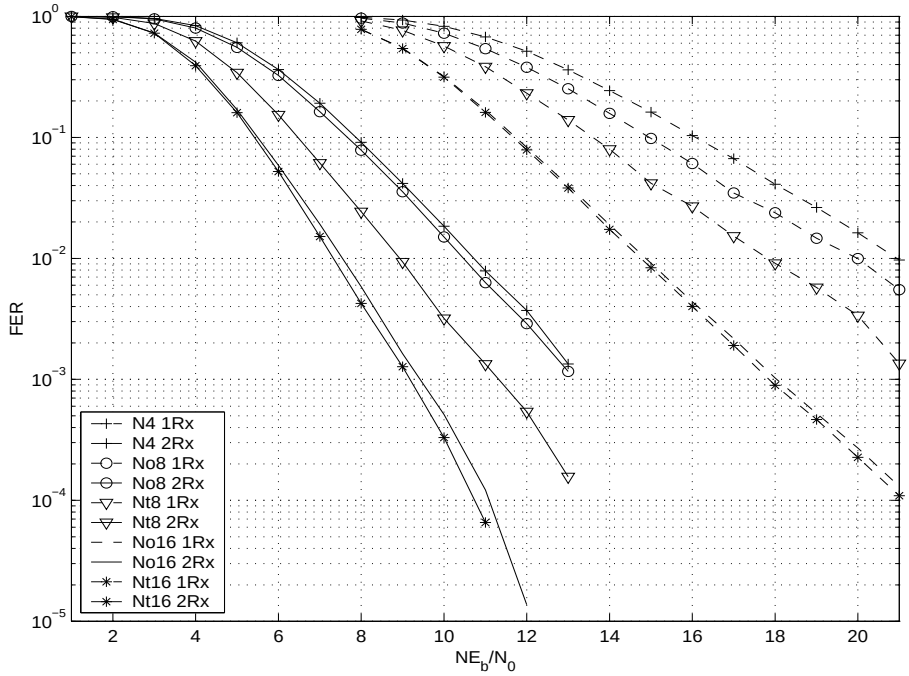


Figure 3.16: Performance of 4-, 8-, and 16-state codes in rapid fading channel

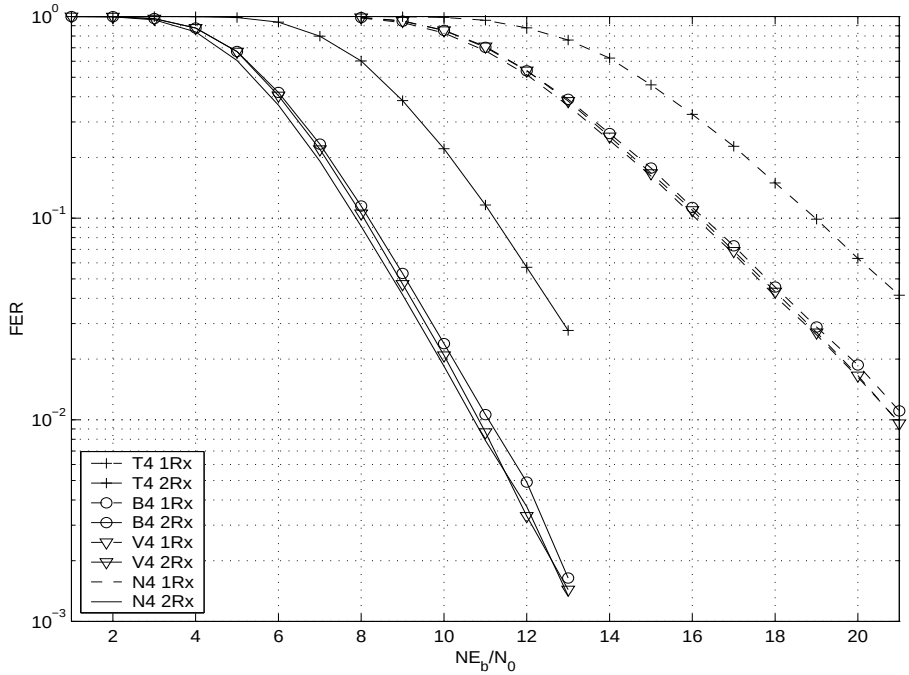


Figure 3.17: Performance comparison of 4-state codes in rapid fading channel

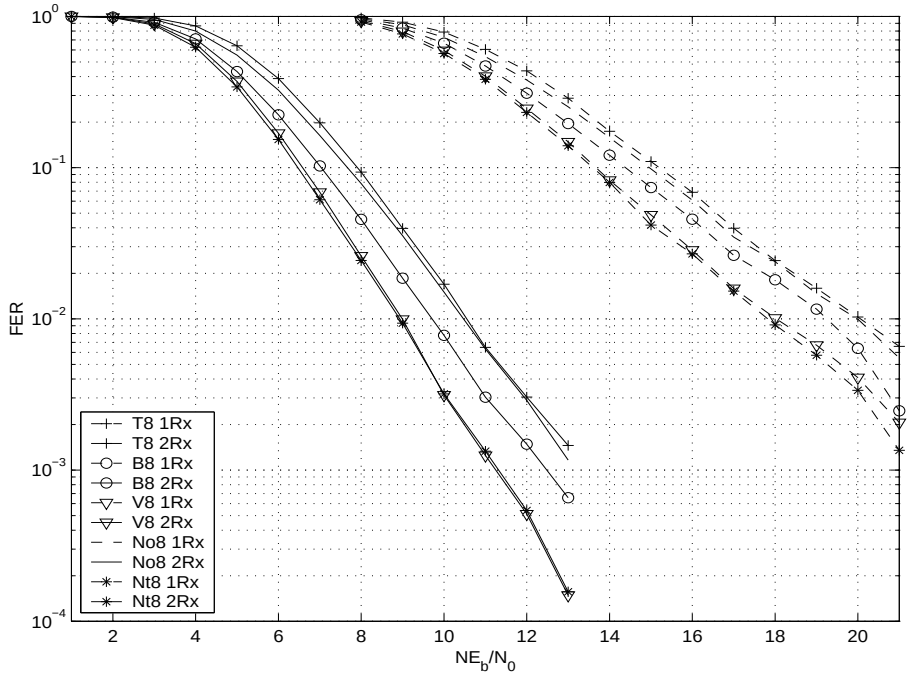


Figure 3.18: Performance comparison of 8-state codes in rapid fading channel

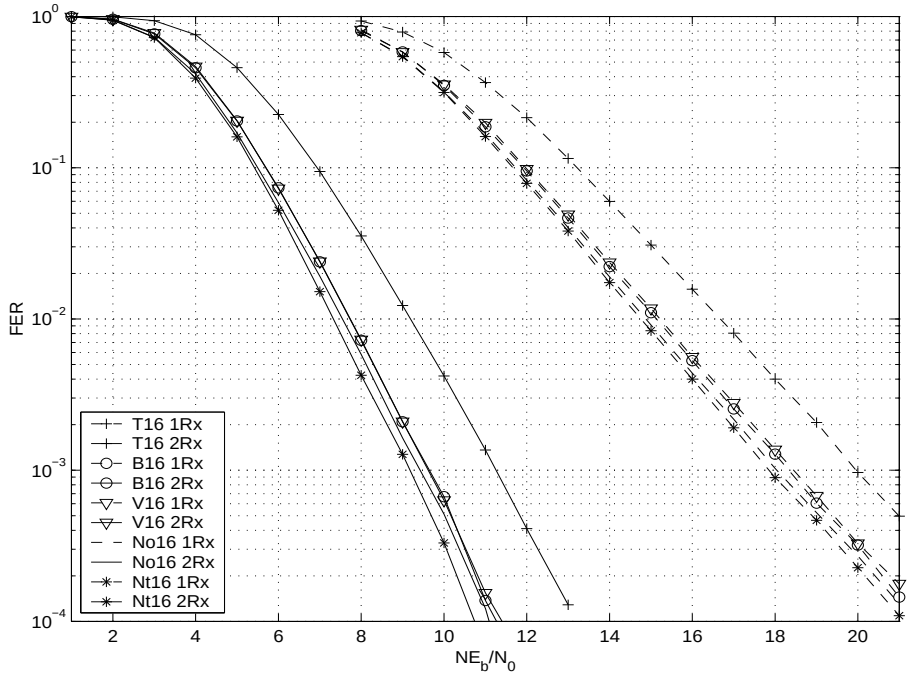


Figure 3.19: Performance comparison of 16-state codes in rapid fading channel

For the codes punctured with period two, Figures 3.20, 3.21 and 3.22 show the performance of the 4-, 8-, and 16-state respectively. Although all punctured codes do not have a good performance, the new codes outperform the existing codes by more than one dB for the 4-state case, and by more than two dB's for the 8- and 16-state cases. As expected for period three (Figures 3.23, 3.24, and 3.25 for the 4-, 8-, and 16-state codes respectively), there are improvement in the codes performance and the new codes also outperform the existing ones at least by three dB's for the three state cases. Similarly for puncturing period four, the new codes have better performance over the existing ones at least by three dB's for the one antenna systems and about two dB's for the two receive antennas systems as shown in Figures 3.26, 3.27 and 3.28. The performance advantage of the code Nt8 over the code No8 increase as the period increase while the codes No16 and Nt16 have almost the same performance for the period two, three, and four with two receive antennas, the first code outperforms the second one for the one receive antenna systems. As shown in Figure 3.29, the code N4 performance improves as the period increase.

### 3.4.3 Puncturing Pattern Structure

In the previous subsections it has been shown that the new codes have a comparable performance to the best codes without puncturing and perform much better than the existing codes under puncturing. In this subsection it will be shown via

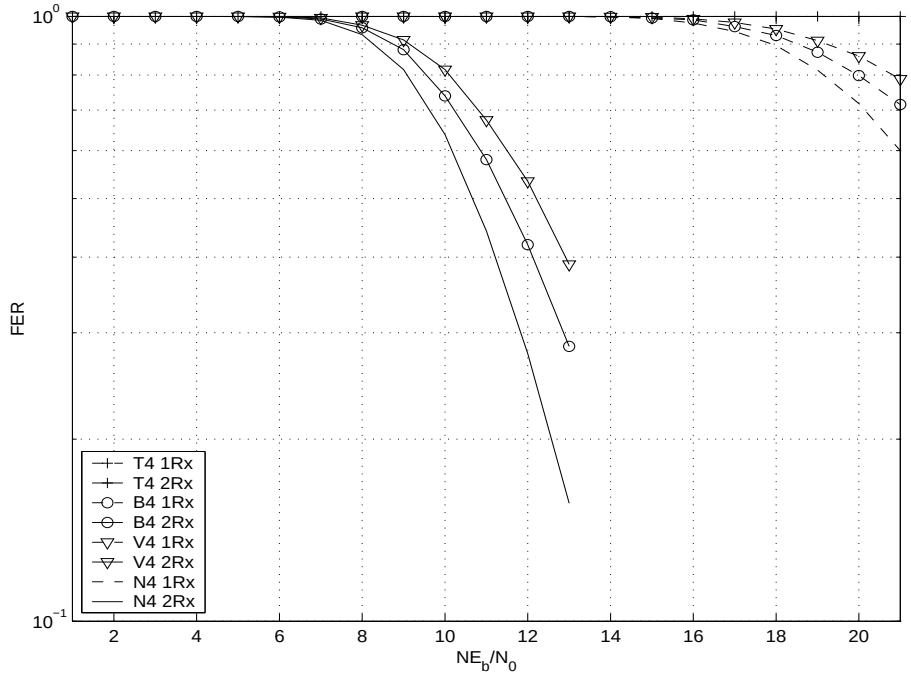


Figure 3.20: Performance of punctured 4-state codes with period 2 in rapid fading channel

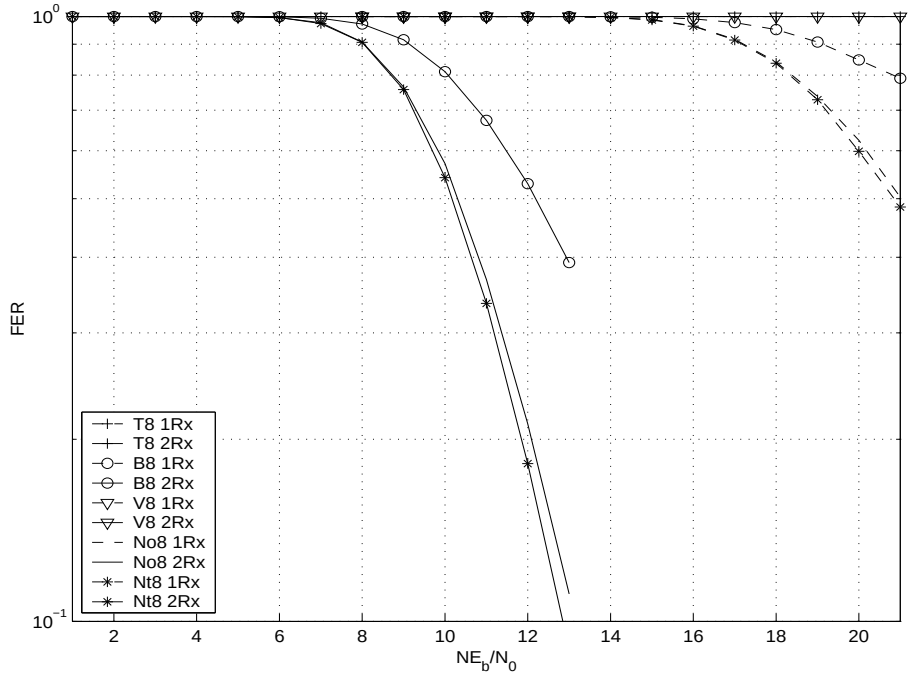


Figure 3.21: Performance of punctured 8-state codes with period 2 in rapid fading channel

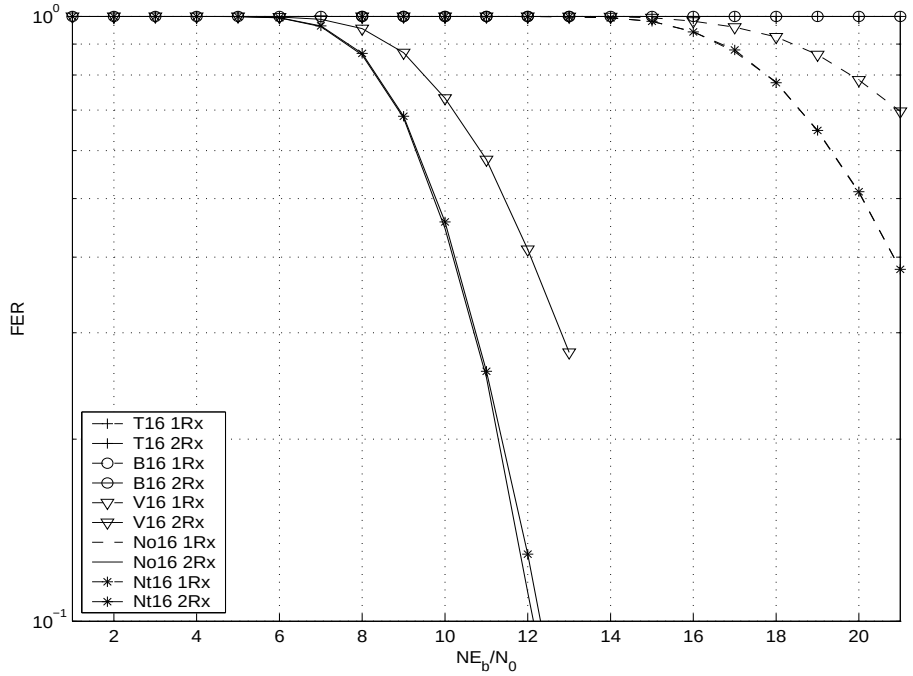


Figure 3.22: Performance of punctured 16-state codes with period 2 in rapid fading channel

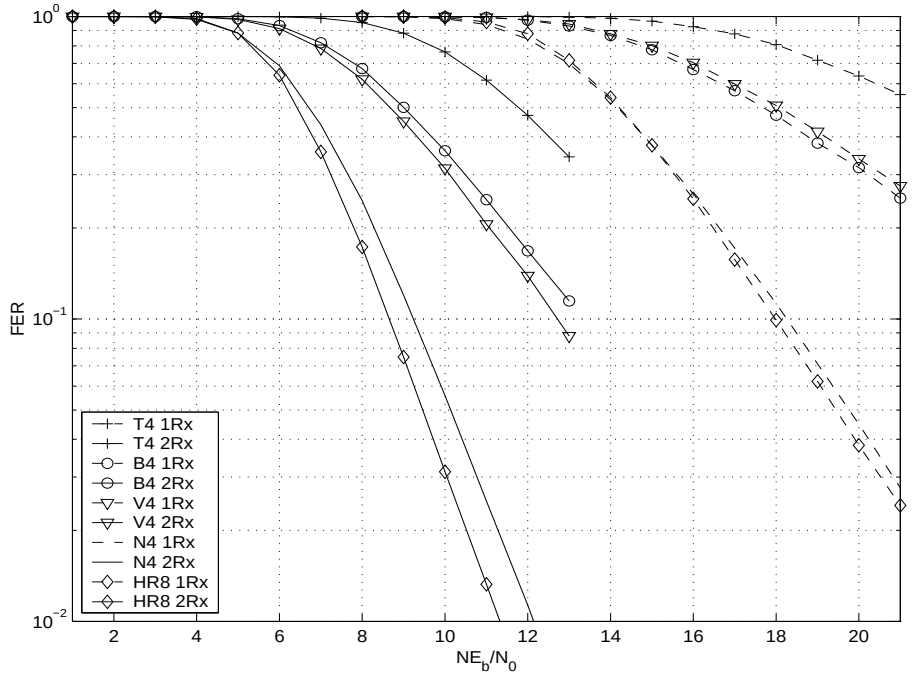


Figure 3.23: Performance of punctured 4-state codes with period 3 in rapid fading channel

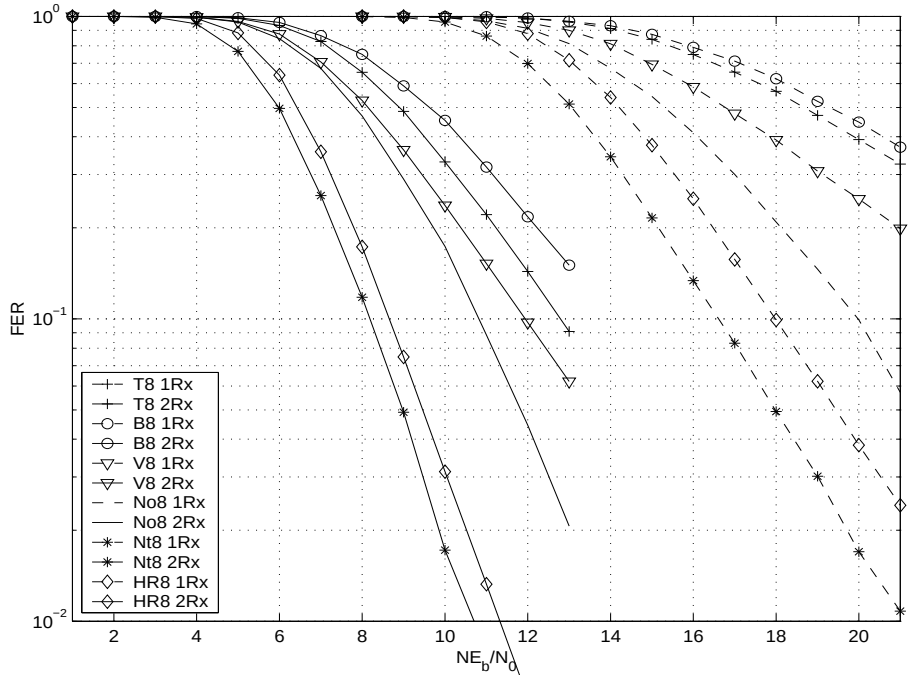


Figure 3.24: Performance of punctured 8-state codes with period 3 in rapid fading channel

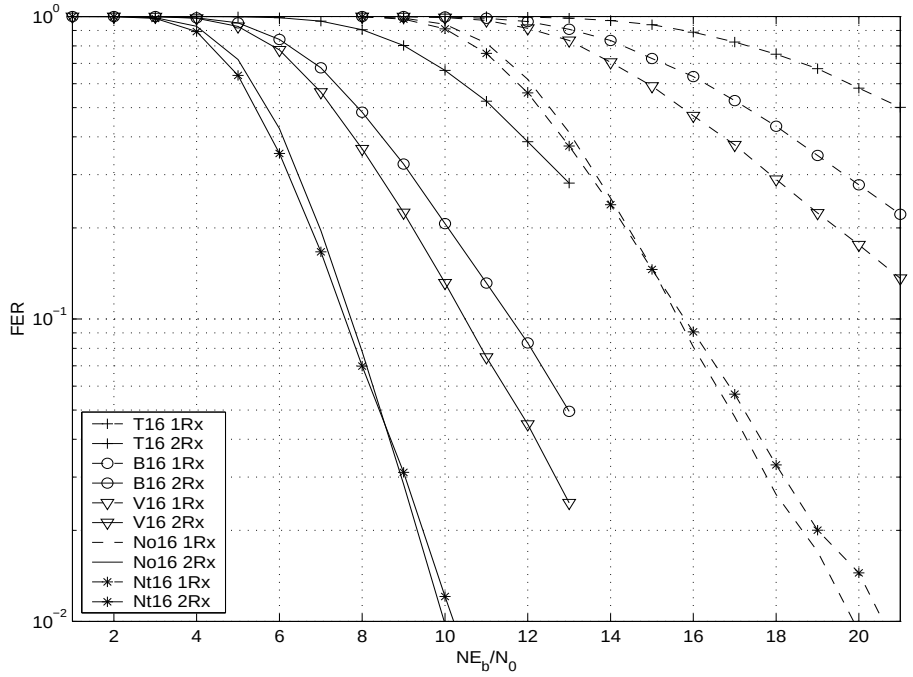


Figure 3.25: Performance of punctured 16-state codes with period 3 in rapid fading channel

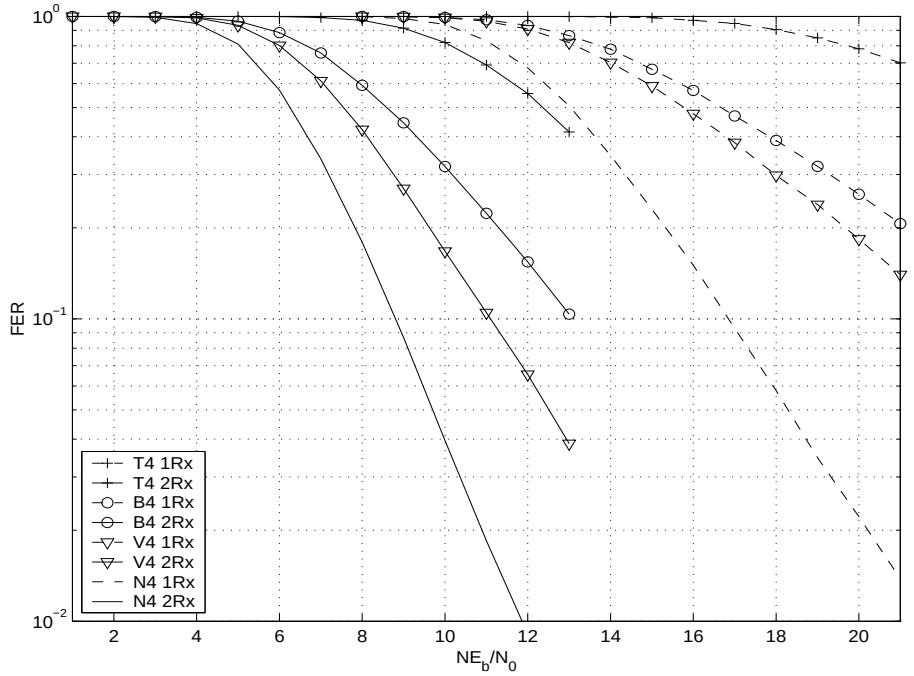


Figure 3.26: Performance of punctured 4-state codes with period 4 in rapid fading channel

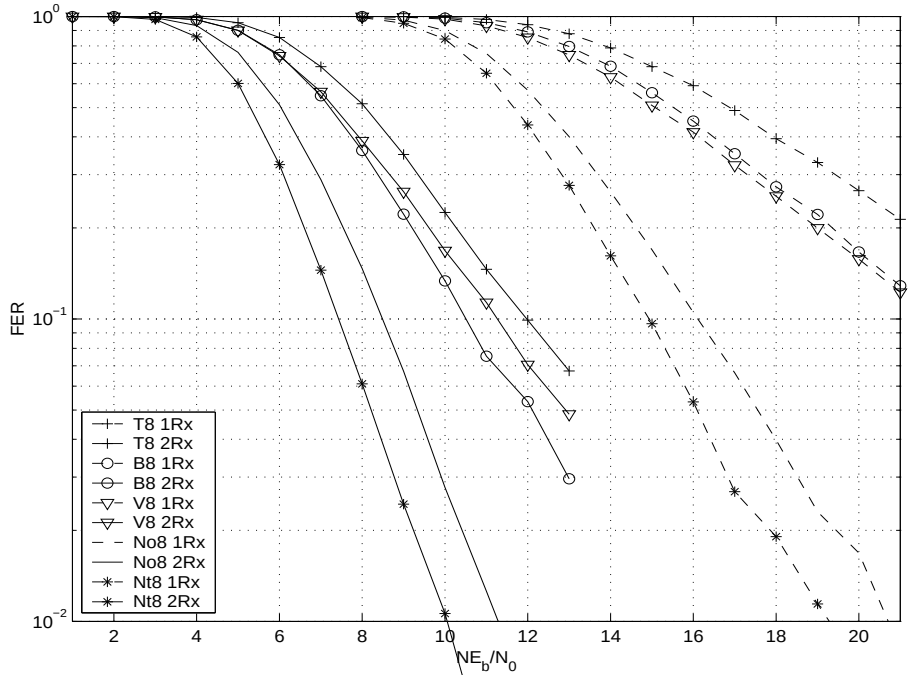


Figure 3.27: Performance of punctured 8-state codes with period 4 in rapid fading channel

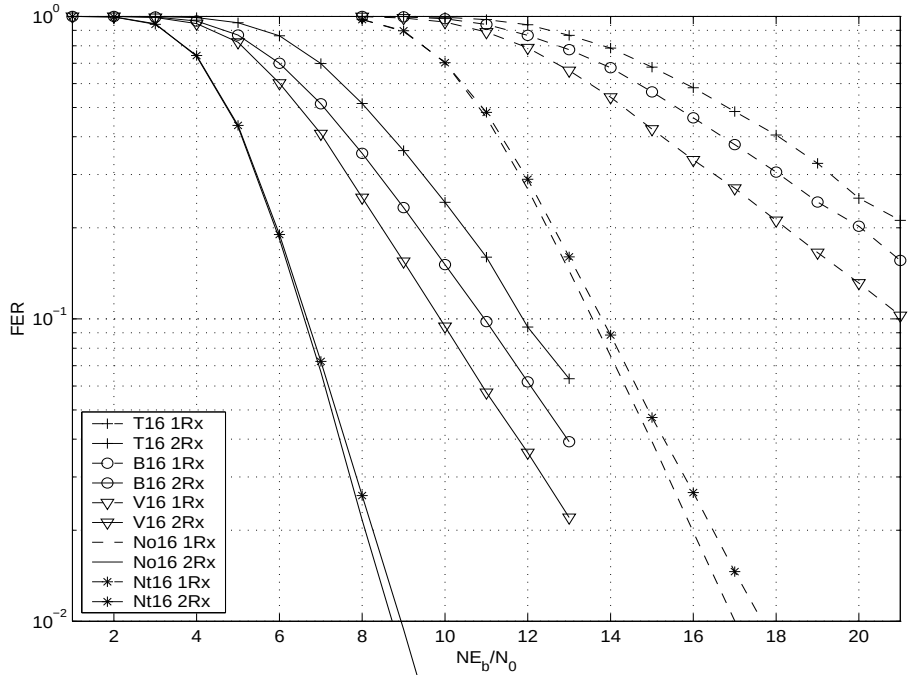


Figure 3.28: Performance of punctured 16-state codes with period 4 in rapid fading channel

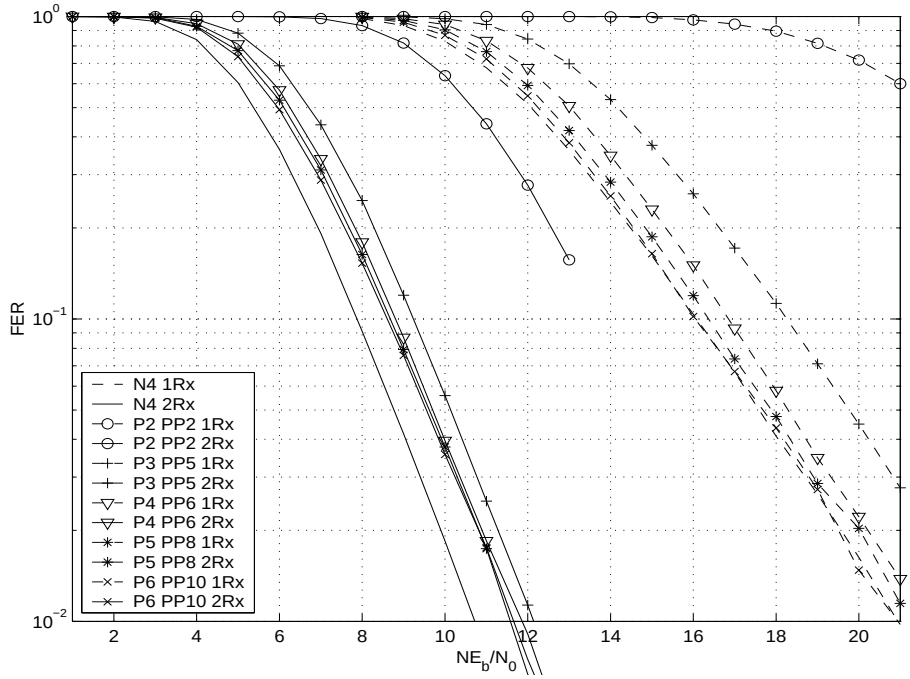


Figure 3.29: Performance of new 4-state code with deferent periods in rapid fading channel

simulation that as the punctured symbols are far from each other in the PP as the performance of the punctured code improved. This is illustrated by using period four PP-(4), PP-(5) and PP-(6) shown in Figure 2.11(4), (5) and (6) respectively where the last PP is the used in the previous simulations. The code N4 is simulated in quasi-static and rapid fading channels with the three PP's and the results are shown in Figure 3.30 and 3.31 respectively. By studying the two figures it can be easily seen that for the one and the two receive antennas systems, as the distance between the punctured symbols within the same PP increases the performance of the punctured code improved.

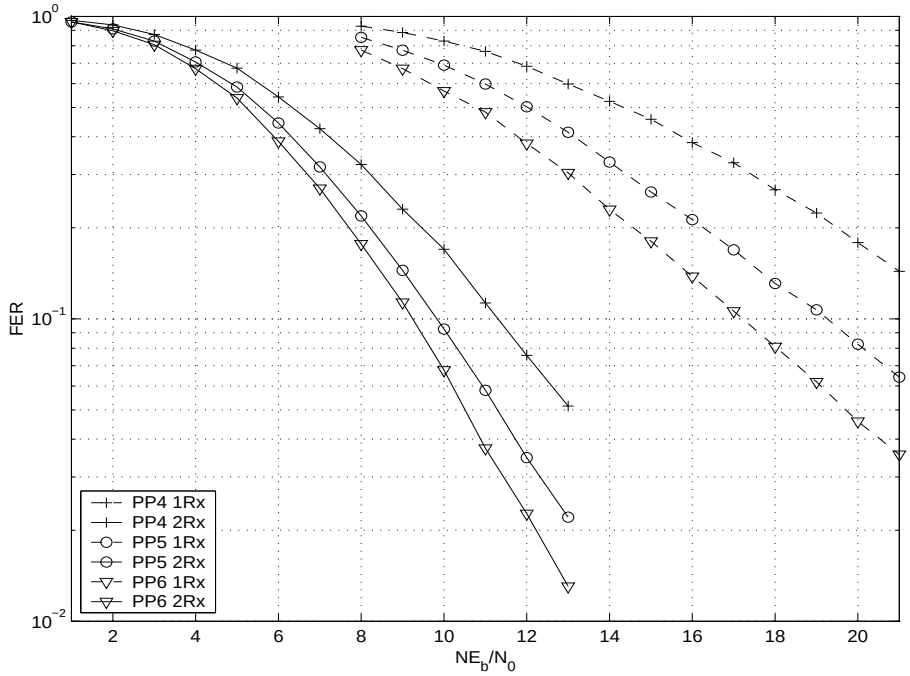


Figure 3.30: Performance of N4 with period four and various PP in quasi-static fading channel

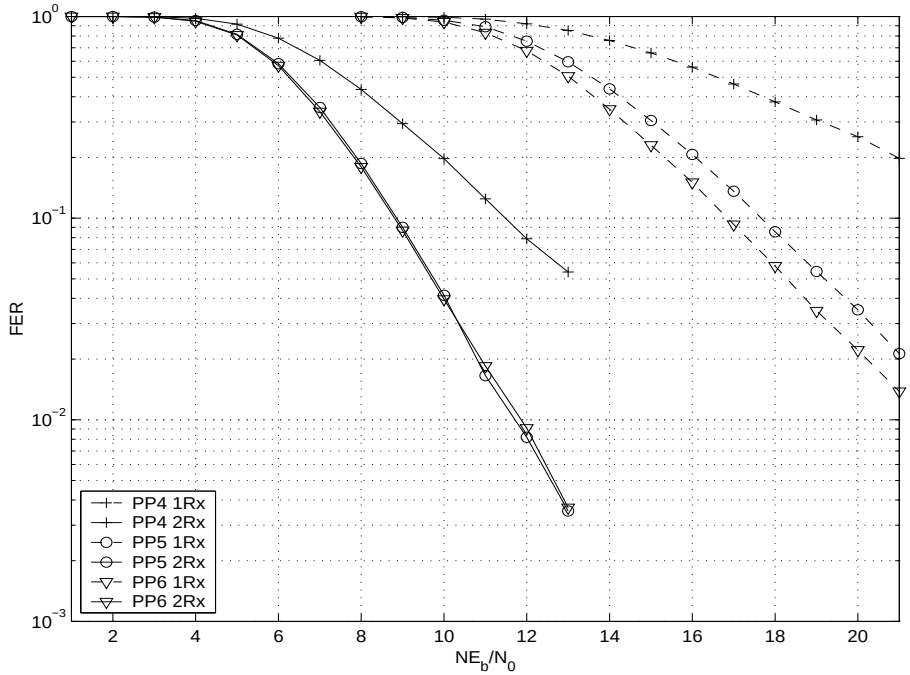


Figure 3.31: Performance of N4 with period four and various PP in rapid fading channel

# CHAPTER 4

# HIGH RATE AND PUNCTURED SPACE-TIME CODES IN AUTOMATIC REPEAT REQUEST SCHEMES

## 4.1 INTRODUCTION

In a simple data communication systems, information follows only in one direction from transmitter to receiver. The information bits are encoded using an error-correcting code (block or convolutional) to combat transmission errors caused by the channel noise. The error control provided in these systems is called forward-error-correction (FEC) scheme [47]. In a FEC system, parity-check bits are added to each transmitted frame to form a codeword depending on the error-correcting

code used by the system. At the other end of the communication channel, if the receiver discovers the occurrence of errors in the received word, it tries to locate and correct the errors and then passes the decoded word to the user. Erroneous data can be delivered to the user if the receiver either fails to discover the occurrence of errors or fails to specify the exact locations of the errors. The system throughput equals to the rate of the error-correcting code employed by the system.

The main drawback of the FEC schemes is that the receiver must deliver the decoded word even if it is incorrect. It is difficult to achieve high system reliability with FEC schemes because the probability of a decoding error is much greater than the probability of an undetected error. To overcome this problem, a long powerful error-correcting code should be used. However, this is not practical solution since it increase the decoding complexity and cost.

A more reliable error control scheme is the automatic repeat request (ARQ) scheme [47]. In an ARQ error-control system, a high rate error-detecting code is employed with a known retransmission strategy. The information bits are encoded where parity-check bits are added depending on the error-detecting code to form a codeword, which is transmitted later. At the receiver, the receiver computes the syndrome of the received word, if the syndrome is zero, the received word is a valid codeword in the code used by the system and it is passed to the user after removing the parity-check bits. If the syndrome is not zero, the received word is erroneous word so that the receiver discards the received word and asks for retransmission of

the same codeword via a feedback channel. Retransmission process continues until an error-free word is received. Erroneous data can be delivered to the user if the receiver fails to detect the occurrence of errors. The probability of an undetected error can be made vary small by using a proper error-detecting code. However, the system throughput is not constant and falls quickly with high channel noise.

To overcome drawbacks in both error-control schemes, they can be combined to form a hybrid FEC ARQ or simply hybrid ARQ scheme. The error-correcting code is used in this scheme to correct the most frequent error patterns and thus reduces the number of retransmission, which increases the ARQ system throughput.

In the next section, types of basic ARQ and hybrid ARQ schemes are studied. Next, hybrid ARQ schemes that employ ST, high-rat ST, and PST codes, are presented. The Chapter is concluded with simulation results and a comparison between the presented hybrid ARQ schemes.

## 4.2 Automatic Repeat Request

### 4.2.1 Basic ARQ Schemes

There are three basic types of ARQ schemes; stop-and-wait ARQ, go-back-N ARQ, and selective-repeat ARQ [47]. These schemes differ in the retransmission strategies implemented in each scheme and in the storage requirement in both the transmitter and the receiver. Before studying the basic ARQ types, it is important to

define some quantities.

- $P_c$= probability that a received word is error free,
- $P_d$= probability that a received word contains a detectable error pattern, and
- $P_e$ probability that a received word contains an undetectable error pattern.

It is clear that $P_c + P_d + P_e = 1$. All three probabilities depend on the channel error statistics while only the probabilities $P_d$ and $P_e$ also depend on the error-detecting code used by the ARQ system. Retransmission depends on the probability $P_d$ since a transmitted frame is accepted by the receiver either if it does not contain errors or if it contains an undetectable error pattern.

The performance of these ARQ schemes is measured by their reliability and throughput efficiency. The reliability of an ARQ scheme can be increased by making the probability of undetectable error pattern very small. Therefore the reliability of an ARQ scheme depends mainly in the choice of the error-detecting code and does not depend on the retransmission strategy. Thus all three basic ARQ schemes achieve the same system reliability. The throughput efficiency or simply throughput of an ARQ scheme is defined as the ratio of the average number of information bits successfully accepted by the receiver per unit time to the total number of bits that could be transmitted per unit time [47]. Because the three basic ARQ schemes differ in the retransmission strategy, they achieve deferent

throughput efficiencies.

### Stop-and-wait ARQ Scheme

The stop-and-wait ARQ scheme is the simplest ARQ scheme. The transmitter transmits the codeword and waits for acknowledgment from the receiver and during this time the transmitter does not transmit any further frames. If the receiver sends a positive acknowledgment (ACK), the transmitter transmits the next codeword. however, if the receiver sends negative acknowledgment (NAK), the transmitter retransmits the same codeword until it is successfully received. This process is shown in the traffic digram in Figure 4.1.

This ARQ scheme does not require any storage in either the transmitter or the receiver. However, it is inefficient because of the ideal time waiting for the receiver acknowledgment. The system can transmit $n + \lambda\delta$ bits if it does not remain ideal, where $n$ is the codeword length, $\lambda$ is the ideal time, and $\delta$ is the bit rate of the transmitter. The number of bits that the transmitter could have transmitted for a successful reception of a codeword is [47]:

$$T_{SW} = \frac{n + \lambda\delta}{P_c} \tag{4.1}$$

Therefore, the throughput of the stop-and-wait ARQ scheme equals [47]:

$$\eta_{SW} = \frac{k}{T_{SW}} = \frac{P_c \cdot (k/n)}{1 + \lambda\delta/n} \tag{4.2}$$

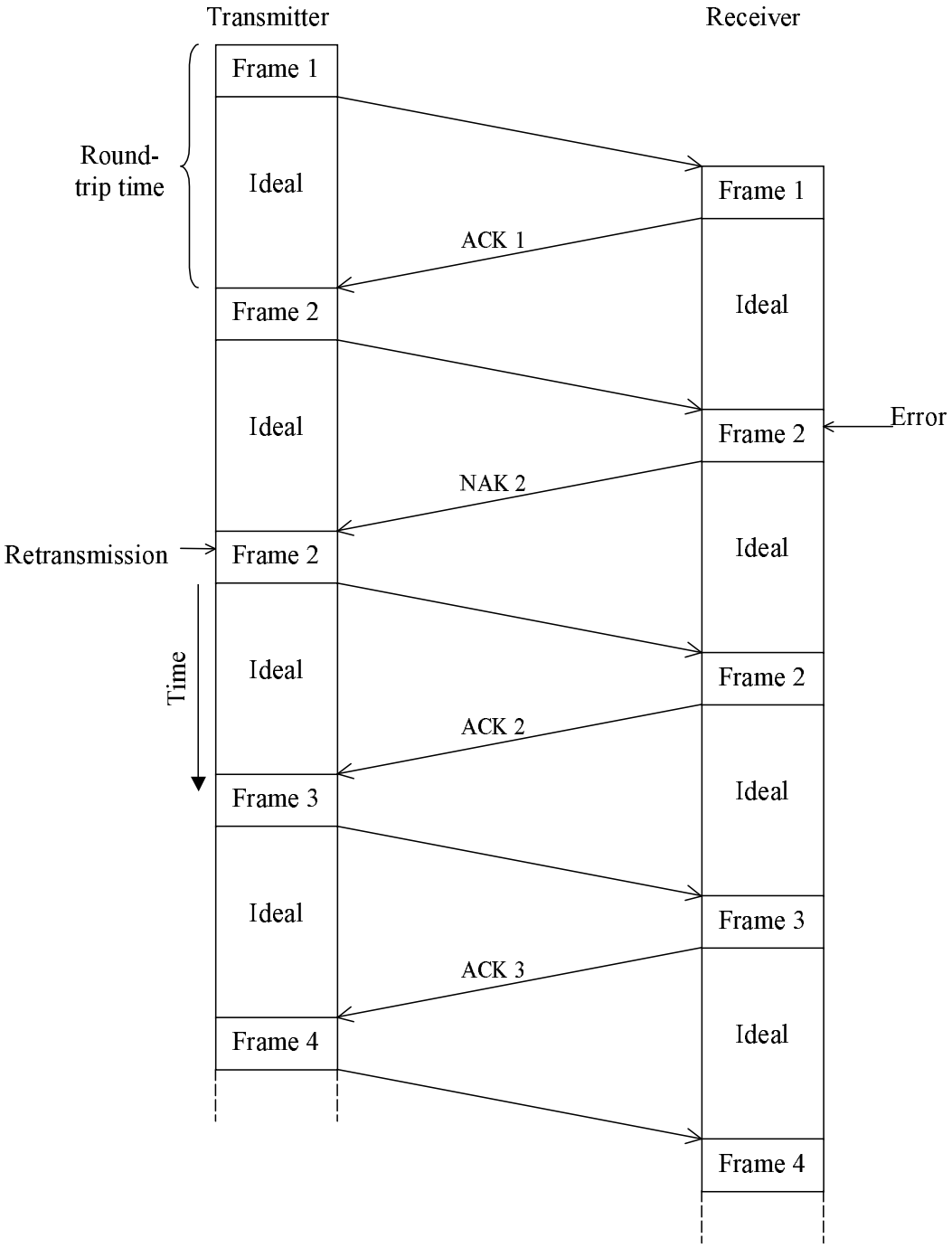


Figure 4.1: Stop-and-wait ARQ scheme

where $k$ is the number of data bits, and $k/n = R$ is the rate of the error-detecting code used by the system. For communication systems with large round-trip delay and high data rate the throughput of the system will be unacceptable.

**Go-back-N ARQ Scheme**

Because the stop-and-wait ARQ scheme was in efficient due to the ideal time, a continuous transmission scheme is needed, which result in introducing the go-back-N ARQ scheme. In go-back-N ARQ scheme, the transmitter transmit the codeword continuously and in order. The transmitter transmits $N-1$ codewords during the period from transmitting a codeword and receiving its acknowledgment from the receiver. The $N$ transmitted codewords are stored in the transmitter for later use. If an NAK of a transmitted codeword for example codeword $i$ is received by the transmitter, it stops transmitting new codewords and goes back to retransmit codeword $i$ and the $N-1$ succeeding codewords. If the same codeword is negatively acknowledged again, the same $N$ codewords are retransmitted until it is positively acknowledged. At the receiver side, if a received word contains a detectable error pattern, the receiver will discard this word and the $N-1$ succeeding received words even if some of them are error free. The traffic digram in Figure 4.2 shows an example of a go-back-5 ARQ scheme.

The go-back-N ARQ scheme requires a storage of $N$ codewords at the transmitter, but no storage is required at the receiver. It is more efficient than the

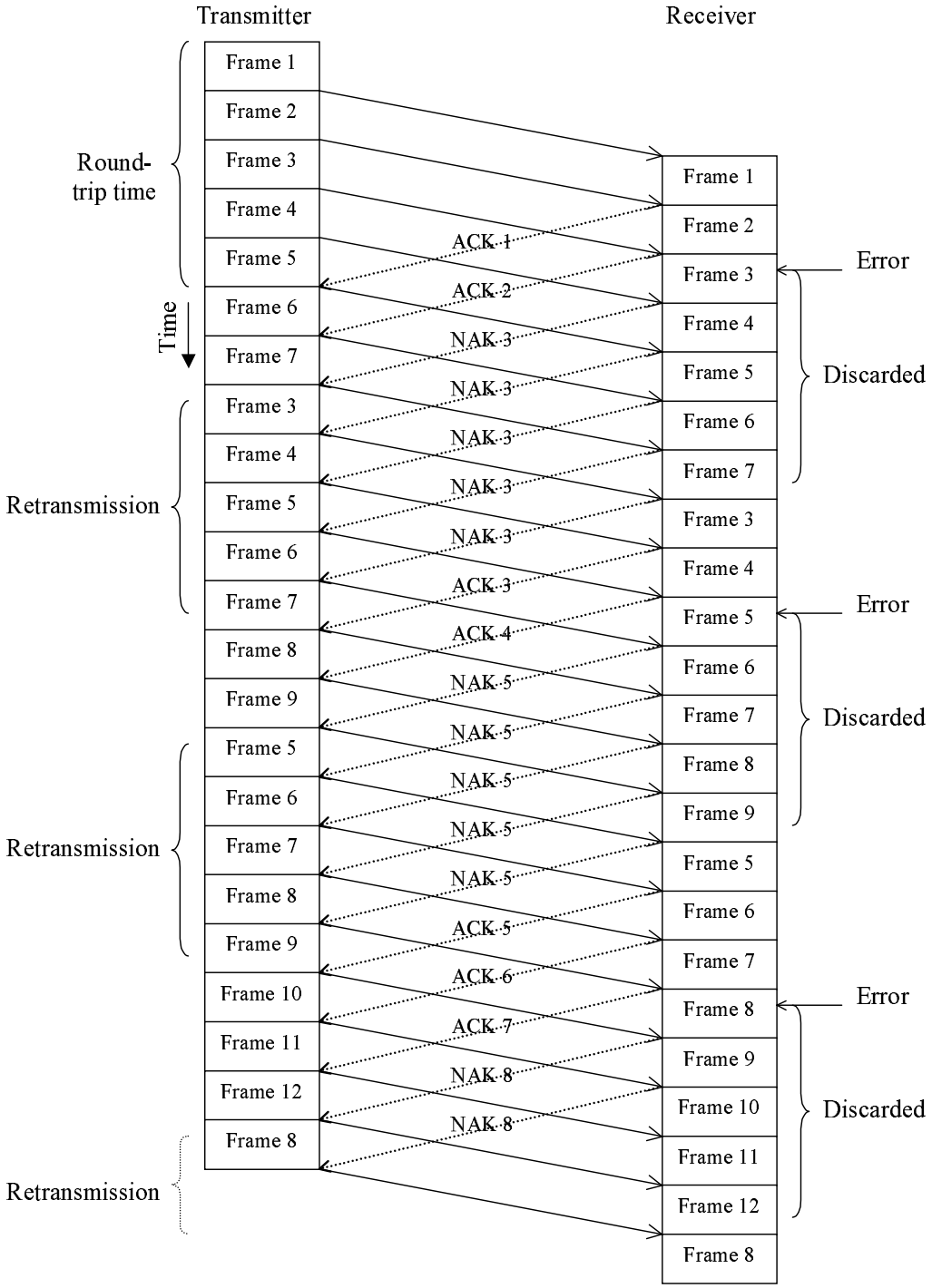


Figure 4.2: Go-back-N ARQ scheme (N=5)

stop-and-wait ARQ scheme since it is continuously transmitting codewords. The average number of bits that the transmitter could transmit for a successful codeword reception is [47]:

$$T_{GBN} = n \cdot \left(1 + \frac{N\,(1 - P_c)}{P_c}\right) \tag{4.3}$$

Therefore, the throughput of a go-back-N ARQ scheme equals [47]:

$$\eta_{GBN} = \frac{k}{T_{GBN}} = \frac{P_c \cdot (k/n)}{P_c + (1 - P_c)\,N} \tag{4.4}$$

However, for data communication systems with high data rates and long round-trip delays, the throughput of the go-back-N ARQ scheme would be unacceptable since $N$ will be very large and thus for each negatively acknowledged codeword, $N$ codeword should be retransmitted and a huge storage is required at the transmitter.

**Selective-repeat ARQ Scheme**

The main drawback of the go-back-N ARQ scheme is the retransmission of $N$ codewords for each codeword detected in error. To overcome this drawback only the codeword detected in error should be retransmitted, which is done in the selective-repeat ARQ scheme. In the selective-repeat ARQ scheme, codewords are transmitted continuously. Each transmitted codeword is stored in the transmitter buffer until it is successfully received. At the receiver, if a received word contains

a detectable error pattern, it is discarded and the next words are received and checked for errors then they are queued to be delivered to the user in order. This is illustrated in the traffic diagram shown in Figure 4.3.

The selective-repeat ARQ scheme requires theoretically infinite buffer at both the transmitter to store transmitted codewords for possible retransmission and the receiver to store error free received words. This scheme is called ideal selective-repeat ARQ scheme. The average number of bits that the transmitter could transmit for a successful codeword reception assuming infinite buffering is given by [47]:

$$T_{SR} = \frac{n}{P_c} \tag{4.5}$$

Thus the throughput of an ideal selective-repeat ARQ scheme equals to [47]:

$$\eta_{SR} = \frac{k}{T_{SR}} = P_c \cdot \frac{k}{n} \tag{4.6}$$

This scheme provides superior throughput performance compared to the stop-and-wait and the go-back-N ARQ schemes. However, infinite buffers are practically not possible. So a mixed mode where two or even the three basic ARQ schemes are combined to limit the storage size were proposed.

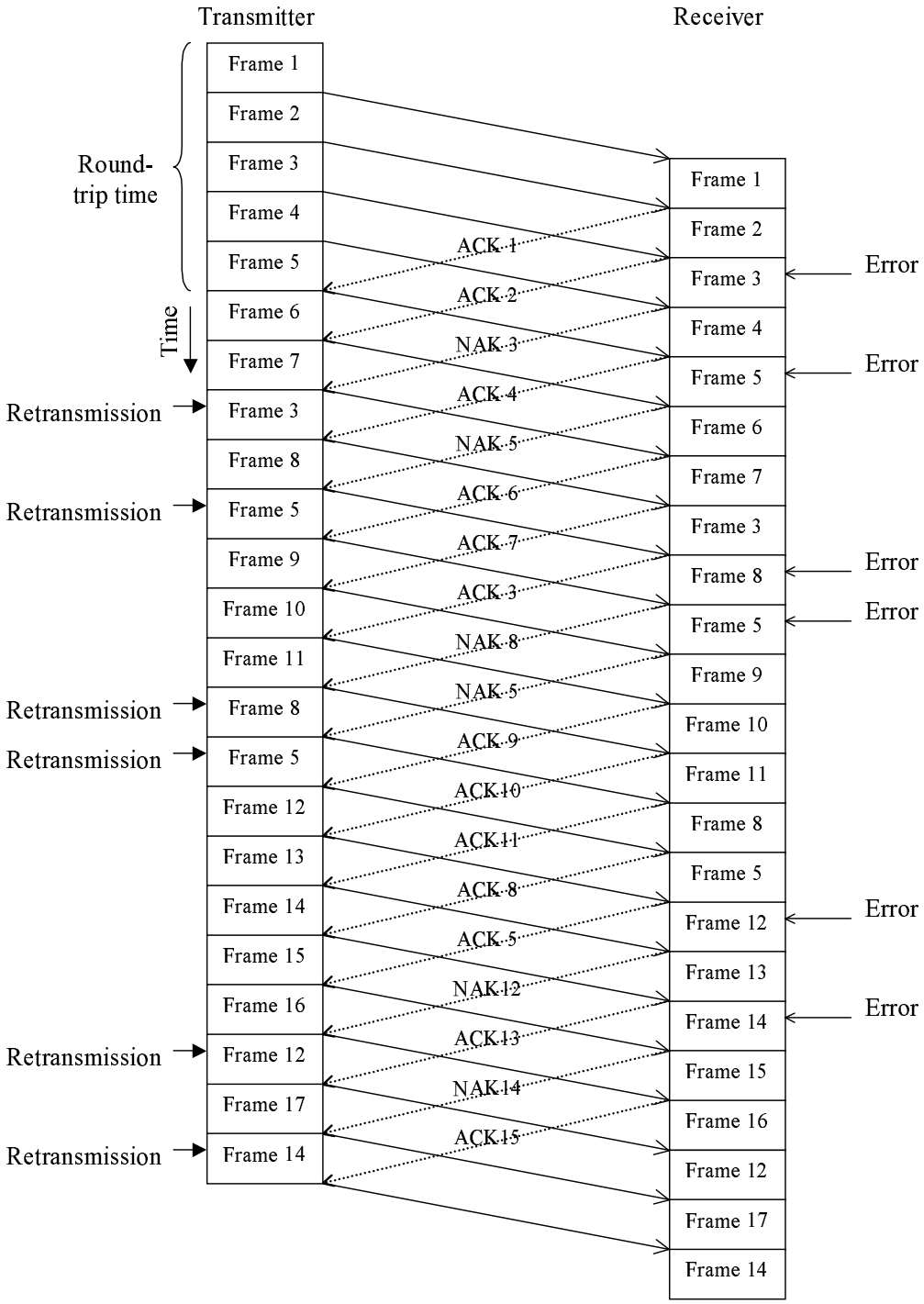


Figure 4.3: Selective-repeat ARQ scheme

### 4.2.2 HYBRID ARQ SCHEMES

A hybrid ARQ (HARQ) scheme is essentially a FEC error-control subsystem contained in a basic or a mixed-mode ARQ system. The error-correcting code implemented by the FEC subsystem is used to reduce the retransmission events by correcting the most frequent error patterns. HARQ schemes are classified depending on the usage of the previous erroneously received words, into two categories; type-I and type-II HARQ schemes.

In both HARQ scheme types, if a received word contains a detectable and correctable error pattern, the errors in the received word are corrected and the decoded word is passed to the user. In a type-I HARQ scheme, if a received word contains a detectable but not correctable error pattern, the erroneously received word is discarded and a retransmission of the same word is requested. Retransmission continues until an error free word is received or the number of retransmission reaches a predetermined value.

However, in a type-II HARQ scheme, if a received word contains a detectable but not correctable error pattern, the erroneously received word is stored for later use and a retransmission of the same word is requested. If the second transmission of a codeword received with detectable and not correctable error pattern, the receiver combines the two copies of the erroneously received word to increase the redundancy available to the decoder. There are two ways of combining the previous erroneously received word with the retransmitted one; code combining and

diversity combining. In a code combining system (proposed by Chase [48]), the erroneous $L$ copies of a codeword are concatenated and decoded using low-rate $R/L$ code where individual received words are decoded using rate $R$ error-correcting code. In a diversity combining system, the erroneous copies of a codeword are added or concatenated to form a single word whose symbols are more reliable than those in individual words. An example of diversity combining scheme is the parity retransmission (first proposed by Metzner [49]) where the first transmission attempt of a codeword contains no or few parity bits for error correction and the successive retransmissions contain more parity bits for error corrections. Clearly type-II HARQ scheme has a better throughput performance than type-I HARQ schemes.

## 4.3 HYBRID ARQ SCHEMES USED

Before describing the hybrid ARQ schemes used in this thesis, few assumptions have to be made.

- Ideal channel state information.
- Low capacity noise-free feedback channel.
- Perfect error detection.
- Independent effect of channel noise on each frame.

- Infinite buffering in both the transmitter and the receiver.

The selective-repeat ARQ scheme is used with high-rate ST, ST and PST codes as FEC schemes to form different type-I and type-II HARQ schemes.

### 4.3.1 Type-I HARQ Schemes

Three type-I HARQ protocols are presented here. The first protocols uses the high-rate ST codes, the second one uses ST codes, and the third one uses PST codes family. The three protocols are presented in the following.

#### Type-I HARQ Protocol using HR ST codes

The information bits are encoded using a high-rate ST code. The channel symbols are transmitted and at the same time stored at the transmitter buffer for possible retransmissions. At the receiver, the received word is decoded and the decoded bits are checked for errors. If the received word contains no errors (undetectable error patterns are are not counted because perfect error detection is assumed), the decoded bits are passed to the user and the receiver will send an ACK so that the stored copy of this codeword is removed from the transmitter buffer. However, if the received word contains a detectable error pattern, the receiver will discard the received word and request a retransmission of the same codeword. Retransmission continues until a successful reception of the codeword occurs or a preset number of retransmissions is reached.

### Type-I HARQ Protocol using ST codes

This protocol is identical to the previous type-I HARQ protocol but employing normal rate ST codes instead of the high-rate ST codes. This protocol and the previous one are illustrated in Figure 4.4.

### Type-I HARQ Protocol using PST Codes Family

The information bits are encoded using a normal ST code. The frame of channel symbols is punctured using a known period and PP. The punctured frame is transmitted and the un-punctured frame is stored at the transmitter buffer for later use. At the receiver, the received word is decoded and the decoded bits are checked for errors. If the received word contains no errors, the decoded bits are passed to the user and the receiver will send an ACK so that the stored copy of the un-punctured codeword is removed from the transmitter buffer. However, if the received word contains a detectable error pattern, the receiver will discard the received word and request a retransmission of the same codeword but with more redundancy. Retransmission continues until a successful reception of the codeword occurs or a preset number of retransmissions is reached, which is in this case equals to the number of members in the PST codes family including the mother ST code. For example if a mother ST code is punctured using period three PP, a family of two members is formed. If the normal frame length is 120 ST symbols, the punctured frame is of length 80 ST symbols. The transmitter first transmits

the 80 ST symbols punctured frame and stores the 120 ST symbols un-punctured one. If the transmitter received NAK for this codeword, it transmits the 120 ST symbols frame and removes the frame from the transmitter buffer. This protocol is illustrated in Figure 4.5.

### 4.3.2 Type-II HARQ Schemes

There are also three type-II HARQ protocols presented here. The first protocol uses the high-rate ST codes, the second one uses ST codes, and the third one uses PST codes family. The three protocols are discussed in the following.

#### Type-II HARQ Protocol using HR ST codes

The information bits are encoded using a high-rate ST code. The channel symbols are transmitted and at the same time stored at the transmitter buffer for possible retransmissions. At the receiver, the received word is decoded and the decoded bits are checked for errors. If the received word contains no errors, the decoded bits are passed to the user and the receiver will send an ACK so that the stored copy of this codeword is removed from the transmitter buffer. However, if the received word contains a detectable error pattern, the receiver will store the received word and request a retransmission of the same codeword. If the second transmission of a codeword fails, both copies of the codeword are combined and decoded as one frame. If the decoded bits contains no errors they are passed to the user and

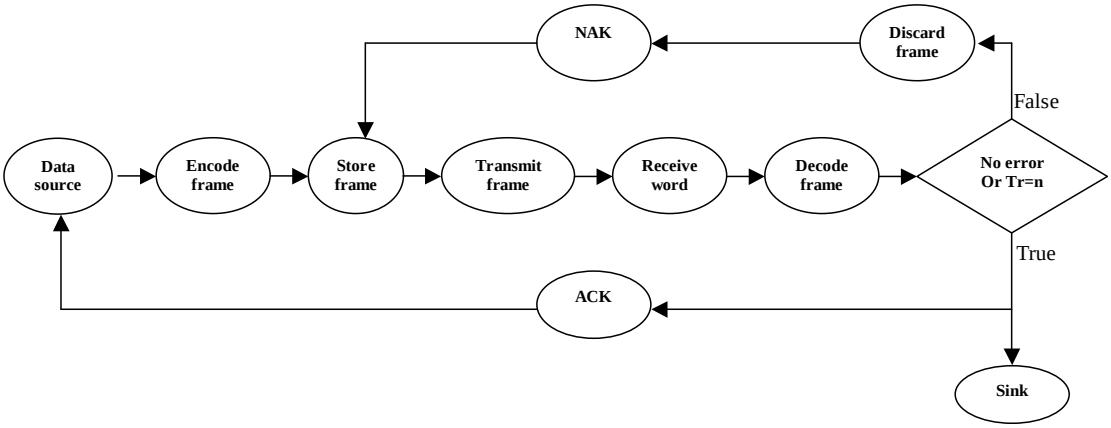


Figure 4.4: HARQ type-I protocols employing either normal or high-rate ST codes

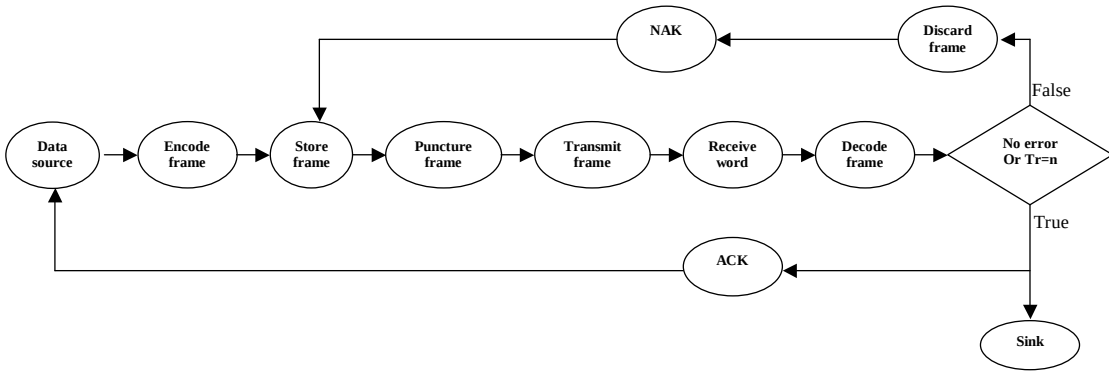


Figure 4.5: HARQ type-I protocols employing PST codes family

ACK is sent to the transmitter. If the decoded bits contains errors, the new frame (combination of the two erroneously received frames) is stored at the receiver buffer and a retransmission request is sent to the transmitter. Retransmission continues until a successful reception of the codeword occurs, successful decoding of the combined frame occurs or a preset number of retransmissions is reached.

Frames combining is not a simple addition of the ST symbols from the first transmission to the corresponding ST symbols from the second transmission. In fact the receiver stores the received signals from the $M$ receive antennas. At the second transmission (first retransmission) attempt, the stored signals are manipulated as received signals from other $M$ receive antennas. So the effect of the first retransmission is simply doubling the number of receive antennas and the successive retransmission increase the diversity which increases the probability that the frame is accepted. Frame combining is a type of diversity combining.

**Type-II HARQ Protocol using ST codes**

This protocol is identical to the previous type-II HARQ protocol but using normal rate ST codes instead of the high-rate ST codes. This protocol and the previous one are illustrated in Figure 4.6.

**Type-II HARQ Protocol using PST codes Family**

The information bits are encoded using a normal ST code. The frame of channel symbols is punctured using a known period and PP. The punctured frame is

transmitted and the un-punctured frame is stored at the transmitter buffer for later use. At the receiver, the received word is decoded and the decoded bits are checked for errors. If the received word contains no errors, the decoded bits are passed to the user and the receiver will send an ACK so that the stored copy of the un-punctured codeword is removed from the transmitter buffer. However, if the received word contains a detectable error pattern, the receiver will store the received punctured word and request a retransmission of the same codeword but with more redundancy. If the second transmission of a codeword with more redundancy fails, both copies of the codeword are added and decoded as one frame. If the decoded bits contains no errors they are passed to the user and ACK is sent to the transmitter. If the decoded bits contains errors, the new frame is stored at the receiver buffer and a retransmission request is sent to the transmitter for the same codeword with more redundancy. Retransmission continues until a successful reception of the codeword occurs, successful decoding of the summed frames occurs or a preset number of retransmissions is reached, which is in this case also equals to the number of members in the PST codes family including the mother ST code. This protocol is illustrated in Figure 4.7.

Unlike the type-II HARQ using HR codes and HARQ using ST codes protocols, in this type-II HARQ protocol, the frames of the first, second and other transmissions of a codeword have different lengths. So they can not be combined directly. Unfortunately, as explained in Chapter two, rate-compatible ST (RC-ST) codes are

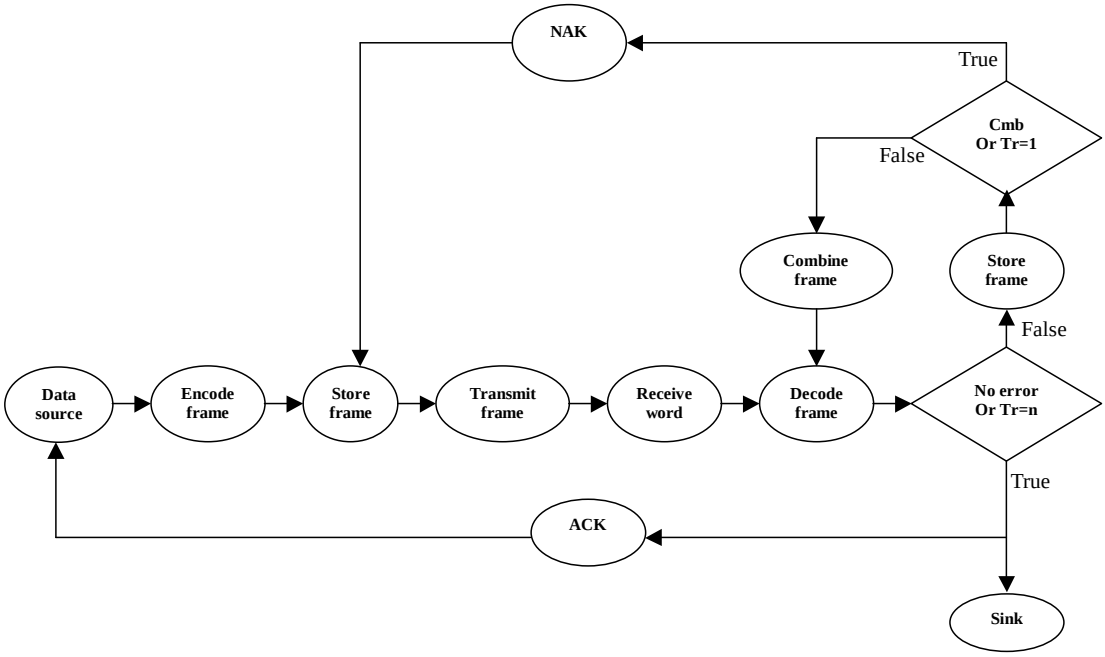


Figure 4.6: HARQ type-II protocols employing either normal or high-rate ST codes

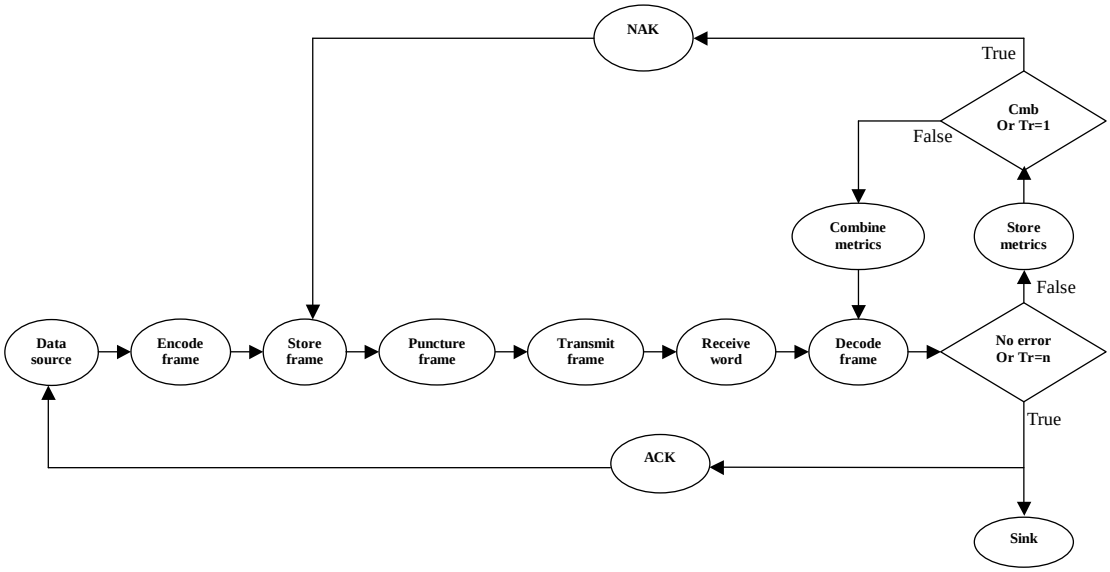


Figure 4.7: HARQ type-II protocols employing PST codes family

unlike rate-compatible trellis (RC-TCM) codes [46], simply because of the shifting process in PST codes. So combining methods used for RC-TCM codes are not applicable to RC-ST codes. However, frame combining problem can be solved by noticing that each $P - N_z/2$ ST symbols in the punctured frame represents the same information bits as the $P$ ST symbols in the original (un-punctured) frame. Since each member of a family of PST codes uses the same trellis diagram of the mother ST code, the stage metrics ($P$ transitions path metric) of the mother ST and PST codes represent the same $P$ transitions. Thus, instead of storing the erroneously received frame at the receiver buffer, the stage metrics are stored and added to the stage metrics of the second transmission of a codeword with different frame lengths. This method is called metric combining and it can be classified as a type of diversity combining. Metric combining can also be used with frames with the same length where in this case it is equivalent to frame combining.

For example if period three PP is used to puncture a frame of length 120 ST symbols, the resulting frame length is 80 ST symbols. Each three ST symbols in the un-punctured frame represents the same information bits as the corresponding two ST symbols in the punctured frame. In this case, for each received successive two ST symbols from the punctured codeword, all 16 3-transition paths starting at an initial state and ending at a final state are numbered and their 3-transition branch metrics are stored (assuming 4-state code). At the second transmission attempts, the un-punctured frame is transmitted. The receiver tries to decode the

received frame, if no errors found, the decoded bits are passed to the user. If there is an uncorrectable error pattern, for each received successive three ST symbols, all 3-transition paths metrics are computed and added to the corresponding stored 3-transition metrics, and then decoding according to the new paths metrics. At this stage, decoded bits must be passed to the user even if they contain errors.

## 4.4 NUMERICAL RESULTS

The hybrid ARQ schemes are simulated in both quasi-static and rapid fading channels. Frame length is set to 120 ST symbols and for type-I and type-II hybrid ARQ schemes using PST code family, period three PP-(5) is used. Since in period three there are only two puncturing rates, the number of transmission is set to two (only one retransmission) for all HARQ schemes presented in the previous section. Moreover, for both type-I and type-II HARQ schemes using high-rate codes, the high-rate code HR8 from Chapter two is used, while for the remaining HARQ schemes the new 4-state code N4 from the previous Chapter is used.

The system throughput is computed using the following equation:

$$Throughput = \frac{l \cdot R_m \cdot d}{l_1 \cdot R_1 \cdot t_1 + 1_2 \cdot R_2 \cdot t_2} \tag{4.7}$$

where

- $R_m$ = Mother ST code rate (or spectral efficiency)

- $l$ = Frame length (120)
- $d$ = Number of delivered frames
- $l_1$ = First transmission frame length
- $R_1$ = First transmission code rate
- $t_1$ = Number of first transmission frames
- $l_2$ = Second transmission frame length
- $R_2$ = Second transmission code rate
- $t_2$ = Number of second transmission frames

For all HARQ schemes, $l_2 = l = 120$ and $R_2 = R_m$ (equals 2 b/s/Hz for ST codes and 3 for high-rate ST codes), where as for HARQ scheme using PST codes family $l_1 = 80$ and $R_1 = 3$, and for other HARQ schemes $l_1 = l_2 = l = 120$ and $R_1 = R_m$. The number of delivered frames $d$ includes correctly decoded frames and even erroneous frames after second transmission. Another measure of throughput is given (effective throughput) where only correctly delivered frames are counted in $d$ in equation 4.7. The effective throughput is required because the number of possible frame transmissions is set to two and erroneous frames after the second transmission are delivered to the user and counted in the throughput. So the minimum throughput equals 0.5 even all delivered frames are erroneous.

### 4.4.1 Quasi-static Fading Channel

In quasi-static channels, type-II ARQ protocols outperform the type-I ARQ protocols employing the same ST code at least by three dB's and two dB's for the one and two receive antennas systems as shown in Figures 4.8 and 4.9 respectively. It can also be seen form the two figures that for both type-I and type-II ARQ protocols with one and two receive antennas, the protocols employing N4 perform better than that employing N4 PST family, while the protocols employing HR8 has a worser performance. As can be seen from Figures 4.10 and 4.11, type-I and type-II protocols employing the same coding scheme have identical throughput efficiencies. This s expected because the maximum number of frame transmissions is set to two and erroneously delivered frames are counted in the throughput. It also can be seen that the type-I and type-II protocols employing ST code N4 have better throughput efficiencies than other protocols followed by the protocols employing ST code HR8. However, for low and moderate $NE_b/N_0$, type-II protocols have a better effective throughput efficiencies than type-I protocols employing the same ST code, while for high $NE_b/N_0$ type-I protocols reach the same effective throughput efficiencies as type-II protocols employing the same ST code as shown in Figures 4.13 and 4.13 for one and two receive antennas systems respectively.

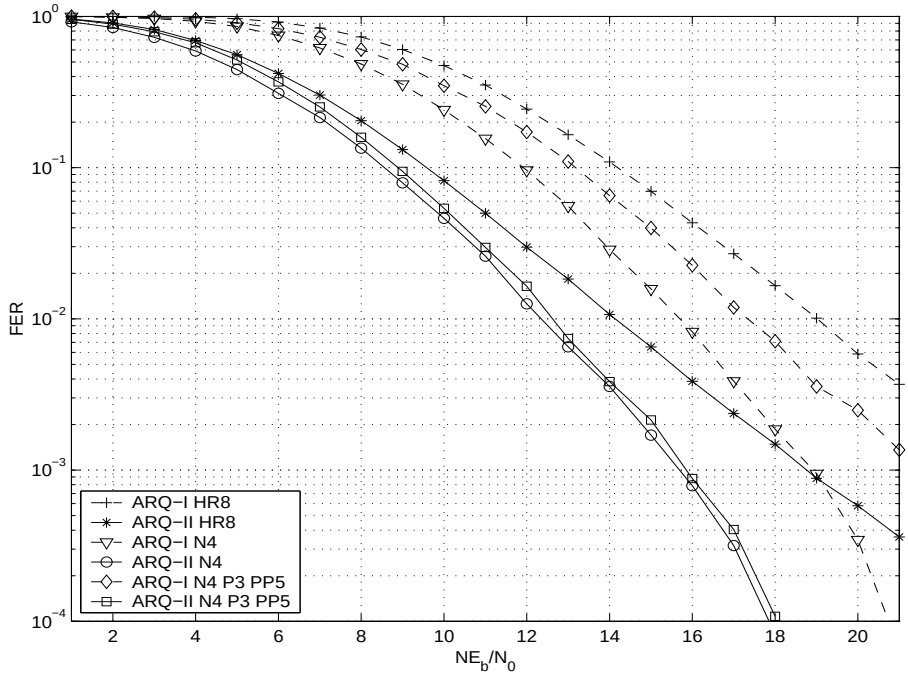


Figure 4.8: Performance of ARQ schemes in quasi-static fading channel with one receive antenna

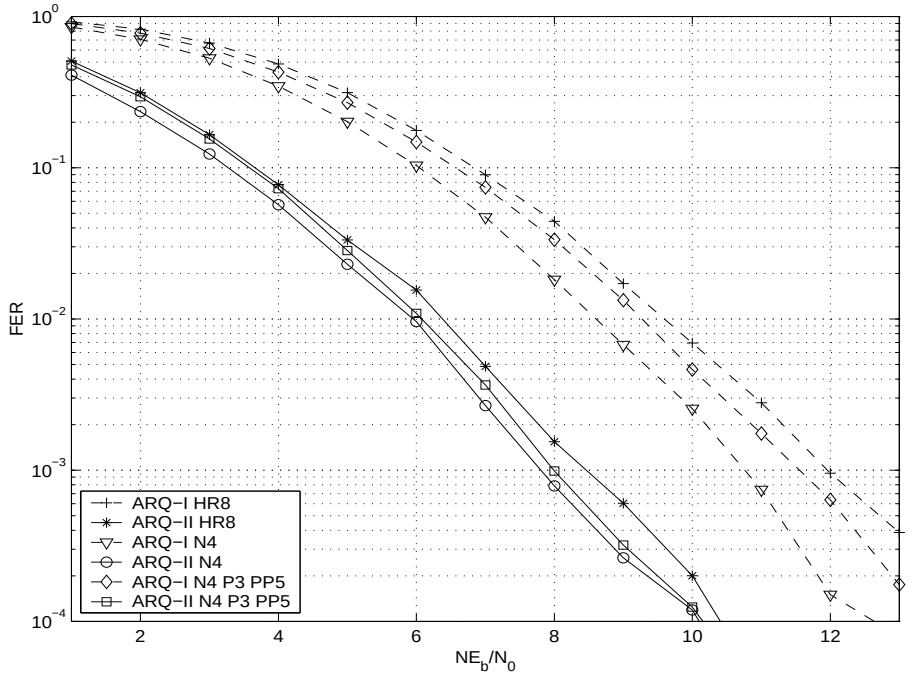


Figure 4.9: Performance of ARQ schemes in quasi-static fading channel with two receive antennas

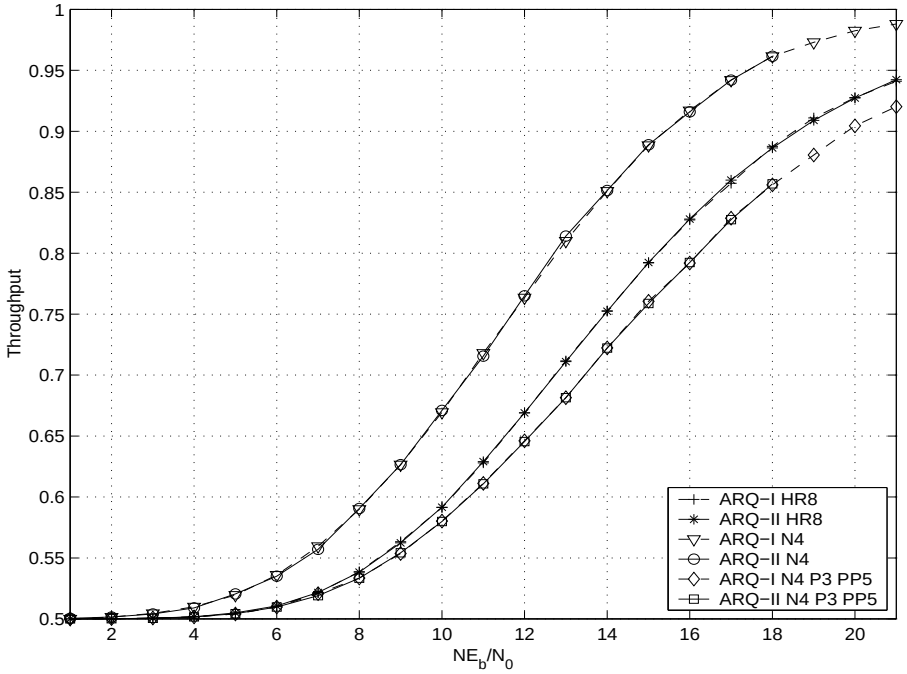


Figure 4.10: Throughput of ARQ schemes in quasi-static fading channel with one receive antenna

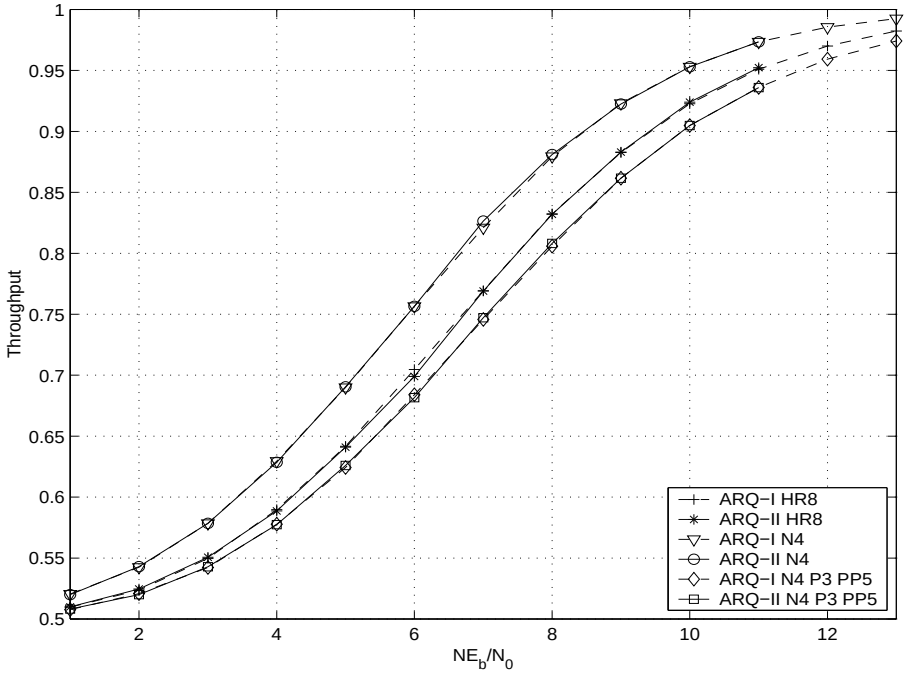


Figure 4.11: Throughput of ARQ schemes in quasi-static fading channel with two receive antennas

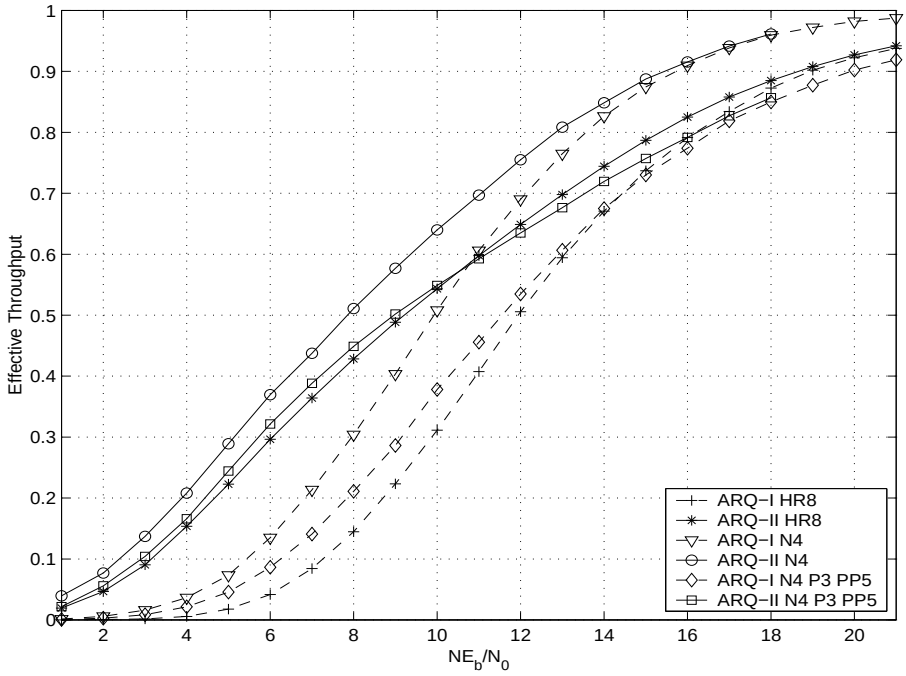


Figure 4.12: Effective throughput of ARQ schemes in quasi-static channel (one receive antenna)

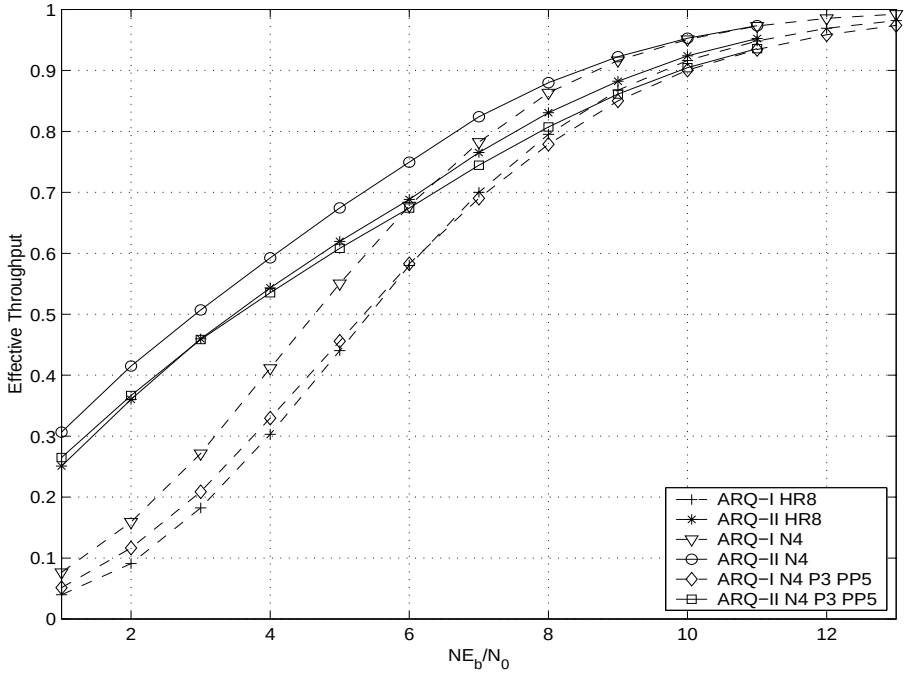


Figure 4.13: Effective throughput of ARQ schemes in quasi-static channel (two receive antennas)

### 4.4.2 RAPID FADING CHANNEL

In rapid fading channels, type-II ARQ protocols also outperform type-I protocols employing the same ST code as shown in Figure 4.14 for one receive antenna and in Figure 4.15 for two receive antennas. As in quasi-static channels, ARQ protocols employing N4 have a better performance than ARQ protocols employing N4 PST code family or HR8. The protocols employing N4 PST code family outperform that protocols employing HR8 except for type-II protocols with two receive antennas. Type-I and type-II protocols employing the same ST code have identical throughput efficiencies as shown in Figure 4.16 and Figure 4.17 for one and two receive antennas. The protocols employing ST code N4 have also better throughput efficiencies than other protocols for one and two receive antennas. Effective throughput of type-II protocols is better than that of type-I ARQ protocols employing the same ST code for both one (Figure 4.18) and two (Figure 4.19) receive antennas.

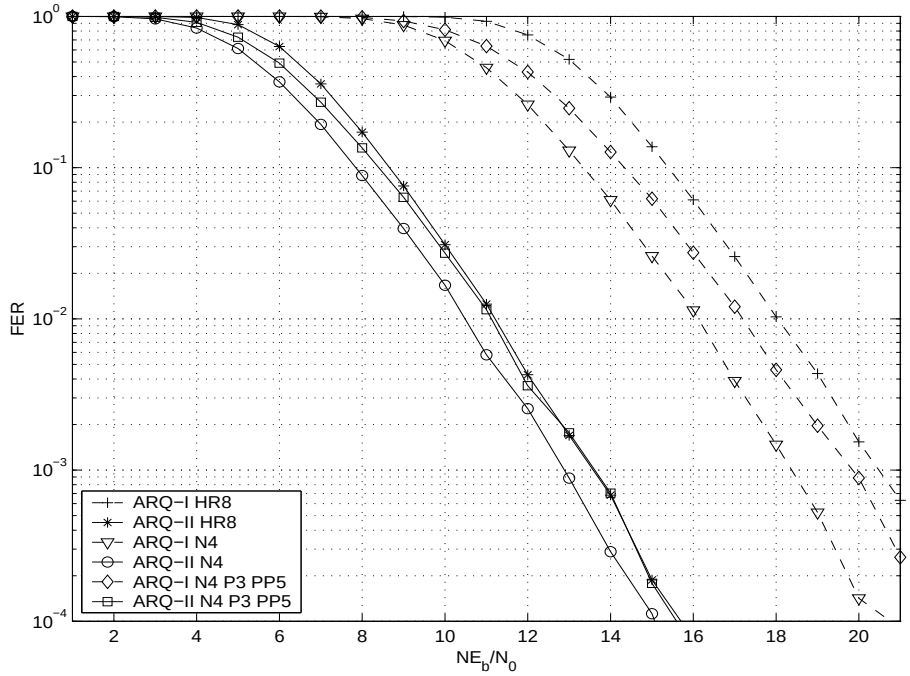


Figure 4.14: Performance of ARQ schemes in rapid fading channel with one receive antenna

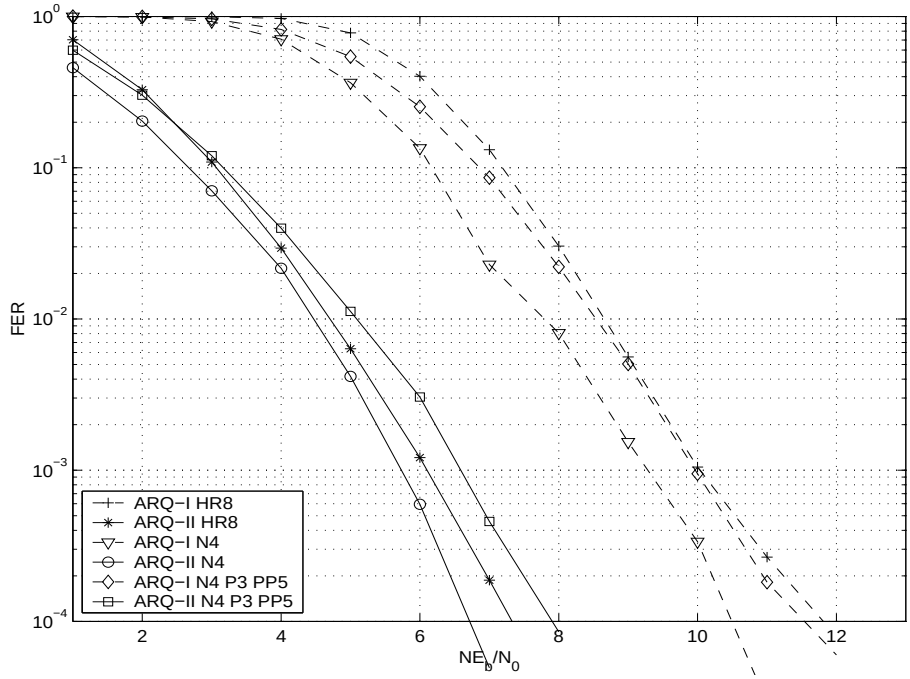


Figure 4.15: Performance of ARQ schemes in rapid fading channel with two receive antennas

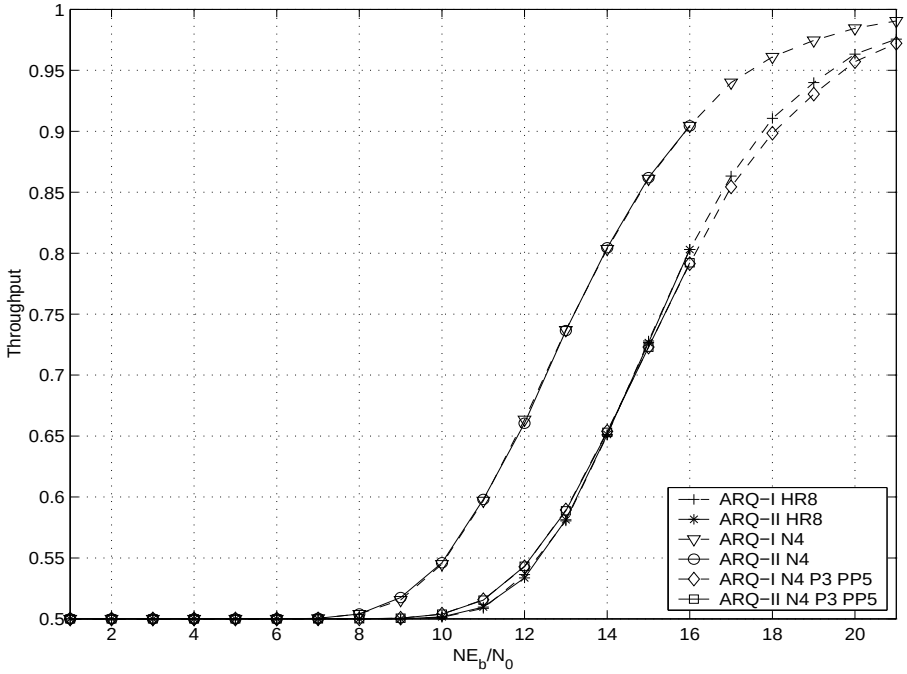


Figure 4.16: Throughput of ARQ schemes in rapid fading channel with one receive antenna

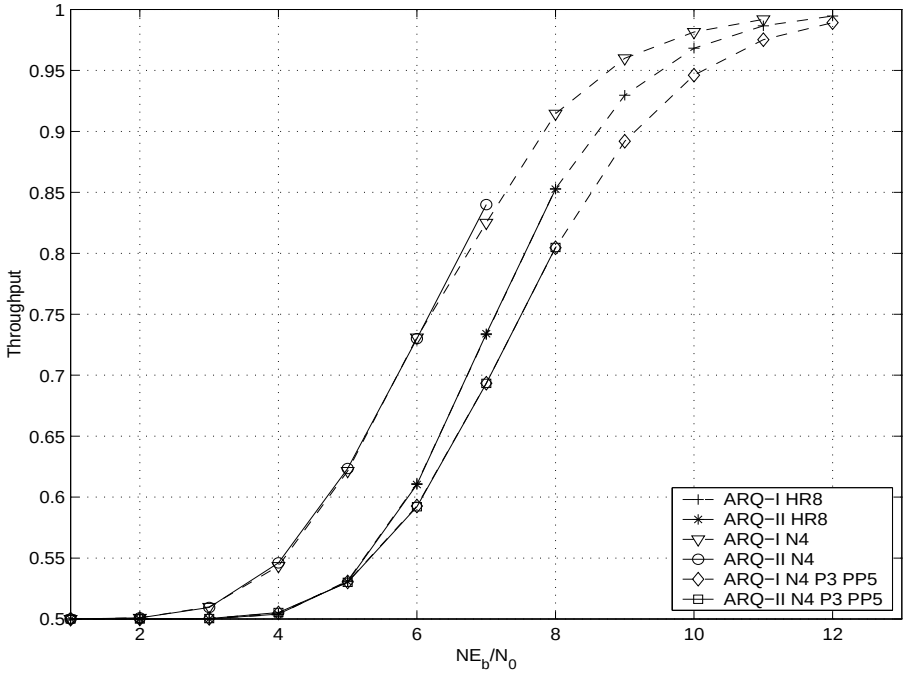


Figure 4.17: Throughput of ARQ schemes in rapid fading channel with two receive antennas

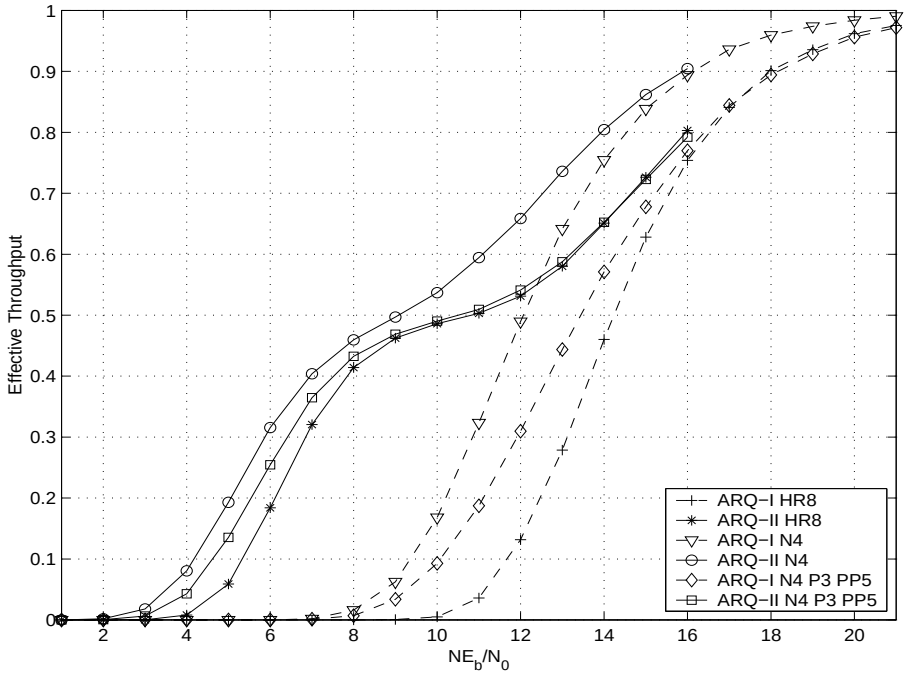


Figure 4.18: Effective throughput of ARQ schemes in rapid fading channel (one receive antenna)

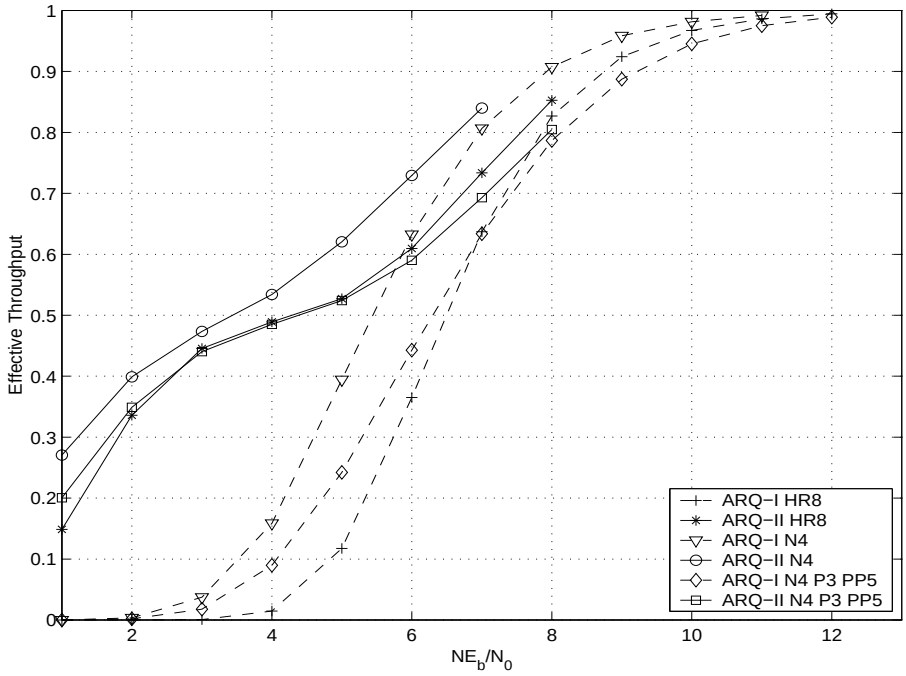


Figure 4.19: Effective throughput of ARQ schemes in rapid fading channel (two receive antennas)

# CHAPTER 5

# CONCLUSIONS AND FUTURE RESEARCH

## 5.1 CONCLUSIONS AND SUMMARY

In this thesis, performance of space-time coding systems over quasi-static and rapid fading channels have been studied. An encoder-transmitter/receiver-decoder wireless communication system is modeled and simulated using C language. The program is tested using some of the existing codes in the literature with deferent number of trellis states over both quasi-static and rapid fading environments.

Performance analysis and design criteria of ST codes are reviewed following [1] and [3] on their approaches where in [1] the analysis is carried assuming high SNR's region while in [3] the analysis is carried for two SNR ranges; low and moderate

SNR's range and high SNR's range. Since these criteria are valid for high-rate ST codes, they are implemented in C program that span all possible high-rate 8-state QPSK ST codes. Fortunately, the exhaustive search result is a code that satisfies quasi-static and rapid fading environments design criteria. This code is simulated and it shows a quite good performance in quasi-static fading channels and a better performance in rapid fading channels.

Increasing the encoder rate is one of two ways used in this thesis to improve ST coding system throughput where the other one is symbol puncturing. In Chapter two a symbol puncturing technique is proposed for ST codes. This technique is detailedly illustrated with some examples. Moreover, punctured system encoder and decoder are also shown where the PST encoder/decoder can be used with normal ST systems. This property of the PST codes suggest the use of PST codes in a rate compatible coding systems. Since in ST coding systems two or more symbols are transmitted at the same time, it is not possible to use the normal Viterbi decoding method in PST systems. A modified Viterbi decoding method for PST systems is presented that use a stage metric instead of branch metrics. Formulas of normal and punctured frame lengths and punctured system rate as a function of puncturing period and number of punctured symbols each period are derived.

Current trellis representation describes only one time transition while puncturing is performed to successive $P$ transitions in time, so they can not be used to

represent symbol PST codes. An alternative trellis representation that describe $P$ transitions in time is presented. Give a puncturing period and pattern this representation completely express symbol PST codes and it also can be used to express un-punctured ST codes. This representation is similar to that of multiple trellis codes and it introduces the idea of *multiple space-time* (MST) codes which is postponed to future research.

In Chapter three, performance of symbol PST codes over quasi-static and rapid fading channels are analyzed. A common design criterion to quasi-static and rapid fading channels is derived which is simply maximizing the symbol-wise Hamming distance. Analyzing performance of un-punctured and punctured ST codes over quasi-static and rapid fading channels leads to design criteria on the un-punctured ST code for each channel that together with the common criterion can be used to design good performing ST codes with and without puncturing. Since for a given puncturing period, PST code performance depends on the un-punctured ST code and the puncturing pattern structure, PP structure is studied. It is found that increasing the distance between the punctured symbols within the PP will improve the PST code performance since the effects of the punctured symbols will be distributed over the remaining (transmitted) symbols within the same period.

Symbol PST code design criteria for both channel models are implemented in an exhaustive search program written in C language. Five QPSK ST codes are found where the first one is a 4-state code (N4) that satisfies the common and both

channels design criteria. The other four codes are two codes (No8 and No16) for quasi-static fading channel and two codes (Nt8 and Nt16) for rapid fading channels where No8 and Nt8 are 8-state codes, and No16 and Nt16 are 16-state codes. Simulation results show that without puncturing the new codes have comparable performance to the best existing codes on their design environments. In fact No16 and Nt16 have better minimum product distance (96 and 144 respectively) than one of the best codes (64) in the literature from (V16) [5] and both codes outperform all other simulated 16-state codes in rapid fading channels. The new codes show superior performance when compared to the existing codes under puncturing with various puncturing periods over quasi-static and rapid fading channels.

ST coding system reliability has been improved by using hybrid ARQ schemes with high-rate, normal or punctured ST codes as forward error correcting codes. Three type-I and three type-II hybrid ARQ protocols are proposed in Chapter four. These protocols are simulated in computer using both channel models. The protocols using N4 perform better than other protocols for one and two receive antennas systems in quasi-static and rapid fading channel models while the protocols employing N4 PST family outperform that employing high-rate code HR8 in most cases except for type-II two receive antennas over rapid fading channel model.

## 5.2 FUTURE RESEARCH

- Higher signal constellations could be used for both high-rate ST codes and PST codes where the design criteria for PST codes may change.

- The designed codes can be tested on other communication channel models such as correlated channels and frequency selective channels.

- Using the alternative trellis representation, better design criteria for both normal and punctured ST codes could be found where in this case the resulting codes are *Multiple Space-time* (MST) codes.

- Increasing the puncturing periods which increases the number of members in the family of PST codes thus improving the rate compatible punctured space-time (RCPST) code reliability.

- Extend the number of transmit antennas to more than two for the PST systems.

- The effects of increasing the number of possible retransmissions on the HARQ system performance and throughput could be investigated.

- Other retransmit strategies and combining methods could be studied for the HARQ systems.

# BIBLIOGRAPHY


[1] V. Tarokh, N. Seshadri, and A. R. Calderbank. Space-time codes for high data rate wireless communication: Performance criterion and code construction. *IEEE Transactions on Information Theory*, 44(2):744–765, March 1998.

[2] J. Hagenauer. Rate-compatible punctured convolutional codes (rcpc codes) and their application. *IEEE Transactions on Communications*, 36(4):389–400, April 1988.

[3] J. Yuan, Z. Chent, B. Vucetic, and W.Firmanto. Performance and design of space-time coding in fading channels. *IEEE Transactions in Communications*, 51(12):1991–1996, December 2003.

[4] Q. Yan and R. S. Blum. Optimum space-time convolutional codes. *Wireless Communications and Networking Conference*, 3:1351–1355, September 2000.

[5] W. Firmant, B. S. Vucetic, and J. Yuan. Space-time tcm with improved performance on fast fading channels. *IEEE Communication Letters*, 5(4):154–156, April 2001.

[6] A. R. Hammons and H. El Gamal. On the theory of space-time codes for psk modulation. *IEEE Transactions on Information Theory*, 46(2):524–542, March 2000.

[7] A. M. Guidi, A. J. Grant, and S. S Pietrobon. Algebraic constructions for psk space-time coded modulation. *Applied Algebra, Algebraic Algorithms and Error-Correcting Codes Springer LNCS 2227*, pages 387–396, November 2001.

[8] Y. Liu, M. P. Fitz, and O. Y. Takeshita. A rank criterion for qam space-time codes. *IEEE Transactions on Information Theory*, 48(12):3062–3079, December 2002.

[9] Z. Safar and K. J. R. Liu. Design of space-time trellis codes for full spatial diversity. *Proceeding IEEE International Conference on Acoustic, Speech and Signal Processing*, 4:2465–2468, 2001.

[10] M. Tao and R. S. Cheng. Improved design criteria and new trellis codes for space-time coded modulation in slow flat fading channels. *IEEE Communications Letters*, 5(7):313–315, July 2001.

[11] C. Kose and R. D. Wesel. Code design metrics for space-time systems under arbitrary fading. *International Conference on Communications*, June 2001.

[12] K. K. Mukkavilli, D. M. Ionescu, and D. Anzhang. Design of space-time codes with optimal coding gain. *IEEE International Symposium on Personal, Indoor, and Mobile Radio Communications PIMRC*, 1:495–499, September 2000.

[13] Y. Liu, M. P. Fitz, and O. Y. Takeshita. Space-time codes performance criteria and design for frequency selective fading channels. *International Conference on Communications*, 9:2800–2804, June 2001.

[14] V. Tarokh, H. Jafarkhani, and A. R. Calderbank. Space-time block codes from orthogonal designs. *IEEE Transactions on Information Theory*, 45(5):1456–1467, July 1999.

[15] S. Li and C. Han. Orthogonally constructed space-time codes. *Proceeding IEEE International Conference on Information Technology and Information Networks*, 2:834–843, 2001.

[16] J. D. Terry and J. T. Heiskala. Spherical space-time codes (sstc). *IEEE Communications letters*, 5(3):107–109, March 2001.

[17] B. M. Hochwald and T. L. Marzeta. Unitary space-time modulations for multiple-antenna communications in rayleigh fading. *IEEE Transactions on Information Theory*, 46(2):543–564, March 2000.

[18] B. M. Hochwald and W. Sweldens. Differentially unitary space-time modulations. *IEEE Transactions on Communications*, 48(12):2041–2052, December 2000.

[19] D. Cui and A. M. Haimovich. Design and performance of turbo space-time coded modulation. *IEEE Global Telecommunications Conference*, 3:1627–1631, November 2000.

[20] D. Tujkovie. Recursive space-time trellis codes for turbo coded modulation. *IEEE Global Telecommunications Conference*, 2:1010–1015, 2000.

[21] D. Cui and A. M. Haimovich. Performance of parallel concatenated space-time codes. *IEEE Communications Letters*, 3(6):236–238, June 2001.

[22] S. A. Zummo and S. A. Al-Semari. A tight bound on the error probability of space-time codes for rapid fading channels. *Wireless Communications and Networking Conference*, 3:23–28, September 2000.

[23] H. Shin and J. L. Lee. Upper bound on the error probability for space-time codes in fast fading channels. *Vehicular Technology Conference VTC*, pages 243–246, September 2002.

[24] G. Taricoo and E. Biglieri. Exact pairwise error probability of space-time codes. *IEEE Transactions on Information Theory*, 48(2):510–513, February 2002.

[25] D. K. Aktas and M. P. Fitz. Distance spectrum analysis of space-time trellis coded modulations in quasi-static rayleigh fading channels. *IEEE Transactions on Information Theory*, 49(12):3335–3344, December 2003.

[26] M. Uysal and C. N. Georghiades. Error performance analysis of space-time codes over rayleigh fading channels. *Journal of Communications and Networks*, 2(4):344–350, December 2000.

[27] R. Gozali and B. D. Woerner. Upper bounds on the bit-error probability of space-time trellis codes using generating function techniques. *Vehicular Technology Conference*, pages 1318–1323, Spring 2001.

[28] G. D. Forney. Geometrically uniform codes. *IEEE Transactions on Information Theory*, 37(5):1241–11260, September 1991.

[29] H. Al-Salman and S. A. Al-Semari. Distance properties of space-time coded trellis codes. *IEEE International Symposium on Wireless Systems and Networks*, 1, March 2003.

[30] S. A. Zummo and S. A. Al-Semari. Space-time coded qpsk for rapid fading channels. *IEEE International Symposium on Personal, Indoor, and Mobile Radio Communications PIMRC*, 1:504–508, 2000.

[31] S. Baro, G. Baush, and A. Hansmann. Improved codes for space-time trellis-coded modulation. *IEEE Communications Letters*, 4(1):20–22, January 2000.

[32] X. Lin and R. S. Blum. On the design of space-time codes employing multiple trellis coded modulation. *Conference on Information Sciences and Systems*, March 2000.

[33] G. A. de Silva. Some new codes for space-time trellis encoded modulation over fading isi channels. *IEEE International Symposium on Personal, Indoor, and Mobile Radio Communications PIMRC*, 1:500–503, 2001.

[34] D. M. Ionescu, K. K. Mukkavilli, and Z. Yan. Improved 8- and 16-state space-time codes for 4psk with two transmit antennas. *IEEE Communications Letters*, 5(7):301–303, July 2001.

[35] X. Li and J. A. Ritcey. Variable-rate trellis coded modulation using punctured codes. *IEEE Pacific Rim Communications, Computers and Signal Processing*, 2:624–627, 1997.

[36] F. Chen and D. Haccoun. Performance of punctured trellis coded modulation over fading channels. *Vehicular Technology Conference*, 1:339–343, 1997.

[37] C. Fraguli, C. Komninakis, and R. D. Wesel. Minimality for punctured convolutional codes. *International Conference on Communications*, June 2001.

[38] K. Majonen and M. J. Heikkila. Higher data rates with space-time block codes and puncturing in wcdma systems. *IEEE International Symposium on Personal, Indoor, and Mobile Radio Communications PIMRC*, pages 36–40, November 2001.

[39] Jaehak Chung, Chan-Soo Hwang, Seunghoon Nam, and Byung Jang Jeong. Punctured space-time trellis codes preserving diversity gain. *Electronics Letter*, 39(13):995–997, June 2003.

[40] Chan-Soo Hwang, Seung Hoon Nam, Jaehak Chung, and Byung Jang Jeong. Design of punctured space-time trellis codes. *IEEE International Symposium on Personal, Indoor, and Mobile Radio Communications PIMRC*, 2:1698–1702, September 2003.

[41] M. Eroz and T. Fuja. A multiple trellis-coded hybrid-arq for land mobile communication channels. *Military Communication Conference*, 2:496–500, November 1995.

[42] A. V. Nguyen and M. A. Ingram. Hybrid arq protocols using space-time codes. *Vehicular Technology Conference VTC*, 4:2364–2368, Spring 2001.

[43] Y. S. Jung and J. H. Lee. Hybrid-arq scheme employing different space-time trellis codes in slow fading channels. *Vehicular Technology Conference*, pages 247–251, September 2002.

[44] E. G. Larsson, P. Stoica, and J. Li. Ml detection and decoding of space-time codes. *IEEE Conference on Signal, Systems and Computers*, 2:1435–1439, 2001.

[45] B. Varadarajan and J. R. Barry. The rate-diversity trade-off for linear space-time codes. *Vehicular Technology Conference*, pages 67–71, September 2002.

[46] M. Eroz. *Rate-Compatible Trellis Codes in Hybrid-ARQ and Combined Source-Channel Codes*. PhD thesis, University of Maryland, 1997.

[47] S. Lin, Jr. D. J. Costello, and M. J. Miller. Automatic-repeat-request error-control schemes. *IEEE Communications Magazine*, 22(12):5–17, December 1984.

[48] D. Chase. Code combining-a maximum-likelihood decoding approach for combining an arbitrary number of noisy packets. *IEEE Transactions on Communications*, 33(5):385–393, May 1985.

[49] J. J. Metzner. Improvements in block-retransmission schemes. *IEEE Transactions on Communications*, 27:525–532, February 1979.

[50] D. K. Aktas and M. P. Fitz. Computing the distance spectrum of space-time trellis codes. *Wireless Communications and Network Conference*, pages 51–55, September 2000.

[51] M. K. Simon and D. Divsalar. Some new twists to problems involving the gaussian probability integral. *IEEE Transactions on Communications*, 46(2):200–210, February 1998.

[52] G. Caire and E. Viterbo. Upper bound on the frame error probability of terminated trellis codes. *IEEE Communications Letters*, 2(1):2–4, January 1998.

[53] R. D. Wesel, X. Liu, and W. Shi. Periodic symbol puncturing of trellis codes. *31st Asilomar Conference on Signals, Systems, and Computers*, November 1997.

# VITA

- Sami Abdul-Hadi Faraj Al-Anazi.
- Born in Al-Jahra, Kuwait on October 21, 1975.
- Received Bachelor of Engineering (B.E) degree with Second Honors in Electrical Engineering from King Fahd University of Petroleum and Minerals, Dhahran, Saudi Arabia in December 1998.
- Email: sami_af@yahoo.com